Fundamentals and Material Science Aspects of Particle Filled Polymer Blends

by

Derrick Amoabeng

Bachelor of Science, Kwame Nkrumah University of Science and Technology, 2011

Master of Science, North Carolina A&T State University, 2014

Submitted to the Graduate Faculty of

Swanson School of Engineering in partial fulfillment

of the requirements for the degree of

Doctor of Philosophy

University of Pittsburgh

2019

UNIVERSITY OF PITTSBURGH

SWANSON SCHOOL OF ENGINEERING

This dissertation was presented

by

Derrick Amoabeng

It was defended on

June 27, 2019

and approved by

Lei Li, PhD., Associate Professor, Department of Chemical and Petroleum Engineering

Ian Nettleship, PhD., Associate Professor, Department of Mechanical Engineering and Material Science

Tagbo Niepa, PhD., Assistant Professor, Department of Chemical and Petroleum Engineering

Dissertation Director: Sachin S. Velankar, PhD., Associate Professor, Department of Chemical and Petroleum Engineering

Copyright © by Derrick Amoabeng

2019

Fundamentals and Material Science Aspects of Particle Filled Immiscible Polymer Blends

Derrick Amoabeng, PhD

University of Pittsburgh, 2019

Filled polymers often comprise thermoplastic polymers and other particulate materials (particles) which are melt blended to form materials with improved mechanical, electrical or transport properties. In many such applications, the morphology of the blend plays a critical role in determining the properties of the blend. This dissertation seeks to exploit capillarity, i.e. interfacial tension forces, to control the microstructure of particle-filled plastics. For instance, by blending together two molten plastics and particles, a variety of structures including space-spanning aggregates, cocontinuous morphologies or fibrillar structures may be realized. These structures arise from a coupling between particle preference for one or both phases of the two immiscible polymers, interfacial tension and mixing conditions.

This dissertation conducts fundamental studies of the relationship between morphology and composition of immiscible thermoplastic polymer blends filled with particles (fused and fumed silica) which are preferentially wetted by one of the polymers. The diverse microstructures that appear in different regions of the composition space are discussed, and morphological maps are constructed for such mixtures. The fundamental knowledge is then applied to develop materials in which the morphology has a significant effect on material properties. In one case, electrically conductive polymer composites are made, where a liquid metal alloy induces the aggregation of copper particles are forced to aggregate within a polymer matrix to form conductive pathways to improve the conductivity of the polymer. In another case, particles are aggregated in the presence of wetting polymer phase by capillary force to test for improvement in mechanical properties.

Table of Contents

List of Tables

List of Figures

Preface

I foremost want to thank the almighty God for how far He has brought me. He made all things possible. I would like to express my sincere gratitude to my research advisor, Dr. Sachin S. Velankar for his continued support, encouragement, supervision and useful suggestion throughout my PhD program. His continued dedication to instilling discipline in me and his guidance enabled me to complete my work successfully. I am also thankful to my committee members, Dr. Lei Li, Dr. Tagbo Niepa and Dr. Ian Nettleship for their suggestions at my proposal and final defense. Furthermore, I would like to thank my lab colleagues, Dr. Junyi Yang and Mr. Junyu Yang for sharing research ideas and techniques on operating certain lab instruments. Lastly, I would like to acknowledge National Science Foundation (NSF) for providing financial support for this research.

1.0 Introduction

Particles suspended in a two-phase liquid mixture can result in complex particle assemblies due to capillarity i.e. interfacial tension forces. Such aggregation of particles induced by capillarity have been explored in the scientific literature for applications such as fabrication of new materials or particle separations [1]. Much of the past research on materials science aspects of capillarity in particulate systems has been on small molecule (i.e. oil/water) systems. This dissertation seeks to exploit that research to large molecule systems using thermoplastic polymers. The overall aim is to understand the effects of capillary forces in filled polymer systems, and to exploit them to develop new materials or material processing approaches which will be discussed in detailed in later chapters.

1.1 Background

Filled polymer blends comprise thermoplastic polymer blends and particulate materials which are melt-blended to form materials with improved mechanical, electrical or transport properties [2-4]. In many such applications, the morphology of the blends plays a critical role in determining the properties of the blends. Capillary forces (i.e. forces stemming from surface or interfacial tension) between particulate materials (particles) serves as a means to controlling structure. Typical examples of such forces include the strength of wet granular materials which comes from particles being bound together by bridging menisci [5], particle stabilization of foams

due to strong adsorption of particles to the air/liquid interface [6-8], and stability of bijels against coarsening [9]. Capillary forces offer a means of binding together particles of such materials to create specific aggregates structures. These structures arise from a coupling between particle preference for one or both phases, interfacial tension and mixing conditions [10, 11].

The focus of this thesis is to examine fundamental aspects of structure development of polymer blends filled with micro-size spherical particles and also nano-size particles permanently fused into fractal like structures. The central idea is to explore the effects of both types of particles on a wide polymer blend composition. For potential applications, the fundamental knowledge was then applied to develop new materials based on polymers as the bulk phases.

This dissertation is outlined in four parts. The first two are about fundamentals of morphology-composition relationship in ternary systems. Specifically, section 2 describes the composition-morphology relation with micro-size spherical particles, and section 3 with fractal-like nanoparticles. The last two parts are exploiting the fundamental knowledge for material science applications. Section 4 describes the material science aspect of developing conductive polymer composite and section 5 discusses the improved mechanical properties of polymer blends with aggregation of particles. These will be described briefly in the following few sections and then in detail in chapters 2.0, 3.0, 4.0 and 5.0.

1.1.1 Composition-morphology relation of fused silica filled polymer blends

There has been much fundamental research on exploiting capillary forces in particle-containing small molecule systems [12-15]. Similar research on particle-filled polymer blends as mostly been restricted to low particle loading [16-19]. There is not much research on high particle

loadings, nor on trying to use capillary forces to aggregate particles to achieve different microstructures. Previous work from our group and others on exploiting capillary forces in filled polymer blends have been used to develop morphology-composition-rheology relations [10, 20, 21]. This includes the relationship between morphology and composition, the effect of particles on polymer blend morphology, phase continuity and rheology. Much work has been done by Domenech et al [20] and Yang et al [22] on the morphology and composition of blends of low (model type) molecular weight thermoplastic polymers with silica particles which were hand blended. In this study, high viscosity polymers with high molecular weight polymers were used which were processed using conventional melt blending [20, 22, 23]. The thermoplastic polymers were selected to have experimentally convenient characteristics such as being completely immiscible, to have comparable viscosity, and an ability to selectively dissolve one species. The particles are spherical, not agglomerated, preferentially wetted by one phase of the polymer, and there was no complication of particle shape. This study has been published as an article in Polymer as Amoabeng et al [23].

1.1.2 Composition-morphology relation of fumed silica filled polymer blends

The research of section 1.1.1 and chapter 2.0 used spherical particles. In fact, many practical fillers are non-spherical with different shapes like acicular, fiber-like and plate-like particles. Therefore, we examined one such complex filler used in practical applications in polymers including reinforcement in polymers for improved mechanical properties, rheology modifiers and reducing friction of films. This work is a similar study of composition-morphology on polymer blends introduced in section 1.1.1 but with particulate materials typically used as

commercial filler, having much smaller and far more complex structure As a step towards practical system, PIB and PEO (same as polymer used with spherical particles) [23] with a common commercially available particulate filler was used. Here, the spherical silica filler was replaced with fumed silica particles (i.e. spherical particles with primary particle size of ~15nm chained together to form open branch aggregates [24]), but with preferential wettability in the PEO phase. This work explored the effects of fumed silica on the immiscible polymer blends, because of the branching structure of the fumed silica, morphology study differed from what was observed with the fused silica particles. One significant difference was the morphology of two percolating polymer phases that persisted almost across the entire composition range.

1.1.3 Conductive polymer composite filled with copper particles and solder

The fundamental concept of particle-aggregation induced by capillarity has been applied in diverse ways to make new materials which will be discussed in detail in later chapters. One relevant point of interest in this thesis common to all chapters is the preferential wettability of particles towards one phase of the immiscible liquids. This idea has can be applied in making materials with diverse application, of which this thesis considers two. In Chapter 4.0, the concept was used to create conductive polymer composites (CPC), where ternary blend of polystyrene/solder/copper were used. The thermoplastic polymer (PS) and molten solder are the two immiscible fluids with copper particles as the solid particulate species. The essential idea is to bind together copper particles using menisci of the solder, thus creating an all-metallic percolating network with high conductivity. The binding of the copper particles using solder is achieved by simply blending under molten conditions is dubbed “bulk soldering”. In the CPC, the solder and

copper particles served as the conductive pathway through the PS polymer matrix. This was published as Amoabeng and Velankar [25]. During this portion of the research, a review article on this topic was also published as Amoabeng and Velankar [26]

1.1.4 Mechanical properties of particle filled polymer blends

Again, the fundamental concept of particle aggregation in filled polymer blends was applied to another property. Here, the goal was to test whether it is possible to improve the mechanical properties by blending it with another polymer and particles up to highly filled fractions. The idea is to selectively fill one phase of an immiscible polymer blend with particles and investigate whether the aggregation of particles by capillary forces can improve the mechanical properties such as tensile and flexural modulus, or ultimate elongation or failure strength. The combined phase with high particle loading exhibits solid-like properties which will significantly affect the modulus of the ternary mixture and processable under molten conditions. One phase of the polymer was melted-blended with particles, along with another polymer that aggregated the particles systematically. The resulting mechanical properties were examined and interpreted based on morphologies.

2.0 A Composition-Morphology of Particle-Filled Immiscible Polymer Blends

2.1 Chapter Preface

The results of this chapter were published as an article: Derrick Amoabeng, David Roell, Kendal M Clouse, Brian A. Young and Sachin S. Velankar. "A composition-morphology map for particle-filled blends of immiscible thermoplastic polymers" Polymer, 119 (2017) 212-223. (listed as reference [23] in the bibliography section). Copyright © 2017 Elsevier. Figures used in this chapter have been reprinted with permission from Elsevier.

2.2 Introduction

Immiscible homopolymers are often blended together to realize blends with improved mechanical, electrical, or transport properties [4, 27, 28]. In many such applications, the morphology of the polymer blend plays a critical role in determining the properties of the blend, and hence there has been much research on structure development in such blends. This includes mapping out the relationship between morphology and composition, the effect of the relative viscosity or elasticity of the constituents on phase continuity [29, 30], dynamic vulcanization [31], processing conditions [32, 33], interparticle forces [34], adding block copolymers [35] and exploiting compatibilizers to modify the morphology [36-44]. In this chapter, we are concerned with polymer blends that are filled with a solid particulate species. The central question motivating this chapter is: how does a particulate filler affect the morphology of an immiscible polymer blend?

Much of the literature on particle-filled polymer blends has been summarized in excellent reviews by Fenouillot et al [16], Taguet et al [45], and Filippone et al [46] and further research in this area continues [47-49]. Most of the existing research has focused on situations in which the particulate filler is present at a low volume fraction, usually less than 5 vol% [16-18, 50, 51]. Even at these relatively dilute loadings, remarkable effects have been noted: morphological stabilization (i.e. morphology remaining stable for extended periods under molten conditions) [52-54], an improvement in dispersion (i.e. a finer-scale morphology) [52, 55, 56], and changes in phase continuity induced by filler [54, 57]. Studies at filler loadings exceeding 5 vol% are uncommon [54, 58-62], and each of these covers only a narrow range of blend compositions. A comprehensive study of particle effects across the entire composition space remains missing.

In contrast to filled polymer blends, studies of small molecule liquid/fluid/particle mixtures span a much wider range of compositions. Much of this literature comes from oil/water/particle or air/water/particle mixtures, although there has been some research on “model” polymer systems with very low molecular weights as well [63-71]. These studies suggest that the full morphological picture is far more complex than recognized in the filled polymer blends community and there is rich morphological diversity as the particle loading and the ratio of the two liquid phases is varied. For illustration, consider for instance a mixture of oil, water, and fully-hydrophilic particles. If the water is in a majority, one obtains a microstructure of oil drops and particles independently suspended in water. If the water is in a minority, the morphology consists of particles suspended inside water drops that are themselves suspended in oil, dubbed a “particles-in-drops” microstructure. If the water is in a very small minority, a completely different structure appears, comprising a network of particles bonded together by small menisci of water. Such a structure has been called a “pendular network” [20] and is analogous to the structure of a sand castle which

owes its strength to small water menisci that bind together sand grains [72, 73]. These three morphologies appear only when the particles are fully-wetted by the water. On the other hand, if the particles are partially-hydrophobic, the morphologies are altogether different since the particles adsorb at the oil/water interface rather than residing in the water [1, 74].

It is immediately interesting to ask whether a similar diversity of morphologies can be realized in filled polymer blends, i.e. when the fluid phases are immiscible polymers rather than oil and water. Indeed at least a few of these morphologies have already been noted in particle-filled thermoplastic blends. For instance, Si et al [52] noted blends of various polymers in which exfoliated clay platelets adsorbed at the interface of the dispersed phase. Such microstructures are analogous to Pickering emulsions in oil/water/particle mixtures. Many similar examples have been cited in reviews [4, 27, 28]. Cai et al [48] examined blends of polystyrene, polyamide, and TiO_2 particles which were fully-wetted by polyamide. They observed a particle-in-polyamide-in-polystyrene morphology which is analogous to the "particles-in-drops" microstructure mentioned in the previous paragraph [48]. Similar particles-in-drops microstructures have been noted by others as well [75-77]. Bai et al [68] quenched a mixture of low molecular weight polybutene and polystyrene with silica nanoparticles from a temperature at which the two polymers were miscible to a temperature at which they phase-separated. Spinodal decomposition led to the formation of an interfacially-jammed bicontinuous morphology which is analogous to bijels noted in oil/water/particle mixtures [78]. All these examples suggest that there are at least some common features between the morphology of particle-filled polymer blends and oil/water/particle mixtures. Nevertheless, a comprehensive comparison of filled polymer blends vs. small molecule analogs remains missing, and more specifically, the effects of particles on polymer blend morphology at high particle loading remain poorly understood.

Motivated by this, we conducted studies of the rheology and morphology of blends of two low molecular weight polymers, polyisobutylene and polyethylene oxide, with particulate filler [20, 79]. These polymers were low viscosity liquids under molten conditions (~10 Pa.s, which is two to three orders of magnitude lower than the viscosity of conventional molten polymers) and could be mixed without needing polymer processing equipment. Using this model system, we constructed a composition-morphology-rheology map across a wide range of compositions [20].

In this article, we now turn to "real" thermoplastics, i.e. polymers that have both, a high molecular weight, and a high melt viscosity. Our primary concern in this chapter is mapping the composition-morphology relationship in particle-filled blends of two immiscible thermoplastic homopolymers, with a focus on the "fully-wetting situation", i.e. the particles have a strong affinity for one of the two polymers. Secondarily we will examine whether their behaviors differ from both, oil/water/particle mixtures as well as from the low-molecular analogs examined previously.

There are good reasons to believe that particle-filled blends of molten thermoplastic polymers will behave differently from similar small-molecule systems. Specifically, the morphology of immiscible polymer blends is determined by two factors, the viscous forces during mixing that seek to mix the two polymers, and the interfacial tension forces that seek to demix the polymers by processes such as coalescence or interfacial coarsening [80]. When filler particles are added, a third factor must be introduced: the affinity of the particles towards one or both two polymers. While these same three factors (viscous forces, interfacial tension, particle affinity for one phase or for the interface) are present in oil/water/particle mixtures, their relative "strength" is quite different. The viscosity of molten thermoplastic polymers is many orders of magnitude higher than of oil and water, and therefore viscous forces are much higher in polymer blends than in small molecule mixtures. Moreover, interfacial tension between immiscible polymers is

typically an order of magnitude lower than between oil and water, and hence the role of interfacial forces is correspondingly diminished. Thus, it is possible that any microstructure that arises due to capillary forces may not survive against high viscous forces. For instance, the pendular aggregate structure mentioned above may be disrupted because virtually all the menisci holding together the particles are broken by viscous forces. Similarly, the particles-in-drops morphology may not survive because the large viscous forces make the mean drop size smaller than the mean particle size. Indeed, Premphet and Horanont [60] show excellent examples of polymer blends in which the drops are much smaller than the particles, and a pendular aggregate structure does not survive. Another example comes from Plattier et al [61] who show that particles prefer to partition into the phase with the higher viscosity regardless of thermodynamics. Thus, merely by changing the relative viscosity of the phases, one can move the particles from one phase to another, or to the interface (if the phases have equal viscosity). Yet another example comes from Dil and Favis [75, 81] who showed that when particles are pre-dispersed into a high-viscosity polymer, they tend to stay in that polymer or at the interface even if their thermodynamic preference is for the lower viscosity phase. These authors argue that the kinetics of particle migration play a major role in particle localization in filled polymer blends. These results are in sharp contrast to the common opinion in small-molecule systems that particles adsorb at the interface strongly with no consideration given to viscous forces [82].

Apart from the effects related to high viscosity, we also anticipate significant differences in phase inversion behavior. In oil/water mixtures, phase inversion is usually abrupt (i.e. appears in a narrow composition range, although the actual phase inversion composition may depend on the mixing conditions or surfactant). The morphology on each side of the phase inversion composition comprises spherical drops of oil in water or vice versa. In contrast, blends of two

immiscible thermoplastics are often characterized by gradual phase inversion over a wider range of compositions within which co-continuous morphologies appear. At compositions adjacent to the phase inversion composition, highly anisotropic or fibrillar morphologies often appear. How particles affect phase inversion and the morphologies near phase inversion of polymer blends is not known at present. Since the behavior of oil/water/particle mixtures is altogether different, past research on phase inversion on such small-molecule systems [13, 14, 83, 84] offers no guidance on what to expect in particle-filled polymer blends.

To summarize the motivation for this study, small molecule liquid/fluid/particle mixtures show rich morphological diversity as the mixture composition is changed. Macromolecular mixtures may offer similar morphological diversity, yet, the higher viscous forces during thermoplastic blending may induce noteworthy differences. The existing literature on particle-filled polymer blends is overwhelmingly at dilute particle loadings, whereas the effect of filler at higher particle loadings, or across the entire range of ratios of the two polymers, is unknown. The goal of this chapter is explored, for the first time, the composition-morphology relationship across a wide range of compositions using a single set of materials.

The materials in this study were selected to permit clean interpretation of the results. The particles are spherical and not agglomerated, and there are no complications of particle shape, quality of dispersion, clustering, or particle porosity. Moreover, the two homopolymers have roughly matched viscosity, and hence the phase-inversion composition is not too far from 50/50 composition, with approximately symmetric behavior on the two sides of phase inversion. Due to this simplicity, we are able to identify the “minimum physics” that arises from the coupling between viscous forces, interfacial tension, and particle affinity for one phase. In that sense, this study serves as a starting point for similar composition-spanning studies with more complex

particles, e.g. fumed silica which has fractal-like particle aggregates, or plate-like nanoclay particles, which thus far have only been examined at dilute particle loadings [52, 85, 86].

The outline of this chapter is as follows. Section 2.3 describes the materials and methods. Section 2.4 presents the morphologies across a wide range of composition space along with a discussion of the various factors governing morphological evolution, and a comparison with small-molecule analogs. Section 2.5 summarizes and concludes the study.

2.3 Experimental Section

2.3.1 Materials and Sample Preparation

Experiments used polyisobutylene (PIB BASF Oppanol B-15, $\rho = 0.908$ g/mL, $M_w = 75000$ g/mol), polyethylene oxide (PEO Dow Polyox N-10, $\rho = 1.1$ g/mL, $M_w = 10^5$ g/mol) and fused silica particles (Industrial Powders SS1205, $\rho = 2$ g/mL). These particles are polydisperse with unimodal size distribution from 0.5 to 5 μm and the mean diameter is 2 μm. An SEM image of the particles is shown in the Appendix Figure A-1. The dynamic oscillatory viscosity of two polymers obtained from frequency sweep experiments is shown in Fig. A2. Both polymers are shear-thinning, and over a wide range of shear rates, the PEO is roughly 1.35 times as viscous as PIB.

As will be shown later, in many blends, the silica particles are completely engulfed by the PEO, i.e. the silica and PEO form a combined phase. This strongly suggests that the silica particles have a strong affinity for the PEO. We believe that the reason for this affinity is that silica surfaces

usually have Si-OH groups which can hydrogen-bond with PEO. In contrast, PIB is much less polar than the silica and is also incapable of hydrogen bonding with silica.

A recent article notes that commercial PEO usually contains a small fraction (~2%) of fumed silica [87]. We have not attempted to test whether that affects the morphology-composition relationships. Given that our blends use filler loadings of at least 10%, we speculate that any effect of fumed silica is dwarfed by effects of the added filler

Blends were prepared using a Brabender Electronic Plasti-Corder model number EPL-V5501 shown in Appendix Figure A-3. It operates on the counter rotation of two roller blades, which induces strong shear forces for efficient mixing of the blends. The maximum mixer capacity with the roller blades installed is 60 mL. The composition is specified by the three volume fractions denoted ϕ_{PIB}, ϕ_{PEO}, and ϕ_p. This study examines particle volume fractions of ϕ_p = 0, 10, 20, and 30%, and the PEO:PIB ratios are varied from 4:96 to 88:12. The PIB/PEO/silica ternary blends were prepared in a two-step procedure. The mixer was first preheated to 95°C, the PIB was added, and allowed to attain the 95°C mixing temperature for 5 min. The PEO was then added in small increments while blending at 92 rpm for 5 min. A small test sample of PIB/PEO blends was taken out of the mixer for later characterization. Then, silica particles were added, also in small increments, and blending continued for 5 min at same speed. For each sample blend, the amount of material at the end of the mixing process was approximately 40 g. The compositions of the blends studied are listed in Appendix Table 1 and also shown on a ternary diagram Appendix Figure A-4. The various symbols in Appendix Figure A-4 correspond to the different morphologies to be discussed later.

2.3.2 Characterization

Structural characterization was performed using Scanning Electron Microscopy (SEM-JEOL JSM6510). Prior to preparing samples for SEM, a portion of each sample was immersed in n-octane. Samples with high PIB content fragmented when immersed in octane, indicating that the particles and PEO did not form a percolating phase (this will be discussed in detail later). For samples that fragmented in octane, the fragments were deposited onto a filter paper (Millipore, 0.1 mm pore size) and washed by dripping excess octane onto the filter paper. Upon drying, the filter paper was stuck onto a carbon-tape on an SEM stub. Samples that did not fragment in octane were first compression-molded into discs of about 0.8 mm thickness. They were then cryo-fractured under liquid nitrogen. The fractured discs were allowed to reheat to room temperature without exposure to moisture (since PEO is water soluble). The fractured surfaces were etched by immersing into octane to remove the PIB. The samples were then were then taped to SEM stubs with the fractured surfaces facing upwards and supported with conducting copper tape. The samples were then coated using a Pd sputtering target for 90 s at 40 mA. Since PIB is removed by selective dissolution in octane for all samples, only the PEO and particles remain for SEM imaging. Thus, the images correspond to either the fragments of PEO and particles remaining when samples disintegrate in octane, or fracture surfaces of PEO continuous samples that do not disintegrate. In the latter, the removal of PIB with octane leaves the appearance of craters or holes.

A limited amount of optical microscopy was conducted with an Olympus Inverted Microscope using 4×, 20× and 40× objectives. For samples that fragmented in octane, the fragmented dispersed phase was pipetted onto a glass slide and imaged directly. For samples which remain intact in octane, direct observation yielded poor images due to the poor transparency of the

semi-crystalline PEO. Accordingly, small portions of the sample were melted on a glass slide at 95 ^{o}C and observed immediately on the microscope.

2.4 Results and Discussion

A total of 11 particle-free and 24 particle-containing blends were prepared and characterized by SEM. Appendix Figure A-4 shows SEM morphologies of all 35 samples that span across the entire composition diagram. This approach of presenting the data on a ternary composition diagram is different from what is popular in the polymer blends literature which usually represents filler effects in rectilinear form (with the filler loading as the primary compositional variable). The rectilinear form is suitable at low filler loadings. However, at the higher filler fractions examined here, the composition of each of the polymer phases reduces significantly as filler is added, making a triangular composition diagram more suitable.

The effects of particles are manifold, and therefore interpreting all of them at once is difficult. To represent the large amount of information in more manageable chunks, we will examine images across specific trajectories in composition space (e.g. change PEO:PIB ratio at fixed particle loading, or vary particle loading at fixed PEO:PIB ratio). By this approach, several trends in morphological evolution with composition can be identified readily. The following discussion is split into six sections: the first on particle-free blends, the next three on particle effects on the morphology, the fifth on particle effects on phase inversion, and the sixth on comparison with small-molecule analogs.

2.4.1 Particle Free Blends

Before discussing effects of particles on the morphology, Figure 2-1 first presents the morphological changes with composition in the absence of particles. When PEO is in a small minority, it forms the dispersed phase comprising roughly round drops with a size of a few microns (Figure 2-1a). With increasing PEO loading, the PEO drops grow in size but remain mostly spherical (not shown in Figure 2-1 but see Appendix Figure A-5 in Appendix A). At a PEO fraction of 33% (Figure 2-1b), PEO is still the dispersed phase but it is increasingly non-spherical, with a large increase in size. This is attributable to a sharp increase in coalescence. At 39% PEO (Figure 2-1c), the sample no longer disintegrates completely in octane, and 56% PEO (Figure 2-1d), the PEO phase remains completely unfragmented. As will be discussed in Section 2.4.5, the PIB phase of these two samples is continuous as well, i.e. the blends of Figure 2-1c&d have a co-continuous morphology. With further increase in PEO content, the PIB loses continuity and becomes the dispersed phase. The PIB inclusions are large and non-spherical at high PIB content (Figure 2-1e) and small and nearly spherical when the PIB is dilute (Figure 2-1f).

In summary, the particle-free blends show behavior that is consistent with that expected from the literature: (1) the minority phase tends to form the dispersed phase; (2) phase inversion appears when the two polymers have comparable volume fractions; (3) the morphology appears co-continuous at phase inversion; (4) the size of the dispersed phase increases greatly approaching phase inversion from either side; and finally, (5) the dispersed phase becomes increasingly elongated near phase inversion on either side.

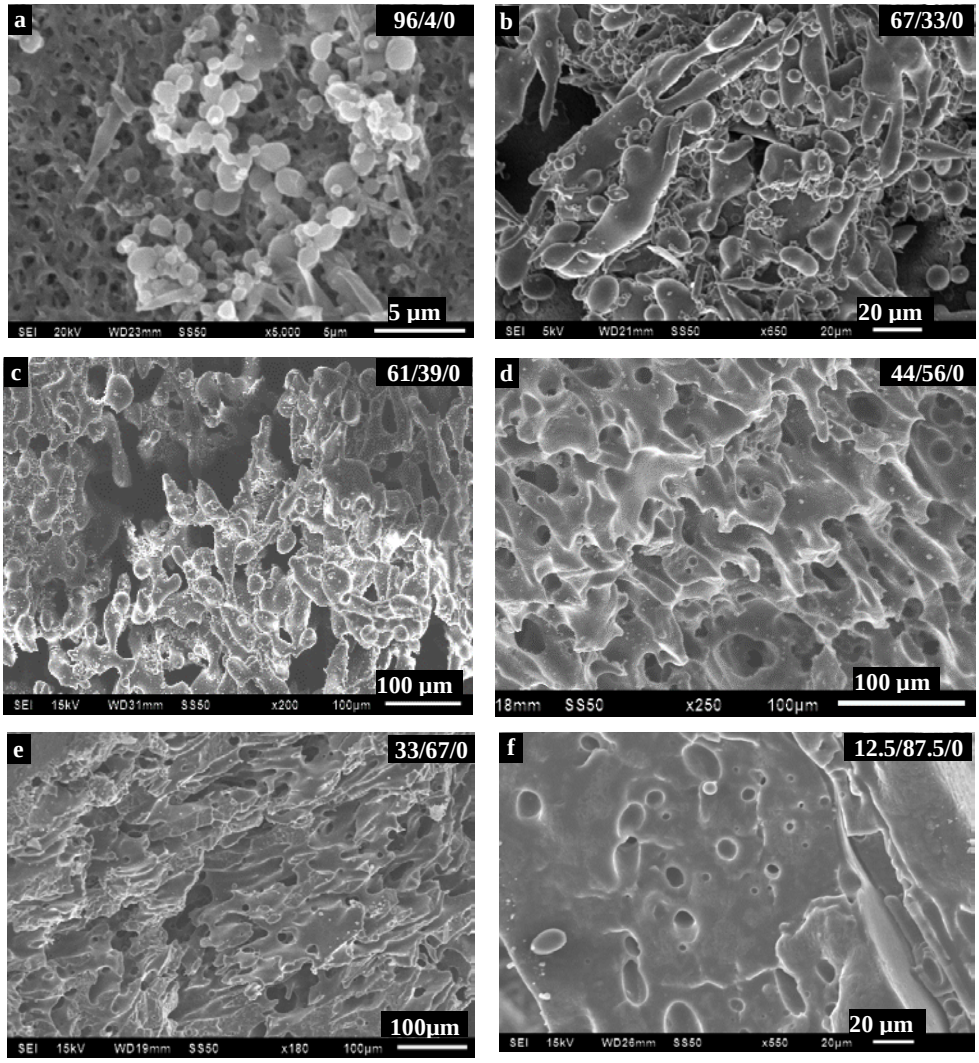

Figure 2-1 SEM images of particle-free samples with the PIB/PEO/fused silica particles ratios listed at the top right of each image. The corresponding compositions are indicated along the bottom edge of the triangular composition diagram in Figure 2-2.

2.4.2 Effects of PEO:PIB ratio at 10vol% particle loading

Figure 2-2 illustrates the effect of changing the ratio of the polymer phases at a fixed particle loading of 10 vol%. These compositions complement those of Figure 2-1. Indeed, most of

the blends of Figure 2-2 were prepared by adding particles to the blends of Figure 2-1, and hence represent – quite literally – the effect of adding particles to the blends of Figure 2-1. We will consider each of these in turn.

Figure 2-2a corresponds to a regime of composition space where the PEO volume fraction (3%) is much less than the particle fraction (10%). Despite the superficial resemblance of Figure 2-2a and Figure 2-1a, these two morphologies are completely different. In Figure 2-1a, the round particles visible are the solidified PEO drops, whereas in Figure 2-2a, a majority of the round particles are silica. The inset to Figure 2-2a shows a higher magnification view of the sample, and the same inset has been reproduced in the Appendix Figure A-6, in a magnified form for clarity. It is clear from these images that the particles are not separated from each other but bound to each other by PEO. As mentioned in the Introduction, such a morphology resembles that of a sandcastle where water menisci bind together grains of sand. The literature on wet granular materials [88] makes a distinction between a "pendular" morphology (where each meniscus is hour-glass shaped and binds two particles), and a "funicular" morphology (where a single meniscus binds together multiple particles). Figure 2-2a suggests a funicular morphology although occasional pair-wise contacts are evident. It is noteworthy that such a morphology has no analog in particle-free polymer blends nor in filled polymers (where particles are dispersed into a single homopolymer). Such a morphology appears only when particles and a small amount of the preferentially-wetting polymer are both dispersed together.

At all the other compositions in Figure 2-2, the PEO fraction greatly exceeds the particle fraction. Since the PEO is completely wetting towards the particles, when it is in large excess, it completely engulfs the particles and hence a silica + PEO combined phase is formed. The changes in morphology with composition are now qualitatively similar to those in Figure 2-1, although

there are some differences. Figure 2-2b consists of a highly elongated dispersed phase, which resembles Figure 2-1b, but with a modest increase in the size of the dispersed phase. Figure 2-2c also resembles Figure 2-1c, however, there is now a significant increase in the size scale of the morphology, i.e. particles induce coarsening, at least at 10% loading. Indeed we have noted previously that addition of particles can sometime accelerate drop coalescence in polymer blends [89, 90] an effect that may be analogous to the "bridging-dewetting" mechanism known in the aqueous foams literature [89].

At even higher PEO loadings (Figure 2-2d and e, and f) there are no changes in phase continuity as compared to the particle-free samples. Some changes in the degree of orientation are apparent, yet, we note that the samples were prepared by batch compounding (not by extrusion) and hence apparent differences orientation may not be significant since different portions of the sample may have different levels of orientation.

It is noteworthy that in all these blends, particles are present in the PEO phase which is thermodynamically preferred. This includes blends such as Figure 2-2b&c where, both before and after addition of particles, PEO is the dispersed phase. In such blends, since particles are added to a well-dispersed PEO-in-PIB morphology, the particles first encounter the PIB; they must cross the interface to enter into the PEO phase. Unlike observations such as Dil and Favis [91] and Gubbels et al. [92], such interphase migration appears to be quite fast.

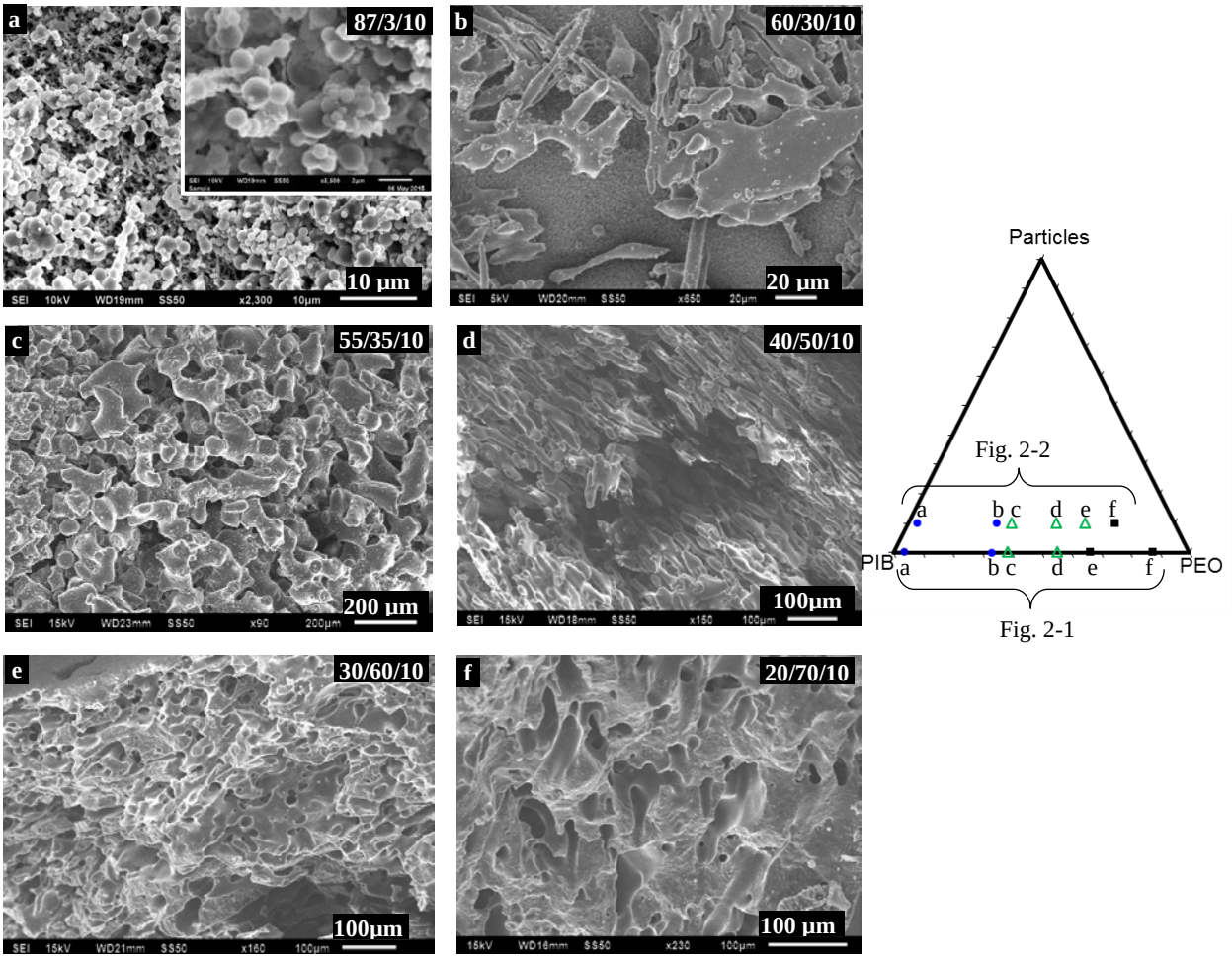

Figure 2-2 SEM images of samples with 10vol% particles. The PIB/PEO/particle ratios are listed at the top right of each image. The triangular composition diagram right shows the compositions of the samples in Figure 2-1 and Figure 2-2.

2.4.3 Capillary Aggregates

The compositions of Figure 2-2 were selected to parallel those in Figure 2-1. However, Figure 2-2 skipped over one interesting range of compositions, viz. that between Figure 2-2a $(\phi_p \gg \phi_{PEO})$ and Figure 2-2b $(\phi_p \ll \phi_{PEO})$. That composition range, when $(\phi_p \approx \phi_{PEO})$, is the

topic of this section. Since the discussion in this section revolves around the PEO loading relative to the particles, it is useful to define the parameter ϱ as [11, 93].

$$\varrho = \frac{\phi_{PEO}}{\phi_p} \tag{2-1}$$

The values of ϱ for all the samples are included in Appendix Table 1. Clearly when $\varrho \ll 1$, one expects a pendular/funicular morphology, since the PEO seeks to wet the particles, but there is not sufficient PEO to engulf them completely. On the other hand, at larger values of ϱ, there is sufficient wetting PEO to engulf the particles, and hence a combined particles + PEO phase is formed. This combined phase has an internal particle filling fraction of

$$\phi_p^{combined} = \frac{\phi_p}{\phi_p + \phi_{PEO}} = \frac{1}{1 + \varrho} \tag{2-2}$$

It is clear then that when ϱ is slightly lower than 1, the combined phase is highly filled. For instance, at $\varrho = 0.75$, $\phi_p^{combined} = 0.57$, a filling level that is nearly impossible to blend homogeneously if PEO and particles were to be mixed together by melt blending. At such high filling fractions, the combined phase is internally jammed, i.e. its rheology is expected to resemble that of a paste (e.g. possessing a high yield stress) rather than a molten polymer (e.g. being viscous or viscoelastic). To validate this idea directly, we examined the rheological properties of the combined particles + PEO phase extracted from three blends with ϱ values of 2.5, 1.45, and 1.25. These measurements, detailed in the Appendix Figure A-7 and the discussion on the same page, show that the samples transition from having a liquid-like rheology to solid-like rheology as ϱ decreases. Indeed, we also attempted (see Appendix A) rheological measurements on the combined phases extracted from a sample with ϱ = 1. Even at 95 ºC (far exceeding the melting point of PEO), this sample had a crumbly consistency indicative of strongly solid-like behavior

and could not be compression molded for rheometry. In a recent study on small molecule analogs to the present blends, we showed that such solid-like behavior greatly affects the morphology [20]: the dispersed phase takes on the form of irregular "lumps" which cannot be broken under mixing conditions. To our knowledge, this region of composition space - where particle loading is close to the wetting polymer loading - has not been explored in thermoplastic blends, and we do so here.

The effect of ϱ can be illustrated most clearly, by comparing blends with three different values of ϱ (Figure 2-3). At ϱ much lower than 1 (e.g. Figure 2-3a has ϱ = 0:16), there is insufficient PEO to engulf the particles completely, and the particles are bound together by the small menisci of PEO. Figure 2-3a suggests that some PEO menisci are pendular (i.e. each meniscus bonds exactly two particles) whereas most are funicular (several particles are held together by a single shared meniscus). Regardless, the morphology is broadly similar to that in Figure 2-2a.

Figure 2-3e corresponds to a relatively large value of ϱ = 2, and hence $\phi_p \ll \phi_{PEO}$. At this composition, there is sufficient PEO to engulf all the particles. Furthermore, the combined phase has $\phi_p^{combined} = 0.33$, i.e. the combined phase is (in a rheological sense not very concentrated with particles. Accordingly, we expect this combined phase to have liquid-like rheology. Indeed, the corresponding morphology (Figure 2-3e), which consists of a smooth (and mostly round) dispersed phase, confirms that the dispersed phase behaves like "normal" liquid drops. This was dubbed a "particles-in-drops" microstructure in the Introduction.

Figure 2-3c corresponds to an intermediate value, $\varrho = 0.6$. At this loading, there is barely sufficient PEO to engulf all the particles. Indeed, if the particles were fully engulfed and homogeneously distributed in the PEO, then the combined phase would have $\phi_p^{combined} = 0.625$. This value far exceeds the highest value of 0.44 examined rheologically in Appendix Figure A-7, but it even exceeds the value of 0.5, a value at which the combined phase was too crumbly to be

molded. At this extremely high value of particle loading, one may therefore expect the combined phase to be highly solid-like. Indeed, the appearance of the dispersed phase in Figure 2-3c is quite different from Figure 2-3e: the interface in Figure 2-3c appears irregular due to protruding particles and furthermore, the dispersed phase is highly non-spherical. Previous research on oil/water systems [12, 94, 95] suggests that the non-spherical shapes appear because the highly concentrated dispersed phase has a yield stress, and the interfacial tension forces are not sufficient to enforce spherical shaped aggregates. Thus, the aggregates retain whatever shapes they achieved during the mixing process. Following the literature on wet granular materials [88], such aggregates were dubbed "capillary aggregates" [12]. It is noteworthy that the dispersed phase size in Figure 2-3c is much smaller than in Figure 2-3e. We believe that this is because capillary aggregates do not coalesce readily, both due to their high yield stress, and because the protruding particles hinder contact of the molten PEO that is on the interior of the aggregates [12]. In contrast, the dispersed phase in Figure 2-3e can undergo coalescence like "normal" liquid drops thus resulting in a larger size.

Figure 2-3b, d, and e in the right column of Figure 2-3 show samples with roughly the same ϱ values as in the left column, but with a higher total dispersed phase fraction, i.e. going from left to right, the particle loading and PEO loading are increased simultaneously. Since ϱ is held nearly constant, the composition (and hence rheology) of the combined phase is almost identical in the left and right columns of Figure 2-3. However, the much larger amount of combined phase raises the possibility that the dispersed phase may percolate throughout the sample. Indeed, the samples of Figure 2-3d and Figure 2-3f, remain intact upon immersion into octane, i.e. at these ϱ values, the increase in dispersed phase loading (as compared to Figure 2-3c and Figure 2-3e) was indeed able to induce percolation of the combined PEO + particles phase. In contrast, the sample of Figure

2-3b was found to disintegrate when immersed in octane, i.e. the PEO and particles - even at a particle loading of 30% - are not able to create a percolating network. In analogous small molecule mixtures, we and others have noted percolation under similar compositions [93, 96], which is useful for fabrication of porous materials by removal of the less-wetting phase [1]. We speculate that the lack of percolation in Figure 2-3b is because the much higher viscous stresses in the current thermoplastic polymeric system disrupt the formation of a large-scale network. This point will be reiterated in Section 2.4.6.

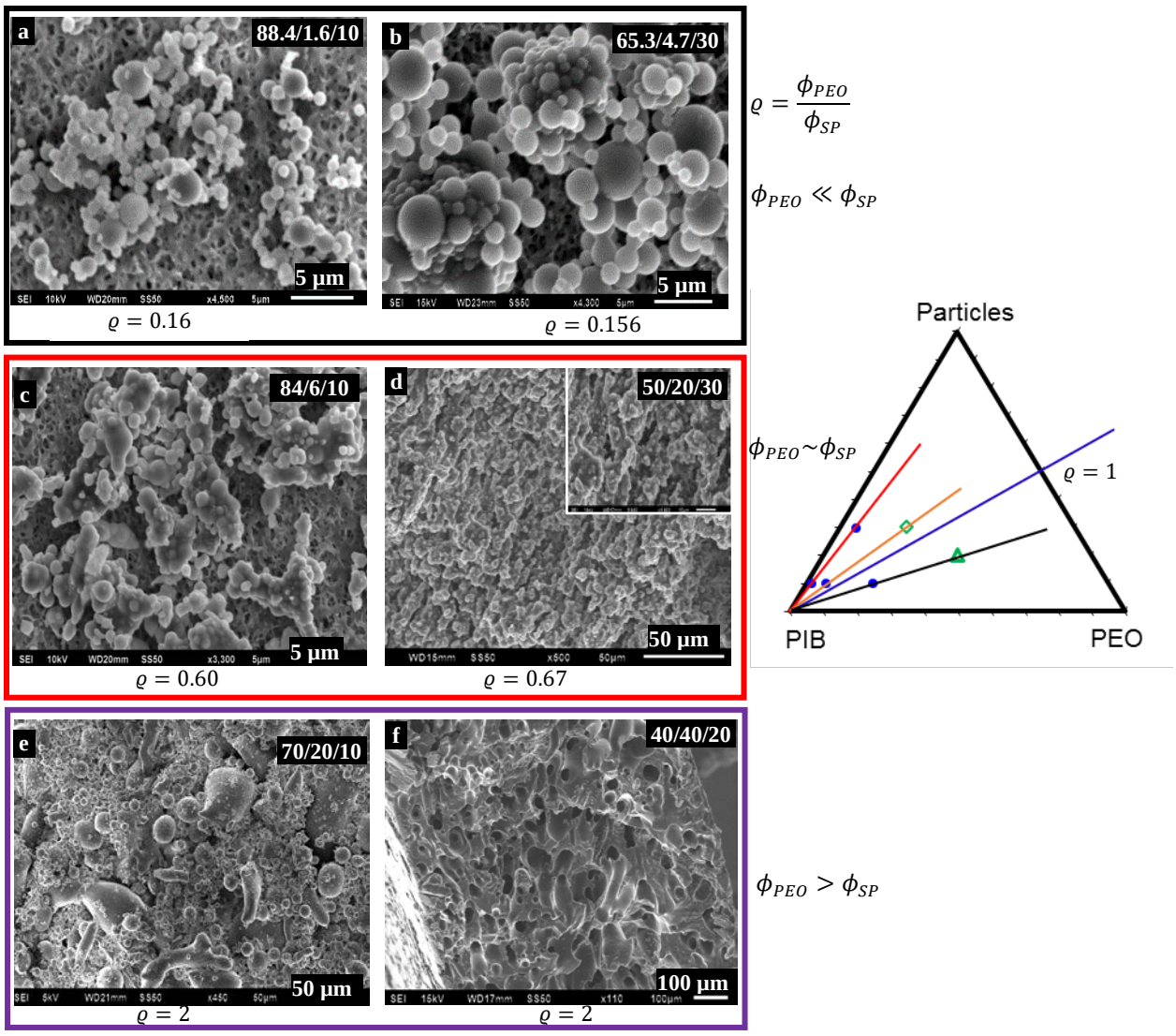

Figure 2-3 SEM images of samples which each pair of images in each horizontal row has roughly similar ϱ value. The PIB/PEO/particle ratios are listed at listed at the top right of each image.

2.4.4 Effects of Particle loading

Figure 2-2 discussed the morphological changes when the ratio of the two polymers was changed at a fixed particle loading of 10%. At this relatively low loading, particles significantly affect the morphology (as compared to Figure 2-1) only when the PEO loading is less than the

particle loading. In contrast, at $\phi_{PEO} > \phi_p$, particle effects were modest. What happens at much higher particle loadings is the concern of this section. Figure 2-4 examines a much higher particle loading of 30%. Even at this far higher particle loading however, the qualitative changes in morphology resemble those in Figure 2-2: pendular/funicular aggregates a low PEO loading, followed by capillary aggregates, and phase inversion into a PEO-continuous structure. One notable difference is in the nature of phase inversion which will be discussed in Section2.4.5.

It is more illuminating to examine the effects of increasing particle loading along composition trajectories at a fixed ratio of the two phases. Accordingly, Figure 2-5 follows four composition trajectories at PEO:PIB ratios of 22:78, 44:56, 50:50, and 88:12. Since the ratio of the phases is kept fixed, increasing particle loading has two inevitable consequences: increasing the volume fraction of the (PEO + particle) combined phase, and (at sufficiently high particle loadings) endowing the combined phase with a yield stress.

At the ratio of 22:78, the particle-free morphology is PIB continuous with round PEO drops (Figure 2-5c). With increasing particle loading, the size of the combined phase first increases (Figure 2-5b), and then the combined phase percolates (Figure 2-5a). Since the PIB remains continuous, at this highest particle loading, both phases percolate (see next section).

For the sequence of images at PEO:PIB ratios of 44:56, the most visible effect is on phase continuity: in the absence of particles (Figure 2-5f&i), the PEO is highly non-spherical and cocontinuous, however Figure 2-5f is on the verge of losing continuity (next section). At higher particle loadings, the cocontinuity appears much better developed and PEO and particles form a continuous phase which percolates throughout the sample. The samples at the PEO:PIB ratio of 50:50 also appear cocontinuous visually (this is verified in the next section).

Finally, at the PEO:PIB ratio of 87.5:12.5, PEO + particle phase is continuous, whereas the PIB phase is dispersed. The only apparent effect of particles is a decrease in PIB drop size in Figure 2-5j as compared to Figure 2-5k.

To summarize, the qualitative changes in morphology are similar at relatively high (30%) loading as at low (10%) loading. In both cases, particles induce large qualitative changes when the PEO content is small but have only modest effects when the PEO content is large. Particles generally increase drop size, but the results at high PEO loading are not entirely consistent with this.

2.4.5 Co-continuity, Percolation and Phase Inversion

We have already alluded to changes in phase continuity in the previous sections. Here we will examine phase continuity for all the samples comprehensively. The phase inversion composition has received much attention in the polymer blend community. Various methods including image analysis, solvent extraction, electrical conductivity measurements and rheological measurement have been considered for judging the phase continuity of polymer blends [97, 98]. Here we use a combination of image analysis and solvent extraction using octane to judge phase continuity. Samples that fragmented in octane were immediately deemed as having PIB as the only continuous phase. Samples that remained intact in octane or broke into no more than two or three large fragments, were further quantified as follows. The intact samples were withdrawn from octane, dried, and weighed. The fraction of PIB extracted, f, was calculated as

$$f = \frac{m_{PIB,o} - m_{PIB,f}}{m_{PIB,o}} \tag{2-3}$$

$m_{PIB,o}$ is the mass of PIB originally present in the sample and $m_{PIB,f}$ is the mass of PIB still remaining in the sample after extraction. In fact, these two quantities are not measured separately; instead, the numerator (the change in mass after octane extraction) is measured directly, whereas the denominator is estimated from the known sample composition. Thus $f = 1$ corresponds to extracting all the PIB (implying that the PIB is continuous throughout the sample), whereas $f = 0$ implies that the PIB is entirely trapped within the PEO matrix. In practice, the f values were either in the vicinity of 1 or below 0.6. We occasionally obtained f values somewhat exceeding 1 suggesting that some portion of the PEO may also have been extracted.

The samples were then classified into one of four categories using the following criteria. PIB-continuous (filled blue circles): The samples disintegrated when immersed in octane.

PEO-continuous (filled black squares): The samples remained intact in octane, but the fraction of PIB extracted, f, was less than 0.9.

Cocontinuous (hollow green triangles): The samples remained nearly intact in octane, the fraction of PIB extracted, f, exceeded 0.9, and the interface appeared smooth.

Capillary aggregate network (hollow green diamonds): The samples remained intact in octane, the fraction of PIB extracted, f, exceeded 0.9, and the interface appeared rough with particles protruding out.

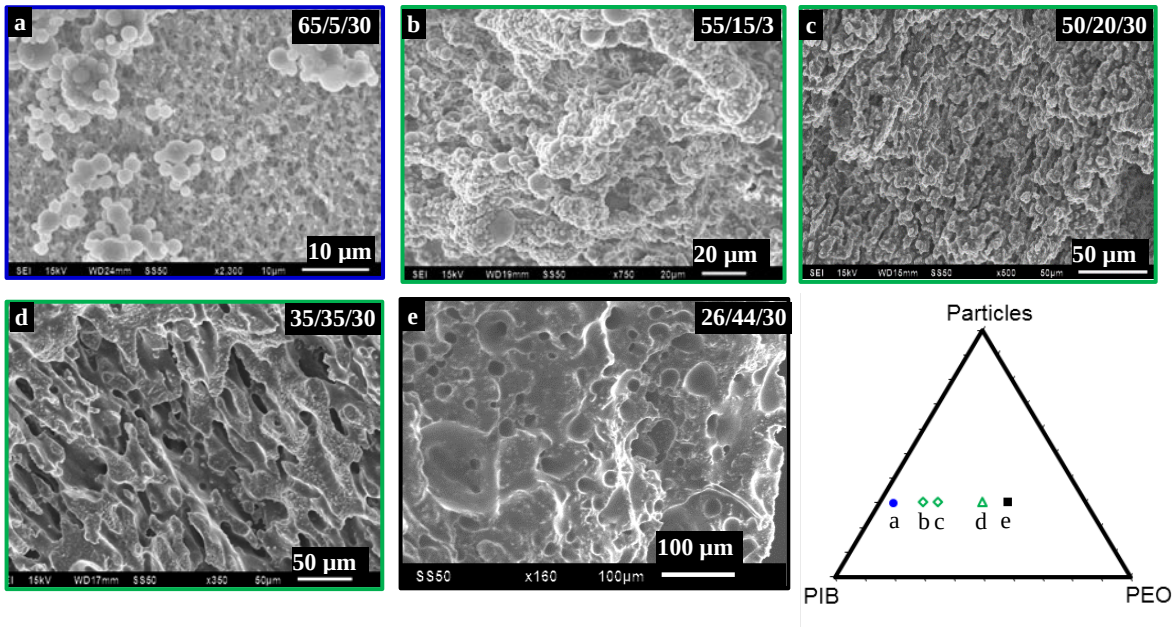

Figure 2-4 SEM images of samples with 30 vol% silica. The PIB/PEO/particle ratios are listed at the top right of each image.

We note that some points in Figure 2-6 that are classified as cocontinuous were on the verge of losing continuity; they fragmented into 2-3 large pieces when immersed in octane. These samples are circled in red in Figure 2-6. A comparison of a sample that is on the verge of losing continuity vs those that are "firmly" in the cocontinuous region is shown in Appendix Figure A-8.

It must be emphasized that the "cocontinuous" and the "capillary aggregate network" both have two percolating phases. However, the ones classified as capillary aggregates networks do not visually resemble the cocontiunuous morphologies common in the polymer blends literature, and indeed they may be stabilized by different mechanisms. Specifically, we pointed out [93] that in analogous small-molecule systems, interfacial tension plays a destabilizing role in cocontinous morphologies, i.e. induces coarsening or breakdown into a dispersed phase microstructure. In contrast, capillary aggregate networks are either unaffected by interfacial tension, or (if the liquid-

liquid interface is concave) may even be stabilized by interfacial tension. Indeed Appendix Figure A-9 shows that a cocontinuous sample coarsened when held molten at a high temperature for a long time whereas a capillary aggregate network did not show any changes/breakdown.

Examining Figure 2-6, it appears that up to 20% particles, the regime of cocontinuity expands due to the addition of particles. More specifically, it is possible to retain continuity of PIB even when it is in a minority (e.g. the sample with a PIB:PEO:silica composition of 30:50:20 is cocontinuous even at 30% PIB). This trend of widening the range of cocontinuity is even more obvious if we exclude the red-circled points in Figure 2-6 in which the PEO + particle phase is not robust enough to stay completely intact. However, the “right” edge of bicontinuity appears non-monotonic, i.e. at 30% particles, more PIB is needed to retain PIB phase continuity than at 20% particles. The reasons for this are not clear. We note that at high particle loadings, the combined phase is expected to have solid-like rheology. The difficulty of dispersing such a solid-like phase may be the reason why the combined phase tends to retain continuity.

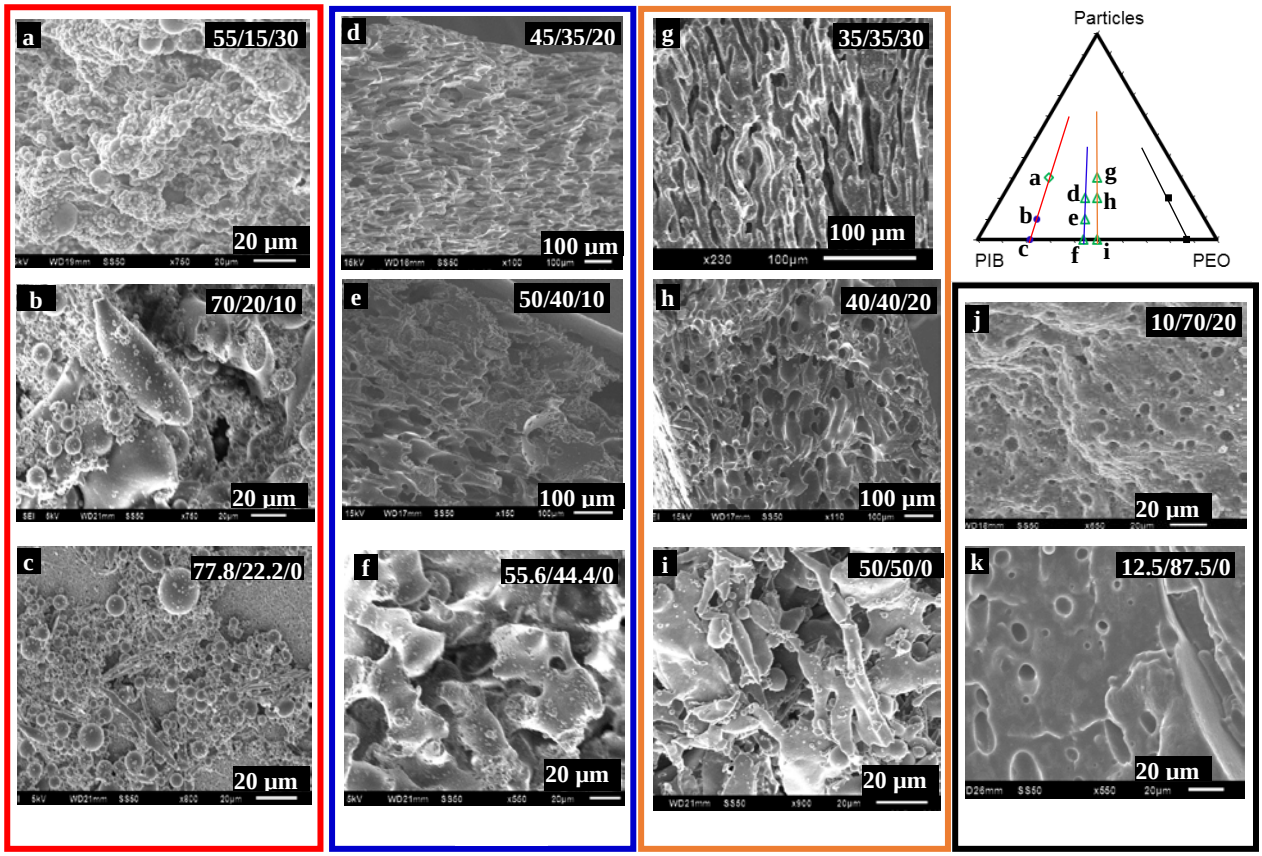

Figure 2-5 SEM images showing effects of particle loading at various fixed volume ratios of the two polymers listed along the bottom of each column. The PIB/PEO/particle ratios are listed at the top right of each image. The top right shows the ternary composition diagram with four lines indicating the four volume ratios corresponding to each column of images.

We sought to develop a simple model to capture changes in phase continuity with particle loading. The essential idea is that since $\phi_{PEO} > \phi_p$ near phase inversion, there is sufficient PEO to entirely engulf the particles. Thus, as a first approximation, near phase inversion, the three-phase blend may be treated as an "effectively" two-phase blend of PIB and the combined phase of PEO + particles. In this picture, the particles affect phase inversion in two ways: they increase the volume of the combined phase, and also the viscosity of the combined phase. One may then apply

the well-known Paul and Barlow criterion [36] (which accounts for the volume and viscosity of the phases), and derive a criterion for how particle loading affects the phase inversion composition. This approach is illustrated in the Appendix A and it predicts that particles should increase the PEO:PIB ratio needed for phase inversion. However, the observed shifts in phase continuity do not agree with this prediction even qualitatively (see Appendix Figure A-10 for a direct comparison). Thus, we conclude that treating the ternary mixture as an "effectively binary" mixture is unsuccessful; the effects of fully-wetting particles are more complex than simply increasing the volume fraction and viscosity of the combined phase.

Finally, we note that the sequence of morphologies involved in phase inversion is quite different at low vs high particle fraction. Phase inversion is, by definition, a transition from a morphology in which PIB is the only continuous phase to one in which PEO is the only continuous phase. At low particle loading (lower three schematics in Figure 2-6) phase inversion involves transitioning from a particles-in-drops morphology (PIB-continuous) to cocontinuous, and finally, to the drops-in-suspension morphology (PEO-continuous). Qualitatively at least, the morphologies on the two sides of phase inversion are symmetric; both consist of roughly spherical drops of one phase in the other. This symmetry is lost at high particle loading because the particles-in-drops morphology does not exist. Instead the pendular/funicular aggregates are the only morphology that is PIB-continuous. Thus, phase inversion proceeds as per the upper four schematics in Figure 2-6: from pendular/funicular aggregates (PIB-continuous), followed by capillary aggregate network and cocontinuous (both of which have two percolating phases), and finally to drops-in-suspension (PEO-continuous). Indeed, at even higher particle loading, we speculate that the cocontinuous morphology may disappear as well; capillary aggregate networks will directly invert into the PEO-continuous structure.

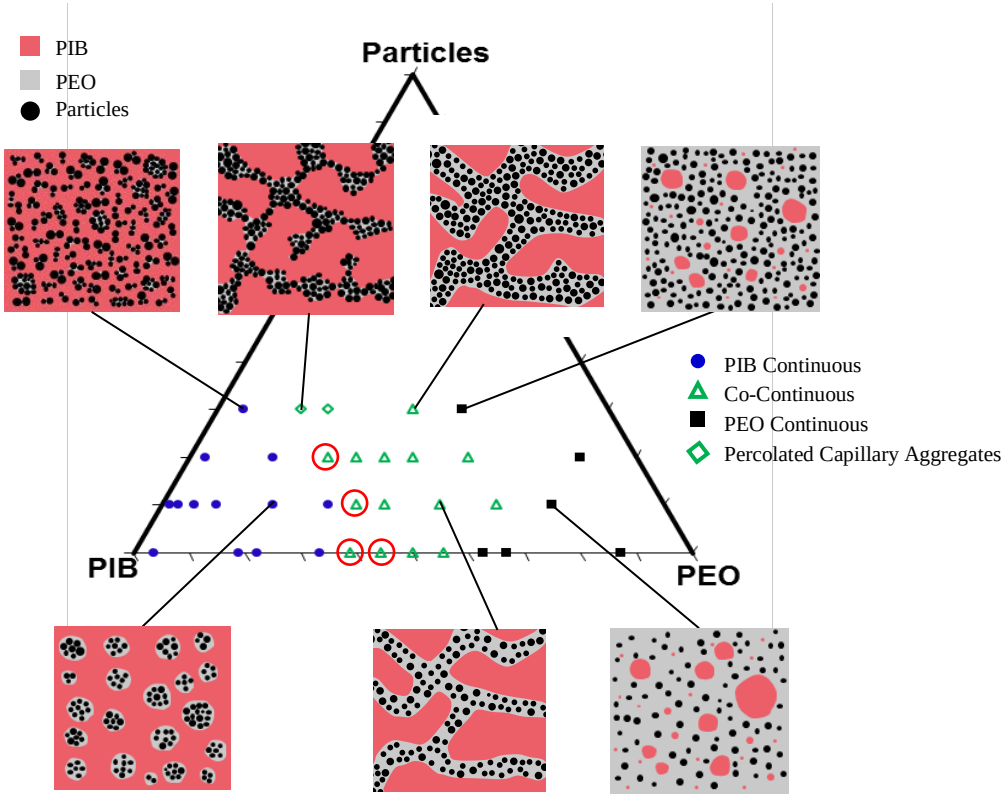

Figure 2-6 A classification of phase continuity on the ternary composition diagram. Schematic images of the four different morphologies at 30 vol% particles with particle-in-drops morphology at low particle loading are shown.

2.4.6 Difference Against Small-Molecule Mixtures

One of the goals of this research was to identify the ways in which particle-filled thermoplastic blends resemble or differ from both oil/water/particle mixtures as well as blends of immiscible polymers of very low molecular weight (and hence low viscosities). There appear to be broad similarities, and similar morphologies appear in similar regions of composition space [12, 20, 93]. Two noteworthy differences are apparent. First, in small molecule systems, it is quite easy to realize a pendular/funicular network that percolates across the entire sample [1]. Indeed in

oil/water systems, such a network can survive removal of the less-wetting phase even at a particle loading as low as 20% [99]. Here on the other hand, we were unable to create a pendular/funicular network that can survive removal of PIB, even at a particle loading of 30%. We believe that this is because, even though the particle-scale capillary interactions do bind together the particles, the high viscous stresses prevent the association of pendular aggregates into a space spanning network. A second difference is the existence of cocontinuous or fibrillar morphologies. To our knowledge, a cocontinuous morphology has never been realized in analogous oil/water/particle mixtures with fully-wetting particles. The above results show that there is a range of compositions at which cocontinuous structures appear, and the composition range for cocontinuity becomes wider upon adding particles. Our previous research on blends of very low molecular weight polymers represented an intermediate case in which the particles could stabilize a cocontinuous morphology even though the particle-free blends could not realize a cocontinuous morphology at any composition [93].

2.5 Conclusion

In summary, we have constructed a morphological map of ternary blends comprising two thermoplastic polymers and one particulate species that is fully wetted by one of the polymers. To our knowledge, the present study is the most comprehensive range of compositions to examine particle effects on the morphology of polymer blends. We show a rich diversity of morphologies, of which two are quite different from the morphologies appearing in binary polymer blends. The first is pendular aggregates in which particles are held together by menisci of the wetting polymer.

The second is capillary aggregates comprising inclusions of the wetting polymer that have extremely high particle fillings. Such capillary aggregates can also join together into percolating networks - a morphology that is distinct from conventional cocontinuous morphologies in polymer blends. Finally, a simple model that captures the two main effects of selective filling e that the particles increase the volume and the viscosity of the wetting polymer e does not capture the particle-induced changes in phase inversion composition.

Much of this research was motivated by past observations of analogous small molecule systems, often consisting of particles, oil, and water. Much of the morphology-composition diagram of filled polymer blends is remarkably similar, but with some noteworthy differences: pendular networks appear to be much more stable in small-molecule systems, whereas cocontinuous structures are altogether missing in oil/water systems. We speculate that this is due to the greater capillary forces and smaller viscous forces in oil/water mixtures.

While this chapter was purely a study of composition morphology relationships, it provides the basis for designing filled polymer blends for practical applications. For instance, applications that require a combination of good transport properties and mechanical robustness can be addressed by cocontinuous morphologies. Particles at a high loading can be employed to reinforce one phase and improve overall mechanical properties, or for instance, change the thermal or electrical conductivity of one phase using metal particles. This chapter also serves as the basis for examining more complex situations, e.g. adding plate-like or rod-like particles. If such particles can also be engulfed by one phase, they would be able to induce solid-like behavior at low particle loadings, and hence realize cocontinuous capillary aggregate networks, even at low particle loadings.

3.0 Fumed Silica Induces Co-continuity Across A Wide Composition Range in Immiscible Polymer Blends

3.1 Chapter Preface

The results of this chapter were submitted as an article: Derrick Amoabeng, Andrew J. Tempalski, Brian A. Young, Bernard P. Binks and Sachin S. Velankar, "Fumed silica induces co-continuity across a wide composition range in immiscible polymer blends" Polymer, (2019) Submitted. (listed as reference [100] in the bibliography section). Copyright © 2019 Elsevier. Figures used in this chapter have been reprinted with permission from Elsevier.

3.2 Introduction

This chapter is a continuation of our research on the microstructure and rheology of ternary mixtures composed of two immiscible molten polymers, and one solid particulate species with more complex filler structures. Previous research on such *particle-filled polymer blends* has been reviewed by Fenouillot [101], Taguet [45], Velankar [74], and Salzano de Luna [102]. Most of the previous research covered only a limited range of ternary blend compositions, and specifically, the particle loadings were usually low (under 5 vol%) as mentioned in the previous chapter. To gain a comprehensive understanding of how composition affects microstructure, we undertook investigations on relatively simple model systems that spanned wide range of compositions, including particle loadings as high as 30 vol%. Guided by the previous research, two situations

were distinguished [74]. The first was the case of *fully-wetting particles*, i.e. the particulate filler has high affinity for one of the two polymers [20, 23]. Thus, if the polymer that is preferred by the particles is present at a sufficiently large loading, it engulfs the particles completely to form a combined particle-filled phase, and for this reason, this is sometimes called *selective filling*. The second was the case of *partially-wetting particles* i.e. the particulate filler has affinity for both the polymers [103]. Thus, the particles prefer to adsorb at the interface between the two polymer phases. In both these cases, we constructed detailed composition-microstructure maps where the triangular composition diagram was divided into various regions with distinct microstructures [20, 23, 104]. A rich variety of microstructures was documented in both cases, including some that have no analogs in particle-free polymer blends. Some of that research constituted the previous chapter of this thesis.

These previous studies were conducted with the simplest type of particles – micron-sized spherical, fused silica. The particles could be regarded approximately as polydisperse hard spheres thus allowing for substantial simplification, and the corresponding morphological maps could be rationalized based on the particle wettability, capillarity (i.e. tendency to minimize interfacial area), and the rheological effects of the particles. This chapter seeks to extend that research on mapping the morphology-composition relationship, but with a more complex particle type, fumed silica. As in our previous research, we only focus on the case of *fully-wetting particles*, i.e. the fumed silica selectively fills one of the two polymers.

Fumed silica is marketed [105] for a variety of applications in polymers including rheology modifiers, anticaking agents, anti-blocking agent, reducing friction of films, and as a reinforcing filler, especially for silicone rubber [106]. Fumed silica is recognized to have a very unusual structure consisting of 15-30 nm *primary particles* that are permanently bonded into highly porous

aggregates [107]. These aggregates, which are 100-500 nm in size, are heavily branched and often regarded as fractal-like [108, 109]. An example, taken with permission from Elsevier, has been reproduced in Appendix Figure B-1. Other excellent images can be seen in a technical document [108] from the Evonik company for the Aerosil® family of fumed silicas. The permanently bonded aggregates are themselves clustered together into *agglomerates* which can be broken down under suitable mixing conditions. Appendix Figure B-2 shows an example of an agglomerate of the particles used in this research. Due to the highly porous nature of the aggregates, and the loose clustering of the agglomerates, fumed silica has a fluffy consistency, with a bulk density under 100 kg/m^3. Given this unusual structure of fumed silica, we anticipate the morphology-composition map of ternary blends containing fumed silica will deviate significantly from Figure 2-6 for the spherical fused silica case examined previously. In particular, we anticipate that when selectively-filling one phase of a polymer blend, fumed silica will strongly modify the rheology of that phase even at a low loading, and therefore strongly affect the microstructure.

3.3 Experimentation Section

3.3.1 Materials and Methods

All materials and methods are identical to those followed in our previous chapter; the sole difference is that the particles are now fumed silica, rather than the fused silica used previously. Fumed silicas are much more difficult to handle due to their extremely low density, and their ability to greatly increase the viscosity of the phase into which they are dispersed. Thus, the highest

particle loading practicable was 10 vol% - far lower than the 30 vol% in our previous research with fused silica.

3.3.1.1 Materials

Experiments used polyisobutylene (PIB BASF Oppanol B-15, $\rho \approx 0.908$ g/mL, $M_w \approx 75000$ g/mol), polyethylene oxide (PEO Dow Polyox N-10, $\rho \approx 1.1$ g/mL, $M_w \approx 10^5$ g/mol) as the two fluid phases. The dynamic oscillatory rheology of the two polymers were reported previously [23]. Under mixing conditions, the magnitude of the terminal complex viscosity of the PIB is about 10 kPa.s, whereas that of the PEO exceeds 30 kPa.s. However, at higher frequencies, the complex viscosities are nearly equal. Fumed silica particles were Wacker Silicones HDK N-20, ($\rho \approx 2.2$ g/mL). An SEM image of the particles is shown in Appendix Figure B-2. As will be shown later, in many blends, the silica particles are completely engulfed by the PEO, i.e. the silica and PEO form a combined phase. This strongly suggests that the silica particles have a strong affinity for the PEO. We believe that the reason for this affinity is that silica surfaces usually have silanol with OH groups which can hydrogen-bond with PEO: N-10 has a relative silanol content of 100%, suggesting high polarity. In contrast, PIB is much less polar than the silica and is also incapable of hydrogen bonding with silica. Indeed, in our previous research with fused silica, the particles also had similar affinity for the PEO phase.

3.3.1.2 Blend Preparation

Blends were prepared using a Brabender Electronic Plasti-Corder model EPL-V5501. It operates on the counter rotation of two roller blades, which induces strong shear forces for efficient mixing of the blends. The maximum mixer capacity with the roller blades installed is 60 mL. The

composition is specified by the three volume fractions denoted ϕ_{PIB}, ϕ_{PEO}, and ϕ_p. In all the figures, samples are labeled as x/y/z where x, y, and z are volume percentages in the order PIB/PEO/particles, i.e. $x = 100\phi_{PIB}$, $y = 100\phi_{PEO}$, and $z = 100\phi_p$. This study examines particle volume fractions, ϕ_p up to 10 vol% (roughly 20 wt%) which was the highest loading that could be blended reliably using the Plasti-Corder. The sample compositions examined are shown on a triangular composition diagram in Figure 3-1. The various sample compositions are denoted by three different symbols depending on phase continuity as explained in Section 3.3.1.3. The samples were blended in a two-step procedure. First, the mixer was first preheated to 95°C, the PIB was added, and allowed to attain the 95°C mixing temperature for 5 min. The PEO was then added in small increments while blending at 92 rpm for 5 min. A small test sample of PIB/PEO blends was taken out of the mixer for later characterization. In the second step, fumed silica was added, also in small increments, and blending continued for 5 min at same speed.

3.3.1.3 Structural Characterization

Structural characterization was performed using Scanning Electron Microscopy (SEM-ZEISS Sigma 500 VP). Prior to preparing samples for SEM, a portion of each sample was immersed in heptane. Since PIB is removed by selective dissolution in heptane for all samples, only the PEO and particles remain for SEM imaging. All samples were coated using a Pd sputtering target for 90 s at 40 mA.

Samples with high PIB content fragmented when immersed in heptane, indicating that the particles and PEO did not form a percolating phase. For samples that fragmented in heptane, the fragments were deposited onto a filter paper (Millipore, 0.1 micron pore size) and washed by dripping excess heptane onto the filter paper. Upon drying, the filter paper was stuck onto a carbon-

tape on an SEM stub. An example SEM of such a fragmented sample is in Figure 3-1a. Samples that did not fragment in heptane were first compression-molded into discs of about 0.8 mm thickness. They were then cryo-fractured under liquid nitrogen and allowed to reheat to room temperature without exposure to moisture (since PEO is water-soluble). The fractured surfaces were etched by immersing in heptane to remove the PIB. The samples were then taped to SEM stubs with the fractured surfaces facing upwards and supported with conducting copper tape. Such samples may be either PEO-continuous (the removed PIB appears as craters, e.g. Figure 3-1c) or have two continuous phases (the removed PIB appears as tortuous pores, e.g. Figure 3-1b). In summary, the images correspond to either the fragments of PEO and particles remaining when samples disintegrate in heptane, or fracture surfaces of PEO-continuous samples that do not disintegrate.

For quantitative classification of phase continuity, the same solvent-extraction procedure from our previous paper was followed [23]. The samples that fragmented in heptane were classified as PIB-continuous. The samples that did not fragment in heptane were withdrawn from heptane, dried, and weighed. The fraction of PIB extracted, f, was calculated as

$$f = \frac{m_{PIB,o} - m_{PIB,f}}{m_{PIB,o}} \tag{3-1}$$

$m_{PIB,o}$ is the mass of PIB originally present in the sample and $m_{PIB,f}$ is the mass of PIB still remaining in the sample after extraction. In fact, these two quantities are not measured separately; instead, the numerator (the change in mass after heptane extraction) is measured directly, whereas the denominator is estimated from the known sample composition. Thus, $f = 0$ implies that the PIB is entirely trapped within the PEO matrix, i.e. PEO is the only continuous phase. In contrast, $f = 1$ implies that all the PIB can be extracted while leaving the rest of the

sample intact, i.e. the sample has two continuous phases. In practice, the f values were either in the vicinity of 1 or below 0.6.

The samples were then classified into one of three categories using the following criteria, and shown as corresponding symbols in Figure 3-1 and Appendix Figure B-3:

PIB-continuous (filled orange circles): The samples disintegrated when immersed in heptane.

PEO-continuous (filled black squares): The samples remained intact in heptane, but the fraction of PIB extracted, f, was less than 0.9.

Cocontinuous (hollow green triangles): The samples remained nearly intact in heptane, the fraction of PIB extracted, f, exceeded 0.9, and the interface appeared rough/smooth.

3.4 Results

All the blends were prepared and characterized by SEM with all the images represented on a full composition-morphology diagram shown in Appendix Figure B-3. The blends span the entire composition diagram at fixed 10 vol% particle loading. Additional samples with lower particle loading were also prepared; these had PIB:PEO ratios near either 60:30 or 30:60. Consistent with our previous research on this topic, the composition-morphology relationship is mapped onto a triangular composition diagram. Due to the large number of samples, it is difficult to discuss all the diverse morphological changes across composition space at once. Instead, we will first consider the subset of samples that vary the effect of particles at roughly constant ratio of the two liquid

phases (Section 3.4.1). Section 3.4.2 then examines the subset of samples that vary the liquid phase ratio at fixed particle volume fraction of 10%.

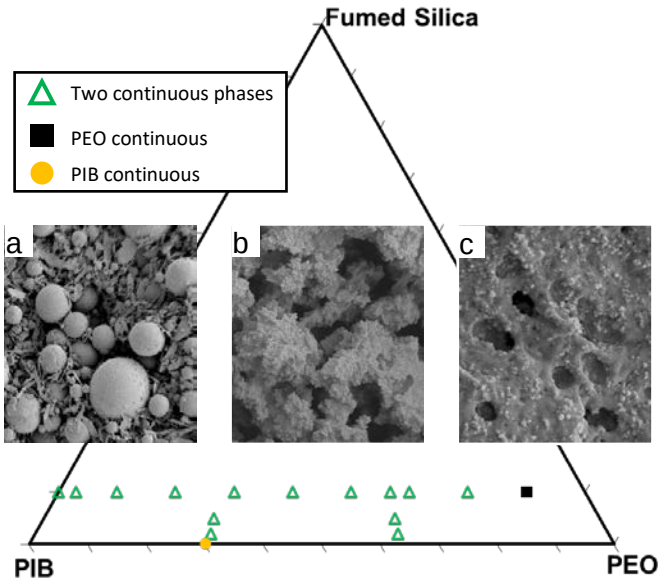

Figure 3-1 Compositions of the particle-containing samples examined in this work represented on a triangular composition diagram. The different symbols have different phase continuity as indicated. Examples of SEM images when (a) PIB is the only continuous phase, (b) both phases are continuous, and (c) PEO is the only continuous phase. Note that only one sample has PEO as the only continuous phase, and only one sample has PIB as the only continuous phase.

3.4.1 Effects of Particle loading at a Fixed PEO:PIB ratio

Previously [23], we had found that in the absence of particles, phase inversion occurs at a PIB:PEO ratio of 61:39. With higher PIB than this, PEO becomes the dispersed phase (i.e. a sample disintegrates upon immersion in heptane), whereas with higher PEO, PIB becomes the dispersed

phase (i. e. the sample remains intact in heptane). There is also a small range of cocontinuty in the vicinity of this composition.

Figure 3-2 illustrates the effects of changing the loading of particles up to 10 vol% at an approximately fixed PEO:PIB ratio. The particle-containing samples Figure 3-2b-e all appear in Appendix Figure B-3, although they are lettered differently, eg. Figure 3-2b corresponds to Appendix Figure B-3a.

Figure 3-2a corresponds to the 67/33/0 sample, i.e. particle-free blend with PEO volume fraction of 33 vol%, in which the PEO forms the dispersed phase. The PEO drops smaller than roughly 10 microns appear almost perfectly round, whereas there are some larger highly non-spherical structures as well. The latter appear to be large, coalesced drops that did not recover spherical shape before being cooled. With addition of very small amount of fumed silica (0.2 vol%, Figure 3-2b), PEO remains the dispersed phase, but with a decrease in average drop size. More specifically, large non-spherical shapes do not appear at all in Figure 3-2b. With increase in fumed silica loading to 2 vol%, there is a drastic change in morphology: the PEO formed a continuous phase with the particles engulfed in the PEO phase. At this loading, the morphology shows a cocontinuous structure: the phase that remains visible in Figure 3-2c is a combined (PEO+particles) phase, whereas the tortuous void spaces correspond to the PIB phase which has been removed. At high magnification, it is clear that the surface of the PEO+particle phase is not entirely smooth. This is a common feature in many blends and will be discussed later.

A further increase in the fumed silica loading to 5 vol% (Figure 3-2d) and 10% (Figure 3-2e) caused a further shift in the morphology (Figure 3-2d). The PEO+particle phase now appears in the form of “nodules” that remain percolating. There is a sharp decrease in size-scale of the

morphology in going from 2 % to 10 % loading (note that the scalebar in Figure 3-2e is much smaller than in the other images).

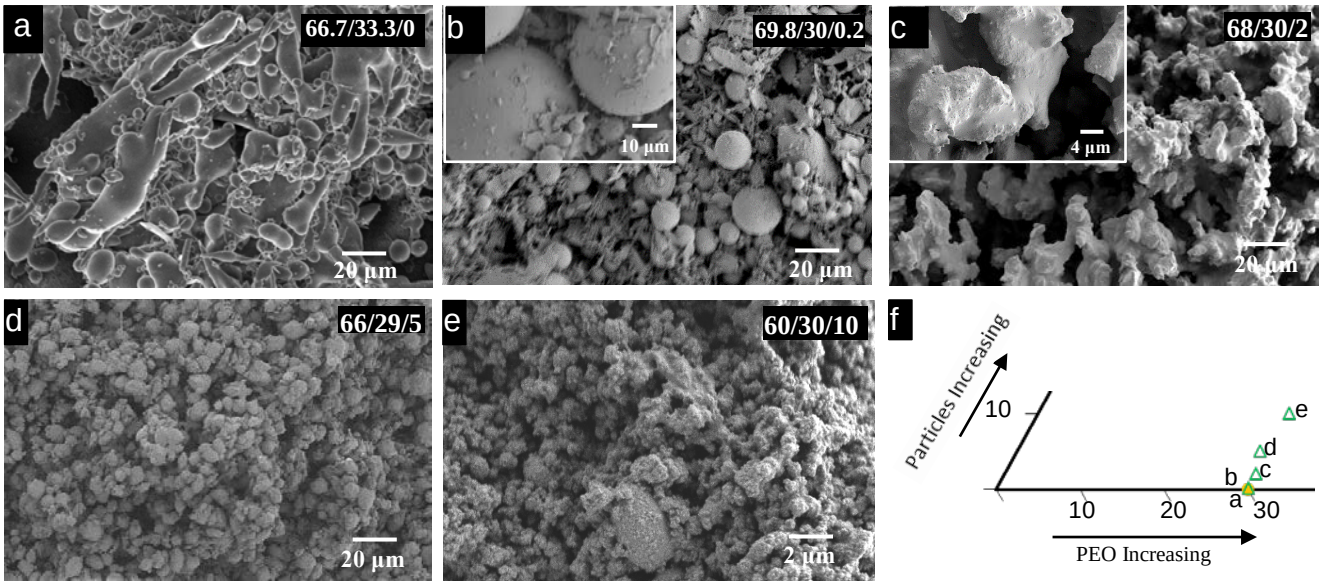

Figure 3-2 SEM images of particle-free and particle containing samples showing effects of particles on microstructure of fixed PEO:PIB ratio at low PEO content. The PIB/PEO/fumed silica ratios are listed at the top right of each image

Similar to Figure 3-2, Figure 3-3 explores the effects of particle loading, but when PEO is in a majority. All the samples in Figure 3-3 show cocontinuous morphologies, i.e. both phases percolate. Figure 3-3a corresponds to the 37.5/62.5/0 sample, which has a typical size-scale of about 30 micron. Adding 2 vol% or 5 vol% fumed silica does not change the cocontinuous morphology qualitatively, however, the size-scale decreases sharply. With a further increase in fumed silica loading to 10 vol%, while both phases still percolate, there is a qualitative change in the appearance. The PEO+particle phase now appears in the form of “nodules” that remained

percolating similar to what was observed in Figure 3-2d & Figure 3-2e. These nodules are only slightly larger than 1 micron, i.e. a much smaller size-scale as compared to Figure 3-3c.

To summarize this section, even at a loading of 2 vol%, particles strongly affect the microstructure: qualitatively, the addition of particles encourages cocontinuity, whereas quantitatively, particles greatly decrease the size-scale of the morphology.

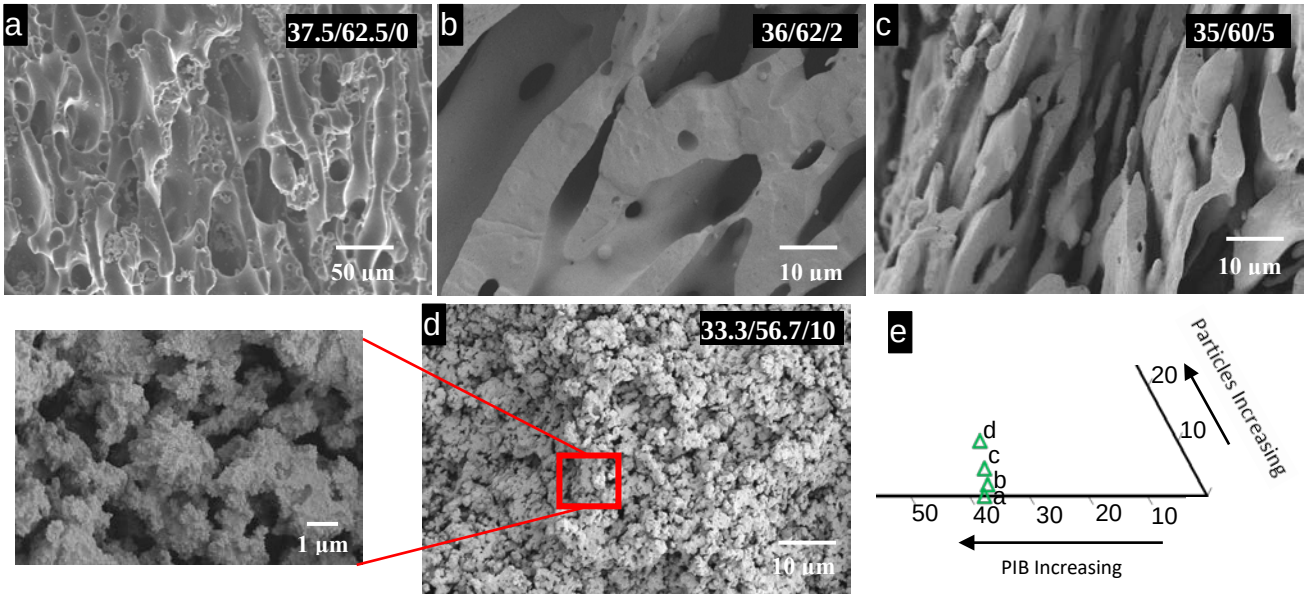

Figure 3-3 SEM images showing effects of particles on microstructure of samples where the PEO loading exceeds PIB loading. The PIB/PEO/fumed silica ratios are listed at the top right of each image Bottom right shows the samples compositions on a portion of the triangular composition diagram (full version is in Appendix Figure B-3)

3.4.2 Effects of PEO:PIB ratio at 10vol% Particle Loading

Figure 3-4 explores the varying effects of PEO:PIB ratio at constant fumed silica loading of 10 vol%. Figure 3-4a shows the microstructure of the 87/3/10 sample, i.e. 3% PEO. Remarkably,

despite the 87% PIB being removed before SEM, the remaining the PEO and the particles are adequate to maintain a monolithic sample. Fumed silica aggregates are known to be highly porous as was illustrated in Appendix Figure B-1, and since the PEO wets the particles readily, one would expect much of the PEO to be "absorbed" into the aggregates. Indeed, it is difficult to identify exactly where the PEO is located in Figure 3-4a. Nevertheless, the presence of a space-spanning (i.e. percolating) network that can survive dissolution of the PIB, and even subsequent drying suggests that at least some of the PEO must be bridging together particle aggregates. Incidentally, we note that even in the absence of PEO, 10 vol% fumed silica in PIB tends to form a network although it is very fragile. This suggests that intermolecular forces between the particles and the interlocking of particles can already form a tenuous particle network on their own even at 10% loading. Addition of a small amount of PEO appears to strengthen this network substantially so that highly porous monoliths can be prepared.

Figure 3-4b and Figure 3-4c show samples in which the PEO loading is increased substantially to values equal to, or far above, the particle loading. In the case of spherical silicas [23] (to be discussed further in Section 3.5), such a transition from $\phi_p \gg \phi_{PEO}$ to $\phi_p < \phi_{PEO}$ caused an enormous change in microstructure. In contrast, Figure 3-3b and c seem to closely resemble Figure 3-4a, at least at first glance. At much higher magnification (Appendix Figure B-4), the structure appears more heterogeneous, with increasing PEO as judged by the increasing size of the pores left behind after removing PIB. These observations suggest that even when the PEO loading significantly exceeds the silica loading, the PEO can still be accommodated within the pores in the fumed silica. While this seems surprising, previous research on the voids within fumed silica aggregates lend support to this notion. Specifically, Ehrburger and Lahaye [110] reported that in dispersion of fumed silica, the void fraction within the aggregates ranged from 80-

90%. Accordingly, voids within the fumed silica aggregates can accommodate fluid that is several times the silica volume. Thus, even at a composition of PIB/PEO/silica of 70/20/10 (Figure 3-4c), it is eminently reasonable for the silica to be absorbed into the pores.

Upon further increasing the PEO loading up to 60 vol% (Figure 3-4d and e), the increasing amount of PEO now encapsulates the fumed silica aggregates almost completely and the sample morphology appears to be a network built from irregular lumps bonded together.

Between 60% and 80% PEO, phase inversion occurs so that PEO becomes the continuous phase. In Figure 3-4f, the combined (PEO+particles) phase forms 90 vol% of the bulk, within which the PIB is dispersed as sub-micron drops. These appear as craters in Figure 3-4f, which were occupied by PIB before immersion into heptane.

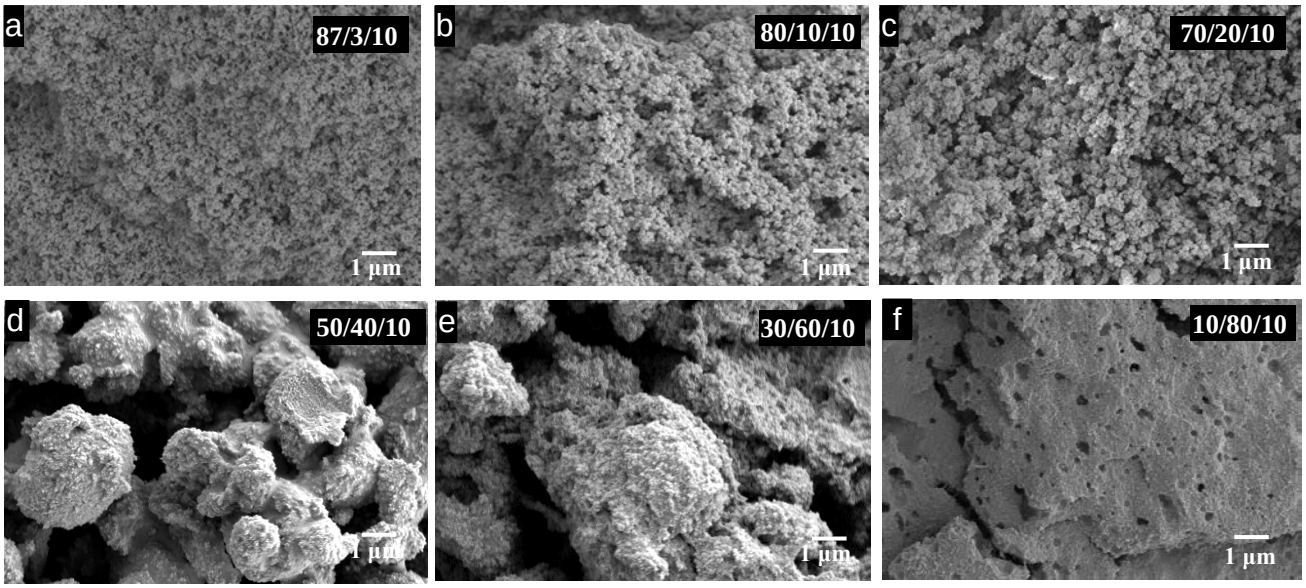

Figure 3-4 SEM images of samples with varying PEO:PIB ratio at fixed 10vol% fumed silica. The PIB/PEO/fumed silica are listed on the top right of each image. Scale: 1µm

Before proceeding, we note that the polymer blends community has conducted much research on the issue of cocontinuity [98, 111-113]. Typically, cocontinuity means that two phases are percolating such that either one of the phases can be removed almost completely while leaving the other intact. Strictly, we are not able to prove cocontinuity by this definition: since the PIB is a liquid at room temperature, it is not possible to test whether it remains intact after removal of the PEO. Nevertheless, all the compositions ranging from Figure 3-4a to Figure 3-4e have two percolating phases, and hence may be regarded as cocontinuous. This leads to the most surprising and interesting aspect of Figure 3-4, viz. at 10% fumed silica loading, morphologies with two percolating phases occupy an extremely wide region of composition space. This is in sharp contrast to the corresponding particle-free blends in which range of cocontinuity is quite narrow. In fact, previous articles had already noted that addition of fumed silica can change the phase continuity or convert a dispersed phase morphology into a cocontinuous one [114, 115]. Yet, the surprisingly wide range of polymer ratios within which both phases percolate has gone unrecognized. Discussion

In the following three sections, we will first rationalize some of the results in terms of the rheology of the (PEO+particles) phase, then construct a morphological map for blends with fumed silica, and finally compare against the fused silica case studied previously.

3.4.3 Effects of Rheology of the PEO+Particles Combined Phase

The chief goal of this section is to comment on the unusual appearance of most of the blends, more specifically that the interface between the PIB phase and the (PEO+particles) phase often appears highly rough and irregular. In particular, contrast Figure 3-2c, Figure 3-2d and Figure

3-2d, all of which have a rough interface vs. Figure 3-3a and Figure 3-3b which appear smooth. Previously we have noted a similarly rough interface with spherical particles, but only at much higher particle loadings of about 30% by volume [20, 23]. In that case we showed that such an irregular interface appears because if the (PEO+particles) combined phase has a very high particle loading (specifically $\phi_p^{combined} = \phi_p/(\phi_p + \phi_{PEO})$ is more than about 0.4) the combined phase develops solid-like rheology. We will therefore first test whether the combined phase composed of fumed silica dispersed in PEO also displays solid-like rheology, but even at a relatively low fumed silica loading. In fact, the idea that fumed silica can convert a free-flowing liquid into a solid-like paste is thoroughly well-recognized in the literature [116-118], and indeed fumed silica is marketed as a rheology modifier. Nevertheless, we seek to quantify the extent of rheological changes for the specific case here.

Rheological experiments were conducted on the (PEO+particles) combined phase that was extracted from the samples by dissolving the PIB. The details of the rheological experiments are explained in Appendix B; here we will only summarize the main points. First, molded discs of the PEO+particles combined phase could not be measured at all by conventional parallel plate rheometry if the particle loading exceeded 6 vol%. These samples made poor contact with the plates (i.e. did not conform to the plates), even when a serrated geometry was used (Appendix Figure B-5a), indicating solid-like rheology. Second, if the combined phase had a particle loading exceeding 15 vol %, it could not be molded into intact discs at all due to a crumbly consistency. Third, indentation experiments were conducted at 95^{o}C on discs of the combined phase using a cylindrical indenter. The indentation force increased steeply with particle loading. Finally, indentation experiments were conducted on a single sample at various rates. The indentation force was found to be only weakly dependent on indentation rate suggesting that (PEO+fumed silica)

blends behave approximately like a plastic material with a yield stress, rather than a Newtonian fluid. These experiments taken together strongly support the notion that the (PEO+particles) combined phase of almost all the blends studied here has a solid-like rheology.

The non-spherical shape of the combined phase and the rough nature of the interface in most of the SEM images therefore seems to have two causes, both related to the solid-like rheology. The first is that the interfacial tension between the two phases (expected to be on the order of 10 mN/m) is not adequate to induce the large-scale flow needed to force a highly irregular dispersed phase to become approximately spherical. In effect, the yield stress of the combined phase exceeds the capillary pressure associated with the large-scale curvature of the liquid/liquid interface, and hence the combined phase appears irregular on a several-micron scale. Second, the particle network is sufficiently strong to resist even small-scale reorganization on the scale of individual aggregates. Thus, the interface appears highly rough even at sub-micron length scales, and even when $\phi_{PEO} \gg \phi_p$, the particles appear to protrude through the interface (Figure 3-4e). This picture is incorporated into the morphological map constructed in the next section (Figure 3-5e and f).

3.4.4 Morphology-Composition Map

The central goal of this research was to construct a morphological map for blends in which fumed silica selectively fill one of the two phases. The SEM images support the morphological map of Figure 3-5 for the blends containing fumed silica. Note that several different colors are used to indicate primary particles belonging to different aggregates, so as to illustrate the interlocking nature of the aggregates. We will briefly discuss each of the cartoon structures

illustrated. The first critical feature to note is that due to the highly porous, fractal-like nature of the particles, the particles can be regarded at dilute only at the lowest particle loadings, e.g. 1 vol%. At such low loadings, the blends usually have a droplet-matrix microstructure analogous to polymer blends (Figure 3-5a&c), although a narrow range cocontinuity may also appear (Figure 3-5b). All the other cartoons represent 10 vol% particles, at which the particles are drawn as being heavily interlocked. At such high particle loadings, when $\phi_{PEO} < \phi_p$ (Figure 3-5d), the structure consists of aggregates that are bound together into a network by some combination of physical interlocking, intermolecular forces, and the portion of the PEO that binds two or more aggregates simultaneously (the remainder of the PEO is presumed to be absorbed "into" the aggregates). We acknowledge that this is speculative since we are unable to see such PEO in the SEM images. Indeed, we have also conducted Transmission Electron Microscopy (TEM) and even in those images (not shown), the PEO could not be identified reliably. Nevertheless, the fact that the 87/3/10 blend survives removal of the 87% PIB (whereas the 87/0/10 breaks into fragments) suggests that the PEO does bind together aggregates to at least some extent. The smallest pores that exist in such a structure are on the length-scale of the primary particles, i.e. several ten nm.

With increase in PEO loading (Figure 3-5e), the aggregates gradually become saturated with PEO and the inter-aggregate binding increases. It is critical to note that the central difference that most of the pores within the aggregates are filled with PIB in Figure 3-5d vs PEO in Figure 3-5e. When PIB is removed, the pores are no longer on the scale of the primary particles; instead, the pores are now a few hundred nm, on the scale of the aggregates.

With further increase in PEO content (Figure 3-5f), the particles are encapsulated more fully, and the pores become much larger than particles suggesting that the details of the aggregate porosity or primary particle size is not as important to the morphology. In such cases, the interface

may be smooth (Figure 3-3b) only at low particle loading. More commonly, the interface is extremely rough, and as mentioned in the previous section, this is attributable to the ability of the particles to form a strong network within the PEO phase. Although this structure fits the usual definition of a cocontinuous morphology as found in particle-free polymer blends, those morphologies invariably have a very smooth interface which coarsens with time, whereas Figure 3-3d does not. In fact, Figure 3-3d is similar to the capillary aggregate network reported previously whose signature feature is the solid-like rheology of the particle-containing phase. However, unlike in the case of spherical particles, with fumed silica, the solid-like rheology develops even at extremely low particle loadings. In fact, we speculate that even other particle shapes such as needle-like or platelet-like particles would form similar capillary aggregate networks at low particle loadings. One important difference of course is that such anisotropic particles would show a strong tendency to develop nematic order, whereas fumed silica does not.

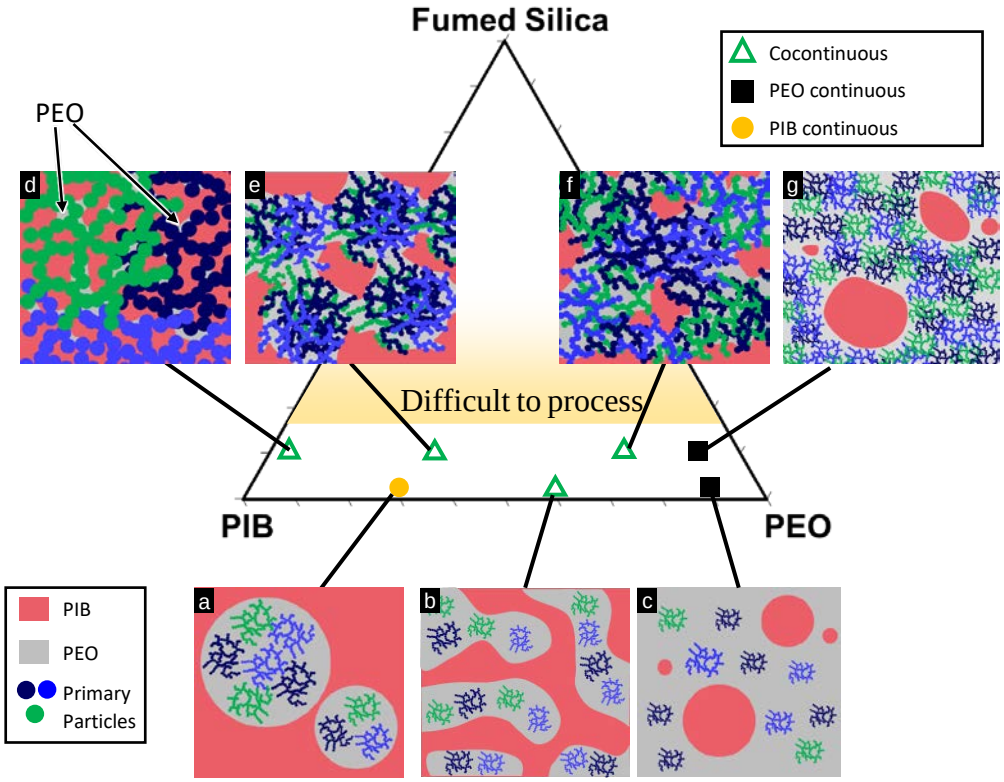

Figure 3-5 A classification of phase continuity on the ternary composition diagram. Schematic images of the four different morphologies at 10vol% particleswith particle-in-drops morphology at low particle loading are shown

Finally, at highest volume fraction of PEO (Figure 3-5g), phase inversion occurs so that PIB becomes the dispersed phase. Note again that the continuous phase remains jammed with particles and has a solid-like rheology. The size-scale of this morphology may be comparable to that of the fumed silica aggregates (e.g. Figure 3-3d), although it is certainly possible for the dispersed phase to be much bigger.

3.4.5 Differences Between Fused and Fumed Silica Particles Filled Immiscible Polymer Blends

Finally, we turn to the second goal mentioned in the Introduction: comparison of the blends with the fumed silica vs those with fused silica studied previously. We will illustrate the differences with SEM images at just two compositions. The first is the blend with a composition of 87/3/10. In the previous research with fused silica, the spherical particles were found to be clustered together by menisci of PEO that connected the particles either pairwise (pendular meniscus) or many-particle (funicular meniscus). These clusters were large, but not percolating, and hence upon dissolving the PIB, the sample disintegrated altogether. An image of the resulting particle-bound clusters collected on a filter paper is shown in Figure 3-6a. With fumed silica, a blend of the same composition has an altogether different morphology which survives intact after removal of PIB. With such highly irregular and porous particles, the concept of a pendular meniscus is no longer meaningful. The particle aggregates can accommodate PEO inside their fractal-like structure, and indeed in the SEM image, it is not possible to identify the location of the PEO at all.

As a second illustration, consider the samples with composition of 40/50/10, at which both particle types show cocontinuous morphologies. The first major difference is that the size-scale of the microstructure is about 10-fold smaller for the fumed silica. Note that the mixing process was identical, and hence the difference cannot be attributed to more intense mixing. Yet, some of the difference in size-scale may be attributed to the larger size of the fused silica particles (~2 micron) as compared with the fumed silica. The second major difference is that the interface of the (PEO+particles) phase in Figure 3-6c appears smooth, as expected for a surface between two immiscible liquids. The morphology is visually similar to cocontinuous morphologies in particle-

free polymer blends. In contrast, the interface of the (PEO+particles) phase in Figure 3-6d appears extremely rough, and the morphology appears to be network of irregular lumps bonded together into a percolating structure.

Yet, even though the morphologies at of the fused vs fumed silicas are altogether different when compared *at the same composition*, overall the type of microstructures appearing in both cases have distinct similarities. For example, droplet-matrix morphologies (with particles either inside or outside the drops) appear at low particle loading in both Appendix Figure B-3 and Figure 2-6. Capillary aggregate networks, i.e. networks built from irregular lumps of the combined phase, appear whenever the particles are sufficiently concentrated to make the filled phase solid-like – in fumed silica, this happens at a much lower particle loading. Thus, the morphology map of Figure 2-6 is somewhat similar to that of Figure 3-5, but with the difference that all the effects of particles are felt at much lower particle fractions. Indeed, the pendular structure is the only morphology from Figure 2-6 that simply cannot appear in fumed silica containing blends.

To conclude, this chapter continues our exploration of the composition-morphology relationship of particle-filled polymer blends in the case when particles selectively fill one of the two polymer phases. The experiments were conducted using blends of PIB and PEO, the latter of which is fully-wetted by the silica. The specific motivation of this chapter was to examine the effect of the nature of the particles, in particular, to examine how the effects of fractal-like fumed silica filler differs from the simpler case of spherical fused silica filler examined previously. Towards that end, this study examines the morphology of immiscible polymer blends filled with fumed silica across the widest composition range probed to date. This includes a wide range of ratios of the two polymers, and up to 10% fumed silica – the highest loading feasible in a Brabender batch mixer.

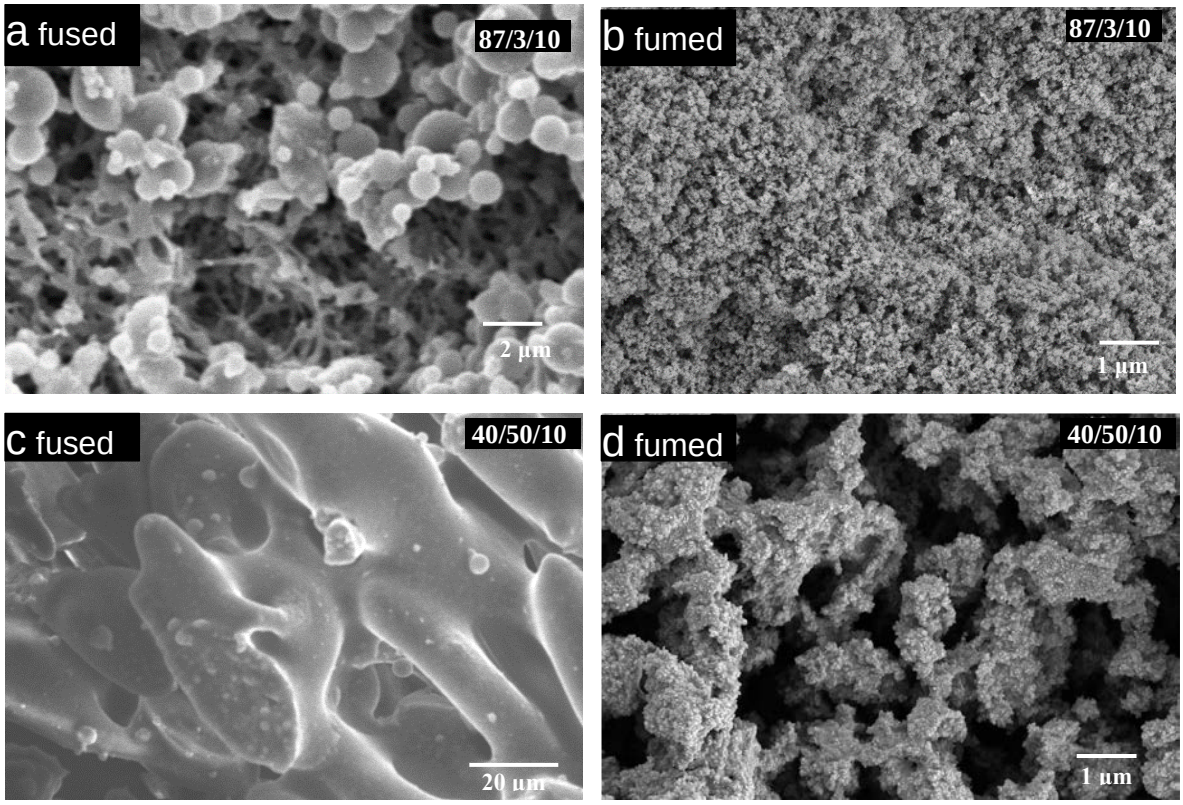

Figure 3-6 Comparison of blends containing 10vol% fused silica (left column) vs 10vol% fumed silica (right column). The PIB/PEO/silica ratios are listed at the top right of each image. a and c have the same composition, as do c and d. Figure 3-6a and c are reproduced from chapter 2.0 with copyright permission from Elsevier.

Almost all the morphologies seen here are heavily influenced by the unusual structure of fumed silica, which consists of highly porous aggregates of silica nanoparticles. Since PEO wets the silica fully, it tends to occupy the pore spaces within the particle aggregates. Accordingly, two cases may be distinguished. At low loading PEO, there is insufficient PEO to fill all the pores. Therefore, the morphology remains on the scale of the individual primary particles (few ten nm). At higher PEO loadings, once all the pore spaces are filled, the PEO engulfs all the aggregates

giving a highly-filled PEO+fumed silica phase. The morphology appears on much larger length-scales ranging from aggregates (few 100 nm) to many microns.

Overall, we conclude with two points. First and not surprising, fumed silica strongly affects the morphology at loadings as low as 2 vol% - far lower than spherical silica. Second and much more unexpected: morphologies in which two phases are percolating appear across a very wide range of PEO:PIB ratio, i.e. co-continuity appears to be a norm in polymer blends filled with fumed silica. One of these phases is always PIB, whereas the other may be a silica-filled PEO phase (high PEO loading) or a silica network held together by PEO (low PEO loadings).

4.0 Bulk Soldering: Conductive Polymer Composite Filled with Copper Particles and Solder

4.1 Chapter Preface

The results of this chapter were published as an article: Derrick Amoabeng and Sachin S. Velankar, "Bulk soldering: Conductive polymer composites filled with copper particles and solder" Journal of Colloids and Surfaces A; 553 (2018) 624-632. (listed as reference [25] in the bibliography section). Copyright © 2018 Elsevier.

In addition, during the course of this research, a review article on this topic was published as Derrick Amoabeng and Sachin S. Velankar, "A review of conductive polymer composites filled with low melting point metal alloys" Polymer Engineering & Science, 58 (2018) 1010-1019 (listed as reference [26] in the bibliography section)

4.2 Introduction

It has been long recognized that capillary forces (i.e. forces stemming from surface or interfacial tension) can greatly affect the structure of particulate systems [1, 74, 119-123]. Examples include the strength of wet granular materials which comes from particles being bound together by bridging menisci [5], "spherical agglomeration" of particles by collecting them within drops [23], particle-stabilization of foams due to strong adsorption of particles to the air/liquid interface [6-8], and the stability of "bijels" against coarsening [9]. The common feature in such

materials is that the capillary force offers a simple means of binding together particles and, hence creating some specific aggregated structure. One may then sinter this structure to make it more permanent [124-127], thus offering a processing route to new materials. The rich variety of microstructures that can be realized due to capillary phenomena in particulate materials has been reviewed recently [74, 128]. Progress on using capillary forces for developing new materials has also been reviewed [1].

Perhaps the most dramatic effect of capillary forces on the behavior of particulate materials is the change in rheological properties. In the above example of granular materials, dry sand can be poured readily, whereas wet sand can be molded into sand castles [5]. The same has been observed in particulate suspensions wherein addition of oil to a particles-in-water suspension (or vice versa) gives the suspension solid-like rheology, e.g. a yield stress [96]. Such changes in rheology have been regarded as the signature of a mechanically percolating network, i.e. capillary forces not only aggregate the particles, but the aggregates form a space-spanning network that is responsible for a very high viscosity or even a yield stress.

Just as a large-scale network can affect the viscosity, it is also plausible that other transport properties of the material might be affected. In fact, electrical conductivity is one transport property that is often strongly affected by the presence of a large-scale network. This is well-recognized in the literature [129-131] on polymers that have been rendered conductive by addition of conductive fillers such as carbon black, carbon nanotubes [132, 133], carbon nanoparticles, or graphene [134]. In that literature, it is commonly observed that high conductivity arises only when the filler loading exceeds a certain threshold (percolation threshold for electrical conductivity) beyond which the filler forms a network. Much research on conductive polymer composites has sought to reduce the percolation threshold, e.g. by using high aspect ratio fillers such as conductive fibers [135, 136].

The goal of this article is to examine the improvements in conductivity of a polymer due to addition of conductive filler particles which are bonded by capillary forces. Specifically, we use polystyrene (PS) as the low-conductivity matrix polymer, copper particles as the conductive filler, and a tin-lead solder alloy as the fluid that induces capillary forces between the copper particles. The essential physical picture can be illustrated in Figure 4-1 (Section 4.3 will provide experimental support for this picture). Figure 4-1a&b depicts the case of copper particles dispersed in PS in the absence of solder. Since the particles do not aggregate to a significant degree, a relatively high particle loading is needed to realize a percolating network. Moreover, neighboring particles make relatively poor contact with each other, and hence low conductivity is expected. This is because even a small separation between the particle surfaces, being filled with the low conductivity matrix, adversely affects conductivity [137, 138]. Figure 4-1c&d shows the effects of adding solder during the blending process. The solder, being fully-wetting towards the copper, can bridge the particles by a meniscus (Figure 4-1c&d) which can lower the percolation threshold. Crucially, the capillary forces are induced by the liquid metal alloy that is itself highly conductive, thus allowing the possibility of a fully-metallic network that spans the entire sample. This idea of bonding together metal particles by mixing them with solder is dubbed “bulk soldering” in this chapter.

Although the term “bulk soldering” is new, the idea of combining non-melting metal filler and low-melting point alloys (LMPA) to improve the conductivity of plastics has been explored to some extent. We have reviewed the broad literature on LMPA-polymer composites recently [139] and cite four papers [140-143] which melt-blend LMPA, non-melting metal filler, and polymer. The LMPA used in these articles were typically alloys of metals such as tin, lead, and bismuth, and had melting temperatures below 250 ^{o}C. The LMPA, the non-melting metal filler,

and polymer were all blended at a temperature above the LMPA melting point. This approach has two advantages: standard plastics processing equipment may be used for blending (and hence the manufacturing approach is readily scalable), and the resulting blends can have high conductivity. A somewhat different example of this approach is from Sun et al [104, 144] who used a cross-linkable epoxy matrix and silver particles that were bonded by an ionic liquid (rather than a liquid metal), although the amount of ionic liquid was only a small fraction of the particle loading.

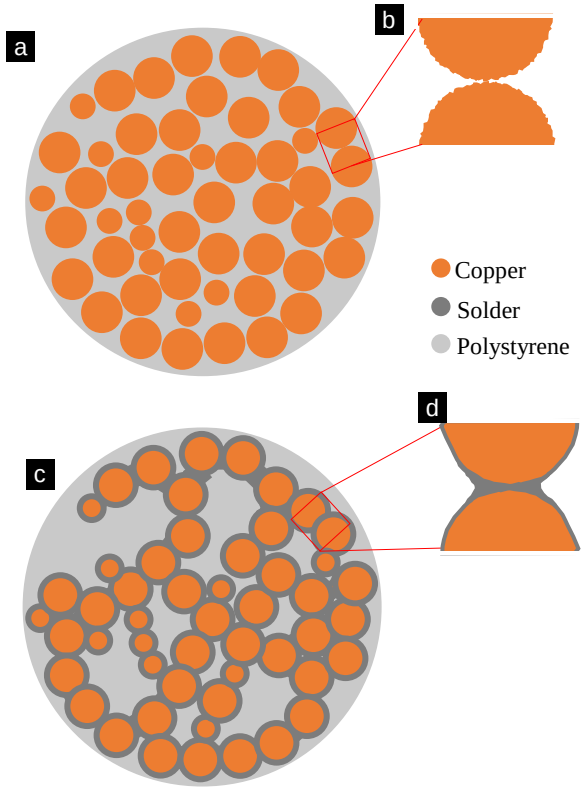

Figure 4-1 Schematic of (a) Copper dispersed in polystyrene without flux and solder to form polymer composite (b) magnified view of a particle contact (c) copper and solder in polystyrene forming metal network (d) magnified view of solder bonding particles via a meniscus

Obviously for practical applications as conductive plastics, it is desirable to achieve high conductivity at as low a metal loading as possible. Much of the previous research used fairly high metal loadings: 40 vol% in Yang et al [143], 53 vol% in Zou et al [141], and over 50% in Mrozek et al [140]. Due to the relatively high cost of the metals (especially solders) as compared to plastics on a volumetric basis as, these high loadings entail a high cost. Moreover, if the particulate metal is present at high volumetric loading, this also causes poor processability, as true for all particle-filled polymers. One may use lower metal loadings using high aspect ratio particles [136, 142, 144], but typically high aspect ratios also tend to significantly worsen processability. Yet, the literature on capillary effects in particulate materials suggest that mechanical percolation can appear at far lower particle loadings. For example, our own research on blends of particles and two immiscible polymers suggests that when particles are bridged by menisci such as shown in Figure 4-1c&d, percolation (judged rheologically) can appear when the particle loading is well under 10% loading [11]. Similar research in oil/water systems [99, 145] also suggests that percolation can occur at particle loadings much lower than those used in LMPA-based composites [140, 141, 143]. As long as the particles are separated from each other, mechanical percolation does not necessarily induce electrical percolation. However, if the particles may be bridged by a meniscus, it may be possible to induce electrical percolation at roughly the same particle loading as mechanical percolation.

We speculate that the previous studies [140, 141, 143] have examined only a very limited range of the composition space, and it is possible that with a more systematic study of compositional effects, high conductivity maybe be achieved even at a particle loading that is much lower than examined previously. In summary, the motivation of this study is to develop the idea of bulk soldering more systematically across a wider range of composition space than examined

previously, with a particular focus on lowering the metal loading needed for realizing high conductivity.

Our research approach in this chapter is heavily influenced by recent research, including from our own group, elucidating structure-composition relationships in ternary liquid/liquid/particle mixtures [74]. These include a wide variety of ternary mixtures of oil/water/particles, air/water/particles, and particle-filled blends of molten polymers. The author's own work in this area was presented in the previous two chapters. Since PS/solder/copper blends constitute liquid/liquid/particle mixtures, many of the insights drawn from the previous research are directly applicable to this research. Two insights are especially relevant. The first is the importance of the relative wettability of the particles towards the two liquids. In the present case, the copper particles are fully-wetted by solder and hence – if there is sufficient solder – the particles can be engulfed by the solder completely. Thus the solder:copper volume ratio, which determines whether engulfment happens or not, is a critical parameter determining structure. The second is the recognition that continuous metallic pathways can be created throughout the sample by three distinct microstructures (Appendix Figure C-1) that correspond to different regions of the ternary composition space [93]. Any one of these pathways should have a high conductivity, however, Figure 4-1c corresponds to one such pathway that creates metallic pathways via a metal-solder composite structure.

The outline of this study is as follows. Section 4.3 first describes the materials and methods briefly (details in Appendix C), followed by experimental results on how the conductivity and microstructure are affected by total metal loading (section 4.3.2), the critical role of flux (section 4.3.1), the solder:copper ratio (Section 4.3.3) and copper particle shape (Section 4.3.4). Section

4.4 discusses the results, especially in regard to how these ternary mixtures compare with previously examined in oil/water/particle or polymer/polymer/particle mixtures.

4.3 Results

Samples were prepared from polystyrene (PS), 30–80 μm diameter copper particles (Appendix Figure C-2), and "solder paste" of a grade typically used in the microelectronics industry. The paste consisted of 15–25 μm diameter particles of $Sn_{63}Pb_{37}$ dispersed in a continuous phase flux. The melting point of the $Sn_{63}Pb_{37}$ is known to be T_m=183 °C). Most samples also included a solder flux to clean the particles (see below). Other details of the materials are given in the Appendix C.

Samples were prepared by blending all components under molten conditions, first mixing the copper particles and the flux, then adding the solder paste, and finally the PS. The temperature during the last mixing step was 220 °C, far above the melting point of the solder particles. All other details of mixing are given in the Appendix C.

The samples were molded into discs at 225 °C and conductivity measured through the thickness. The surface of the discs was sanded lightly to expose the metal particles and ensure good contact with electrodes. Samples were also immersed in toluene to extract the PS, upon which the metal dispersed phase could be recovered and imaged by optical and electron microscopy. All the details of conductivity and structural characterization are given in Appendix C. The composition of the samples is specified by two volume fractions ϕ_{solder} and ϕ_{copper} (the

polystyrene being the remainder). We will frequently refer to the volume ratio of the solder to the copper as ϱ;

$$\varrho = \frac{\phi_{solder}}{\phi_{copper}} \tag{4-1}$$

Two series of samples were prepared: the first that varied ϕ_{solder} and ϕ_{copper} keeping ϱ fixed at 0.15 (Section 4.3.2) and the second that varied ϱ at a fixed metal loading of 0.2 (Section 4.3.3). In most of our previous research on the fundamentals structure-composition relationships, the composition of liquid/liquid/particle mixtures was represented on a triangular composition diagram. Analogously, the compositions of all the three mixtures are shown on such a diagram in Appendix Figure C-6.

Initial experiments were conducted at a single solder:copper ratio of $\varrho = 0.15$. The rationale for selecting this ratio is guided by analogous research on other liquid/liquid/particle ternary mixtures. That rationale is as follows. As mentioned in the Introduction, since the solder can wet the copper completely (see below), we anticipate that solder and copper will form a combined phase in which copper particles are dispersed in solder. Such a combined phase is expected only if the solder volume is adequate to completely engulf all the particles. The schematic picture of Figure 4-1c&d requires the solder to join the particles either pairwise or via a few-particle contacts, but not complete engulfment. Previous research suggests that in analogous ternary mixtures when the particles are fully-wetted by one phase, complete engulfment requires the wetting phase to be roughly 25% of the volume of the particles [74]. Thus, a ϱ value of 0.15 seems suitable to avoid complete engulfment, and hence this value was adopted for initial experiments. Later experiments also examined ϱ values ranging from 0.06 to 1.5.

4.3.1 Critical Role of Flux

Figure 4-2 compares the electrical conductivity at several filler loadings for three different sample families. The lowest set of data (filled triangles) correspond to polymer-copper composites prepared by simply dispersing copper particles (as received) into polystyrene. These samples have low conductivity even at 30 vol% copper loading. One reason for this low conductivity is simply that the copper particles are well separated by an insulating layer of polystyrene. Yet a second reason may be that copper is generally covered with a thin surface layer of oxide which is insulating. Thus, even when two particles make physical contact, there may still be an insulating oxide layer preventing good electrical contact.

Accordingly, samples with the same copper loading were prepared, but with the particles being pre-dispersed into flux prior to blending with polystyrene. The resulting samples (open red circles in Figure 4-2) were found to have a conductivity that was orders of magnitude higher. These experiments testify to the importance of having metal surfaces that are extremely clean: it appears that oxide film poses a significant resistance to electron conductivity and removing it can increase conductivity.

Flux has two important constituents called activators and vehicles [41]. Information provided from the flux manufacturer shows that the activators in the flux used here are NH_3Cl and steric acid. The former can readily decompose at high temperature to produce HCl. Both acids can reduce the CuO layer on the particles. The vehicle (i.e. the carrier phase) for this specific flux is not known, but often includes a solvent, and possibly some non-volatile species.

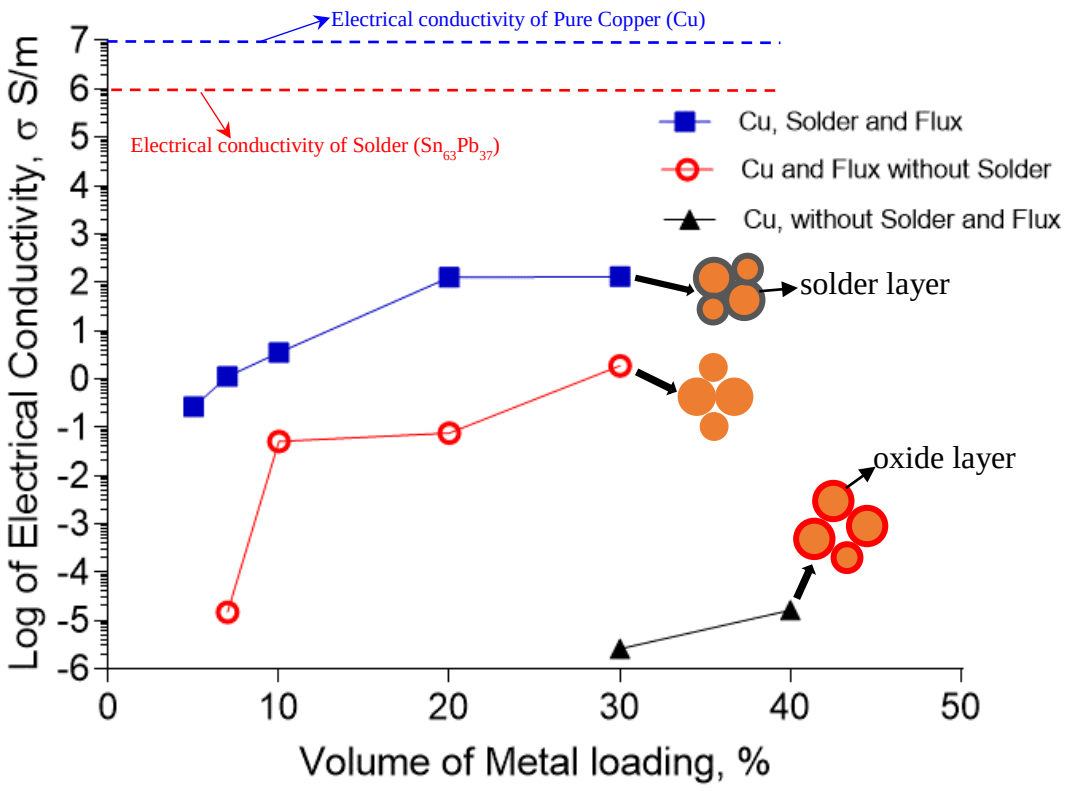

Figure 4-2 Conductivity of PS/solder/copper composites at various total metal loadings where $\varrho = \phi_{solder}/\phi_{copper}$ was kept fixed at 0.15. The points labelled a, c, d, and e refer to the corresponding images in Figure which shows morhologies of these samples

Weighing experiments on the samples before and after mixing suggest that roughly half of the mass of the flux is volatile and is lost during the melt blending process. A separate experiment conducted with a mixture of flux and polystyrene (no metal) shows that the nonvolatile portion remains in the sample in the form of a dispersion. In samples that contain solder and copper particles (discussed in the next section), due to opacity, our experiments are not able to determine the location of the non-volatile portion of the flux. Yet, the fact that the copper is well-wetted by the solder suggests that they do not interfere with the wetting of copper by solder.

4.3.2 Bulk Soldering of Copper Particles

We now turn to samples to which solder is added, and this section is restricted to samples for which $\varrho = 0.15$. Figure 4-2 shows that these samples have far higher conductivity than the flux-containing samples without added solder. We emphasize that the x-axis of Figure 4-2 is drawn at total metal loading, i.e. the conductivity increase occurs not because adding solder raises the metal loading, but because the solder changes the microstructure.

We examined the microstructure directly by Scanning Electron Microscopy (SEM) after removing the PS phase by selective dissolution in toluene. In the absence of solder, the copper particles are well-wetted by PS, as may be judged by their good dispersion. Dissolution of the PS phase gave a slurry of copper particles in toluene indicating that the copper particles were completely separated. With addition of solder, the copper particles were found to be bonded together into aggregates (Figure 4-3a). The aggregate size increased with total metal loading (Figure 4-3b-f) until, at 30 vol%, the solder-copper together formed a fully-self-supporting scaffold that retained the original shape of the molded disc (Figure 4-3e). In fact, a large-scale scaffold was evident at 20 vol% as well (Figure 4-3d), although it was fragile and fragmented upon extracting from toluene. It is the presence of this very open scaffold that provides highly conductive pathways throughout the sample and hence is responsible for the high conductivity.

Higher magnification views (Figure 4-3c and Figure 4-3f) show the details of the particle contact and confirm that the solder wets the particles. Indeed, complete wetting is evident even without any SEM at all: when a blend such as Figure 4-3b is immersed in toluene, the remaining metal aggregates appear to be a dull silvery color (Fig. B4d) rather than the red color of copper (Appendix Figure C-4a&c). This indicates that the solder is not only bonding together copper

particles, but also covers the copper surfaces. Yet, the microscopic picture of particle contact (Figure 4-3c) appears to be more complex than Figure 4-1d. Specifically, the contacts between the particles are not strictly pairwise as sketched in Figure 4-1d, but instead involve multiple particles bonded together by a single meniscus. Such a microstructure was dubbed “pendular/funicular morphology” in our research [23, 74] on immiscible liquids with particles. These images suggest the schematics drawn alongside each set of data in Figure 4-2, with two features being noteworthy (1) particles in the lowermost schematic are depicted with an oxide film, which is no longer present in the middle schematic (after flux treatment), and (2) in the uppermost schematic, the space between the particles is depicted as filled with solder.

Finally, we re-emphasize the critical role of the flux in creating the solder-bonded particle structure. In the absence of flux, the solder by itself is ineffective in raising conductivity. Specifically, a limited number of PS/copper/solder mixtures were prepared by simply melt-blending dry solder powder, copper particles (as received), and PS. These blends had low conductivity suggesting that the copper particles are not well-wetted by solder in the absence of flux. To verify this, we compared the melting behavior of solder on copper foil without and with flux. If dry solder powder was placed on copper foil and melted (Appendix Figure C-5a), it coalesced into large blobs which, upon cooling, were easily chipped off the surface of the foil (Appendix Figure C-5b). In contrast, melting the solder paste (which is the same solder particles dispersed in flux) on foil resulted in excellent wetting (Appendix Figure C-5c) and it was not possible to chip away the solder from the foil (Appendix Figure C-5d), making it easy for the solder to wet the surface of the copper [146, 147]. Thus, the removal of oxide from the copper surface is a critical step in realizing high conductivity.

To our knowledge, there is no prior research on adding flux to improve the conductivity of metal-filled plastics. This idea is potentially applicable not only to copper, but also to other metals that are used to improve the conductivity of plastics. Indeed, specialized solders are available even for making the surface of stainless steel suitable for soldering, and this may be a useful method to improve the conductivity of conductive plastics based on stainless steel fibers [148]. The chief challenge is that such fluxes are corrosive and may be damaging to processing equipment.

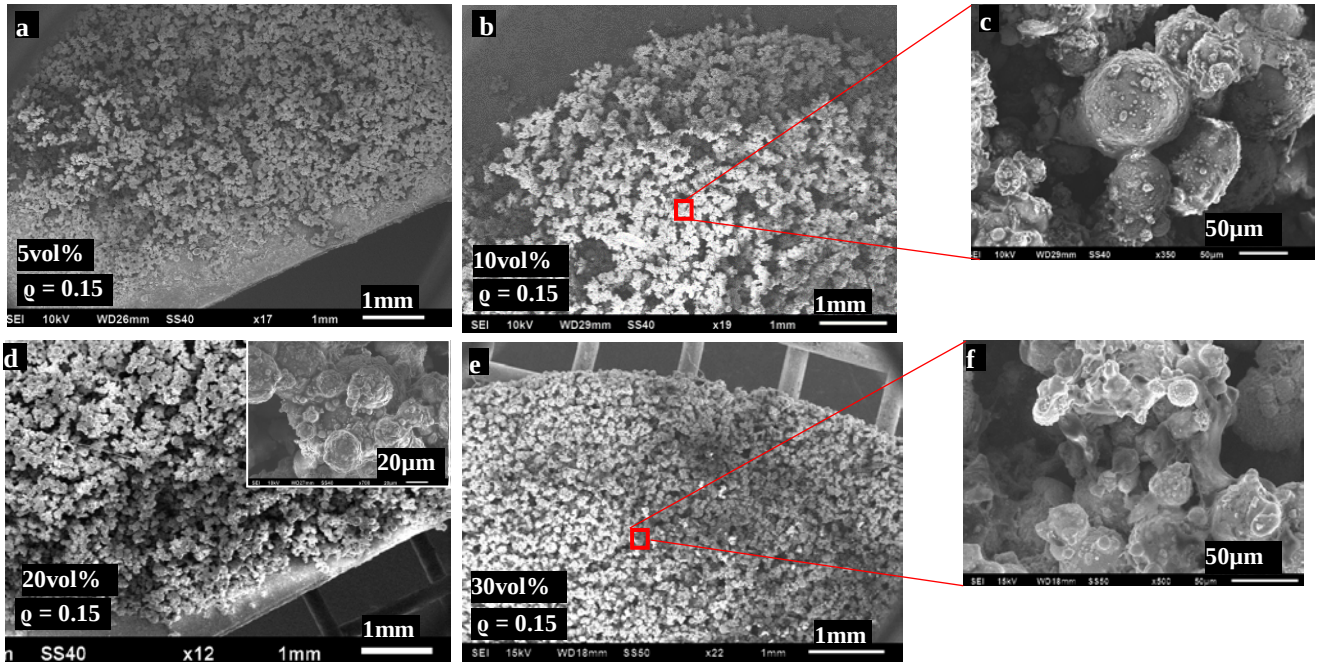

Figure 4-3 SEM images of conductive polymer composite with copper particles, solder, and flux.Samples are prepared at constant ϱ-value of 0.15 with increasing total metal loading after selective dissolution of polymer matrix (PS) with metal loading of (a) 5vol% (b) 10vol% (d) 20vol% and (e) 30vol% showlow magnificatiom images with (c and f) at high magnification of 10vol% and 30vol% metal loading respectively.

4.3.3 Effects of Solder:Copper Particles Ratio on Composite

We now examine the effect of the solder to copper ratio, ϱ. As mentioned in Section 4.3.2 when the particles are fully wetted by one of the two liquids, two possibilities arise depending on the wetting fluid:particle ratio. If the ϱ value is sufficiently large, the particles and the wetting liquid form a combined phase. In contrast, if the ϱ value is relatively small, the wetting liquid tends to form menisci that bond the particles together. Accordingly, ϱ strongly affects microstructure, and in the present case, is likely to influence conductivity. Indeed this was noted by Zou et al. [141] albeit at a very high metal loading (53 vol%), and by Sun et al. [144] in an ionic liquid system, although these latter experiments used highly non-spherical particles and relatively small ϱ values. Here we re-examine this question, but at a much lower metal loading (20 vol%) than Zou et al. [141], and across a range of ϱ values that span the expected transition from meniscus-bound to a particle-engulfed state. Since the total metal loading is held fixed at 20%, these sets of samples trace a trajectory in the triangular composition space that corresponds to $\phi_{PS} = 0.8$ as illustrated in Appendix Figure C-6, and in Figure 4-4f. Practically this trajectory is interesting because it may be possible to improve the conductivity without increasing the metal loading, but by choosing a ϱ value different from the $\varrho = 0.15$ used in Figure 4-2 and Figure 4-3. But conceptually as well, varying the solder:copper ratio is interesting since it allows a direct comparison of this system against the previously-constructed map of microstructure across a wide range of compositions for model polymeric systems [20, 23, 93]. Specifically, we showed that as the volume fraction of the particle-wetting fluid was increased, there was a sequence of structural transitions from meniscus-bound particle aggregates to capillary aggregates to phase inversion, sometimes with an

intermediate cocontinuous morphology. In this section, we will test whether similar structural changes appear and how they affect conductivity.

Figure 4-4 illustrates the effect of changing ϱ at a fixed total metal loading of 20 vol%. Figure 4-4a corresponds to the lowest solder content of $\varrho = 0.06$, which corresponds to ϕ_{solder}=1.1% and ϕ_{copper}=18.9%. As expected at this relatively low solder content, there is insufficient solder to engulf the copper particles completely. Accordingly, the sample dispersed completely upon immersing in toluene, and SEM revealed discrete aggregates of few copper particles bonded by menisci of solder. Figure 4-4b (identical to Figure 4-3d) corresponds to $\varrho = 0.15$. As mentioned above, upon removing the PS, all the metal was consolidated into only a few large fragments which are called a pendular/funicular network of the filler phase. With further increase in the ϱ value to 0.6 (Figure 4-4c), all the particles became bonded into a single percolating network, and immersing the sample into toluene gave a single porous disc of metal. SEM shows the particles appear to be heavily covered with solder and strongly bonded into large aggregates. A further increase in ϱ to 0.9 (Figure 4-4d) led to significant coarsening of the morphology. While a large and fairly open network still exists at this composition, the size-scale of the "building block" of this network is no longer a single particle, but large blobs of particles held together by solder. Previously we called these blobs "capillary aggregates", and the corresponding network as a "capillary aggregate network".

A further increase in ϱ to 1.5 (Figure 4-4e) leads to a breakdown of the percolating network. This can be anticipated based on our previous research [20, 23] and can be explained readily: capillary aggregates are stable against coarsening because they have a very high internal volume fraction of particles, e.g. at $\varrho = 0.9$, the copper particles constitute 53 vol% of the combined (copper+solder) phase. At such a high-volume fraction, the combined (copper+solder) phase is

expected to have solid-like rheology, and hence cannot coarsen. When ϱ increases, the combined phase becomes dilute (e.g. Figure 4-4e has only 40% copper in the combined phase). Due this dilution, the combined phase behaves like a relatively low viscosity liquid and can coalesce or breakup readily. Under these conditions, sustaining a network is difficult due to rapid coarsening induced by interfacial tension [93].

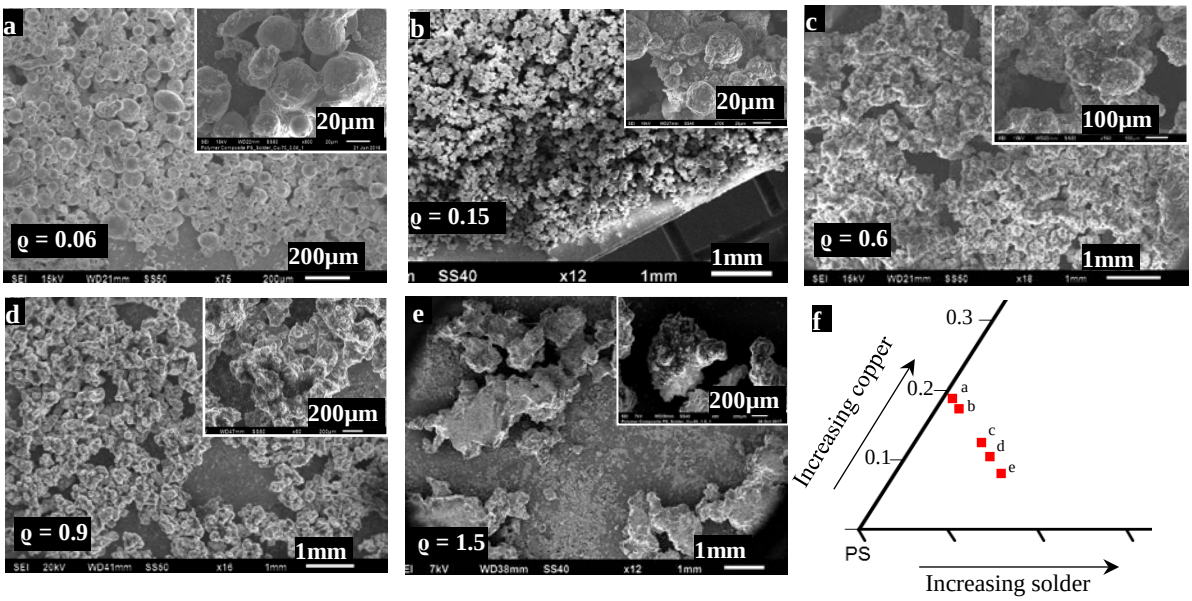

Figure 4-4 SEM images of conductive polymer composites with copper, solder and flux at different ϱ-values at fixed metal loading of 20vol%. The triangular composition diagram shows the compositions fo the samples shown in Figure 4-4a - Figure 4-4e.

One may expect these changes in microstructure to induce significant changes in electrical conductivity and indeed, Figure 4-5 shows a sharp increase in conductivity at small values of ϱ, with the $\varrho = 0.6$ giving the highest conductivity amongst the measured samples. There is clearly an optimum in the solder:particle ratio: not only does the conductivity reduce when ϱ rises to 0.9,

but the microstructure of Figure 4-4e is so coarse that it is not possible to make homogeneous discs for conductivity measurements.

4.3.4 Shape and Mixing Effects

High aspect ratio fillers, for example, acicular, fiber-like, and plate-like particles can generally percolate at much lower volume fraction than spherical particles and hence can give higher conductivity. Indeed conductive polymer blends that use stainless steel fibers as the conductive filler have been commercialized [148, 149]. We examined whether replacing the spherical copper particles with flakes would affect conductivity. Flakes were prepared by ball-milling the spherical copper particles, and their morphology is shown in Appendix Figure C-3. Figure 4-5 compares the conductivity of four blends (two different flake sizes at two different ϱ values) against the corresponding samples with spherical particles. Surprisingly, increasing the aspect ratio did not necessarily increase conductivity. At $\varrho = 0.15$, the conductivity reduced sharply indicating a loss of the percolating network, and indeed immersion in toluene caused a complete disruption of the disc specimens. In contrast, percolation was maintained at $\varrho = 0.6$ and high conductivity was retained. The possible reasons for this are discussed in Section 4.4 below.

Finally, all the research thus far was conducted by mixing by hand with a spatula. For any practical applications, the use of conventional plastics processing equipment to prepare such samples would be needed. We conducted a single experiment using a Brabender Plasticorder, a batch mixer that is commonly used in the plastics processing community. The results of this blending (Figure 4-5) were roughly comparable to those of hand-blending: the sample was found

to retain a percolating network upon dissolution and had high conductivity, thus indicating that in principle, bulk soldering is viable even using standard plastics processing equipment.

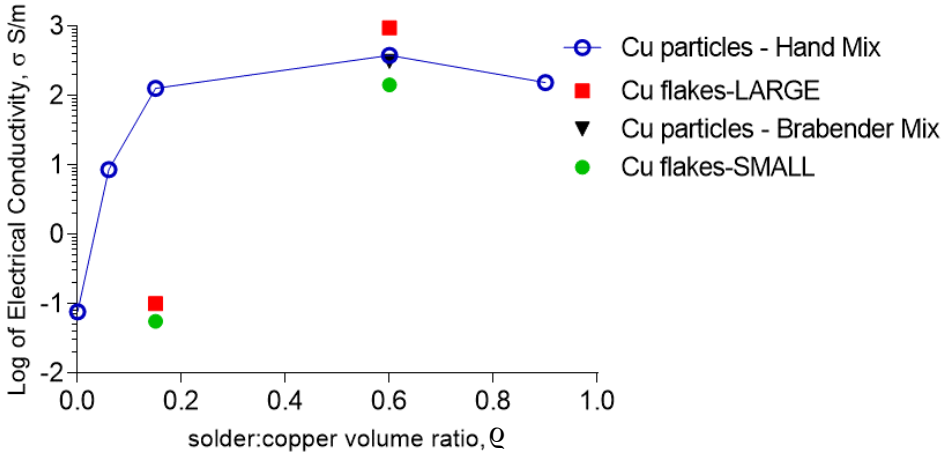

Figure 4-5 Conductivity of polymer composites with 20vol% metal loading at different ϱ-values. Several sizes and shapes of copper particles were used in preparing composite samples and tested

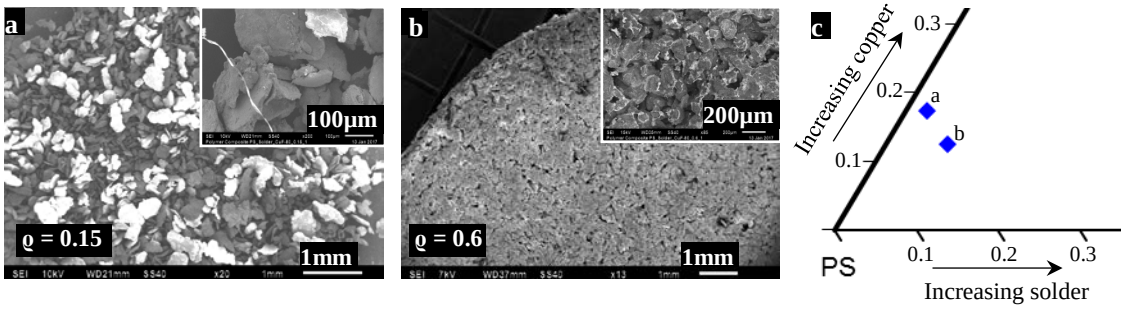

Figure 4-6 SEM images of conductive polymer composite with copper flakes, solder and flux at different ϱ-values

4.4 Discussion

Three aspects of the experimental results deserve further discussion: a comparison of the morphologies against previous research, the behavior of the non-spherical flakes, and a comparison of the conductivities found here against those in the previous literature on combining particles and liquid metals in thermoplastic matrices.

As mentioned in the Introduction, this research was strongly influenced by previous studies of the microstructure-composition relationships in analogous oil/water/particle or polymer/polymer/particle systems [1, 74, 128]. The system studied here behaves in a qualitatively similar fashion, at least with changes in the solder:copper ratio. At the lowest ϱ value studied here, the pendular/funicular morphology (i.e. two or just a few particles bound by menisci of the wetting fluid) appears as was also noted previously [1, 74, 128]. With increasing solder content, there was adequate solder to fully engulf the particles and form a combined phase highly filled with copper particles. This combined phase is expected to have solid-like rheology and hence takes the appearance of irregular lumps which we previously called capillary aggregates [10, 12]. With a further increase in solder, the size-scale of the combined phase increased sharply as the combined phase starts to behave as a “normal” fluid phase capable of rapid coalescence [10, 12]. Previously we also noted non-monotonic changes in rheology: the solid-like behavior of the mixtures peaked at an intermediate value of ϱ corresponding to a pendular/funicular morphology [11, 104]. It is more difficult to conduct rheometric experiments in the present situation, however, qualitatively, the mixtures show similar rheological trends. This is illustrated in Appendix Figure C-7 where samples with various solder:copper ratios (all at fixed metal loading) were allowed to melt. It is clear from those images that the samples with low or high values of ϱ sag under gravity, whereas

$\varrho = 0.6$ corresponds to a relatively high stiffness for which the sample does not flow. Indeed, at the highest ϱ value in Appendix Figure C-7, the size of the combined phase is so large that the PS separates from the metal phase altogether and leaves the sample.

Despite the qualitative similarity of the current system as compared to the previous liquid/liquid particle mixtures, two differences must be pointed out. The first is a quantitative difference between the ϱ values at which various microstructural transitions appear. In our own studies of immiscible polymer blends with spherical silica particles that are fully-wetted by one phase [11, 20, 23], the pendular/funicular morphology appeared for $\varrho < 0.4$. Capillary aggregates appeared around $\varrho = 0.6$. For ϱ values exceeding 1, the combined phase had a smooth interface indicating that the combined phase was liquid-like. These specific values of ϱ refer to our own research on immiscible polymer blends with spherical silica filler (chapter 2.0), but very similar observations have been made in oil/water/particle or air/water/particle mixtures [74].

A glance at Figure 4-4 suggests that the same sequence of transitions is shifted to higher ϱ values in the PS/solder/copper mixtures. For instance, Figure 4-4c (with $\varrho = 0.6$) suggests that capillary aggregates are not well-developed; instead the largest aggregates still comprise solder menisci that bind just a few particles. In contrast, at a similar value of ϱ, well-developed capillary aggregates were noted previously [11, 23]. Similarly, Figure 4-4e shows irregular lumps indicative of capillary aggregates, whereas this $\varrho = 1.5$ was previously found to give a smooth liquid/liquid interface in particle-filled polymer blends indicating that the combined phase behaved like a liquid [93]. We believe that the reason for this shift in the composition at which these morphologies appear is that the copper and solder react with each other. In previous studies or in studies of oil/water/particle mixtures, the combined phase was simply a *physical* mixture of the wetting fluid and the particles. In contrast, in the present case, copper is known to react with the tin in the solder

to form intermetallic compounds Cu_3Sn (in the form of thin sheets) and Cu_6Sn_5 (in the form of scallop-like structures) [150]. This reaction occurs by diffusion of the molten tin into copper, and the resulting intermetallic compounds are responsible for the excellent adhesion of copper and solder. Previous research suggests that this process can happen rapidly (less than 1 min) [150] and hence may indeed be relevant to our samples.

To test for the possibility of intermetallic formation, we conducted SEM imaging of the cross-section of the metal phase; in contrast, Figure 4-3, Figure 4-4, and Figure 4-6 show only the surface of the metallic phase. The sample with $\varrho = 0.6$ was chosen for this purpose for convenience of imaging. A molded disc of the sample was polished to expose the cross section of the metal, and the corresponding images are shown in Figure 4-7. In the absence of reaction, only three distinct gray levels corresponding to three distinct compositions would be expected: polystyrene (darkest), copper, and solder (brightest). Figure 4-7 however shows four gray levels, and based on the expected elemental compositions, we anticipate the following sequence polystyrene (darkest), copper, tin-rich phase, lead-rich phase (brightest). To further confirm intermetallic formation, elemental analysis was conducted by energy-dispersive x-ray spectrometry, and the corresponding results are shown Appendix Figure C-8. These results clearly show that in the region immediately adjacent to the copper particles where grayscale is intermediate between the particles and the meniscus, there is nearly equal copper and tin, but no lead. Moreover, the region far away from the copper particles (brightest grayscale) is depleted in tin as compared to the original solder composition. Both these strongly support the formation of copper-tin intermetallic compounds. The immediate implication is that after some mixing time, a portion of the wetting fluid (tin) turns into a solid intermetallic, thus reducing solder:copper ratio ϱ below its value at the beginning of the mixing process. This reaction can explain, at least

qualitatively, why the microstructural transitions occur at higher ϱ value as compared to analogous non-reacting systems.

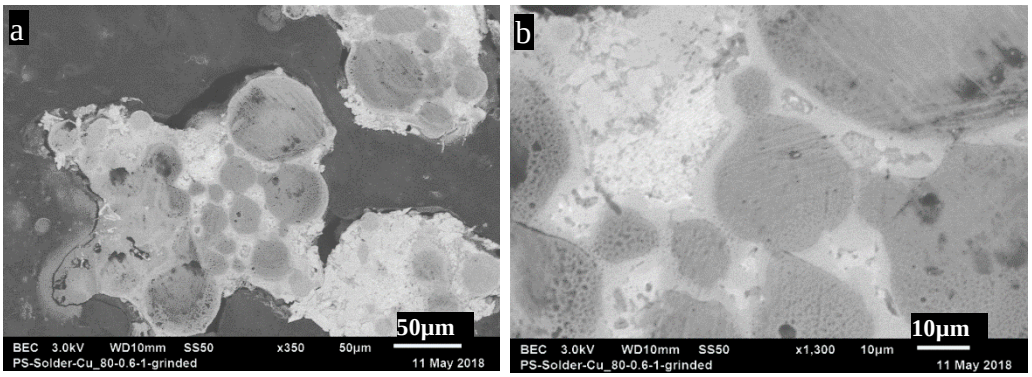

Figure 4-7 SEM images of the polished cross section of the composites. Note the gray region adjacent to the particles which indicates formation of an intermediate compound

It is also noteworthy that a cocontinuous structure of the type shown in Appendix Figure C-1c has not been identified in our research. This structure consists of two phases (one with particles and one without), both of which are continuous. Unlike in Appendix Figure C-1b, in Appendix Figure C-1c, the particle-containing phase is relatively dilute in particles so that it has liquid-like rheology, and hence the interface is smooth. Although we have not seen such a smooth-interface morphology yet, it is possible that that higher ϱ values and higher total metal loadings may yield such a structure. Indeed such a morphology was seen by Mrozek et al [140], albeit at metal loadings exceeding 50 vol%.

The second difference is the observation that the conductivity of the samples based on copper flakes is not significantly different from that of spherical particles. It is generally accepted that conductive fillers with high aspect ratios are beneficial because they tend to percolate at lower

filler loadings. This is the reason why fillers such as carbon nanotubes, carbon nanofibers, graphene, or stainless-steel fibers have attracted attention for conductive polymer composites. Yet, in the present case, only the large copper flakes gave a significantly higher conductivity than the corresponding spherical particles at the same composition. We speculate that there are two reasons for this. The first is that the large surface area of flakes require more solder to wet completely. Thus, at a given ϱ value, the solder loading may be adequate to cover the spherical particles completely, but not adequate to cover flakes of small size. The same may be true for flux as well: the amount of flux may be insufficient to fully clean the flakes. The second possibility is that capillary menisci are highly effective with flat particles, i.e. if two flat particles interact side by side, then, they will bond strongly with a meniscus. Not only is the corresponding solder "lost" (since it cannot participate in forming a network), but furthermore, the two flat particles now behave effectively like a single thicker particle. These speculations suggest that by adjusting the ϱ value, flakes may prove to be more effective at building a network. A further excellent discussion of the effect of particle shapes can be found in Maurath et al [151].

Third, the question underlying this research was whether, with a systematic study of compositional effects, a range of compositions may be identified that give high conductivity even modest metal loading. Detailed comparisons against published data are difficult because of differences in metal loading and in particle shape. The most suitable comparisons are against the two papers [140, 141] that used roughly spherical particles along with liquid metal. Mrozek et al. [140] reported a conductivity of 10 S/m at 30 vol% metal loading. Mrozek et al also reported far higher conductivity exceeding 10^4 S/m, but at a total metal loading of 50% or higher at which the metal and the polymer were both continuous. A second comparison may be made against Zou et al [141] who reported a far higher conductivity, roughly 2.5×10^6 S/m at a total metal loading of

54%. Our own values from Figure 4-4 and Figure 4-5, are typically several hundred S/m, much higher than reported by Mrozek et al [140] at a comparable loading, but much lower than of Zou et al [141], who had a much higher metal loading.

Moving beyond spherical particles, three further articles are worth mentioning although they are not comparable to our current research since they use highly non-spherical particles. Michaeli et al. [142] and Wu et al. [136] both used long copper fibers bonded together by low-melting metal. Wu et al. report a conductivity exceeding $10^3\ S/m$ at 10% metal loading. Michaeli et al. report a conductivity of ~1 S/m at 20% metal loading, but it rose rapidly and exceeded $10^5\ S/m$ at 40% metal loading. Finally, Yang et al [143]. used dendritic copper particles in conjunction with tin. The highest conductivities reported were about $4 \times 10^5\ S/m$ at 40 vol% metal loading although this required many hours of annealing.

It is noteworthy, the conductivity of eutectic tin-lead solder is roughly $7 \times 10^6\ S/m$. Almost all of the reported values in the previous two paragraphs are far lower, even though many of these articles show that the metal forms a continuous phase. An exemplary case is from Mrozek et al. [140], who clearly show a continuous metal phase at 60% metal, yet report a conductivity that is almost 100-fold lower than the corresponding solder. The reason why so many researchers find a surprisingly low conductivity, even when the metal phase is continuous, remains unclear. The sole exception is Zou et al [141] which is a far outlier: their reported conductivity of $2.5 \times 10^6\ S/m$ is only 3-fold lower of pure solder. Even more surprising, the same article reported that copper-in-polymer (without any liquid metal) had roughly the same conductivity – an unprecedented value for metal-filled plastics. Finally, they also reported that bonding copper together with solder *lowered* the conductivity which is surprising considering that there was excellent morphological evidence of 3D network formation.

Finally, we emphasize that, in common with other liquid/liquid/particle mixtures, mixing method may play a role in structure development. For instance, limited experiments early during this research showed that pre-dispersing the solder into the PS and then adding the copper particles during blending gave a highly heterogeneous structure because the solder had coalesced into large drops even before the copper was added. This is similar to our observation that in oil/water systems [12] or in polymer systems [10], if one starts with a droplet-matrix system and adds particles that are wetted by the drops, capillary aggregates from readily. Thus, other mixing protocols or the use of higher rate mixing equipment, may improve or worsen the conductivity.

4.5 Concluding Remarks

In summary, we have developed conductive thermoplastic polymer composites based on blends of polystyrene, molten solder, and copper particles. The essential idea, which is inspired by analogous research on other liquid/fluid/particle systems, is to bind together copper particles using menisci of the solder, thus creating an all-metallic percolating network with high conductivity. Since such binding of the copper particles using solder is achieved by simply blending under molten conditions, this approach is dubbed “bulk soldering”.

We examine the effect of composition on the microstructure and conductivity and show that even at a total metal loading of 20vol%, it is possible to create an all-metal scaffold that percolates throughout the sample. Moreover, the solder:metal volume ratio is a critical parameter determining the microstructure and conductivity of the composites. Specifically, if this ratio is small (e.g. 0.2), the copper particles aggregate due to the solder, but do not percolate. If the ratio

is large, e.g. exceeding 1, the solder engulfs the metal particles and forms a combined copper-in-solder phase that is too liquid-like to remain percolating. The changes in microstructure with ternary composition broadly resemble that of other liquid/fluid/particle mixtures, although at least some of the structural transitions require a higher ratio of solder:copper than expected from previous research. While most of the results of this chapter were realized with samples prepared by hand-blending, however, a single test using standard plastics processing equipment shows similar results.

Finally, our results show the critical role of flux in realizing high electrical conductivity. Copper particles generally have an oxide layer, and it is only after this oxide layer is removed that the solder can effectively wet the particles and achieve bulk soldering.

5.0 Mechanical Properties of Particle Filled Polymer Blends

5.1 Introduction

Some of the common purposes for adding fillers to polymers is to improve mechanical properties, e.g. enhancing stiffness, tensile/flexural modulus and strength of the resulting polymer composites. However, the addition of rigid fillers to polymers often increases brittleness and faces poor processabilities when significant amount of fillers is added.

In general, the traditional approach to increasing the modulus of a polymer is by dispersing particles or fibers of a high modulus materials such as glass into the polymer matrix. To achieve high modulus for the filled polymer requires the use of high filler loadings (30 – 70 vol%) [152] which entails poor processability. Lower loadings of high-aspect ratio fillers may be used to achieve similar values of modulus, but typically high-aspect ratio fillers tend to significantly worsen processability. In this chapter, we propose the use of spherical particles and a wetting polymer phase which serve as a combined polymer phase within a polymer matrix.

This chapter explores how to improve the mechanical properties of a polymer filled with particles which are bound together by capillarity. The focus is on improving the mechanical properties of a polymer blended with another thermoplastic polymer and particulate materials. The strategy of this work is to create capillary aggregates in the combined phase and orient them under flow to behave like a stiff filler of high aspect ratio. This approach has two potential advantages: the wetting polymer phase is molten at processing temperature which may ease processability even

at high particle loading of the combined phase, and the filler aggregates can form large scale structures, possibly percolating to improve the modulus of mixture.

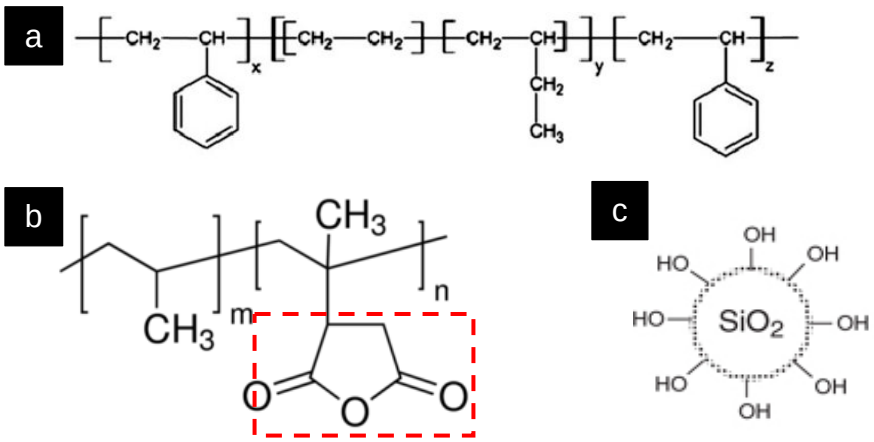

Figure 5-1 Chemical structure of (a) styrene-ethylene-butylene-styrene (SEBS) figure was taken from reference [153] and (b) maleated anhydride polypropylene and (c) silica particle showing hydroxyl group on the surface. The maleic anhydride portion of MaPP reacts with hydroxyl groups on the surface of the silica particle, forming a coupling between OH and maleic anhydride.

In this study, SEBS elastomer (Styrene-ethylene-butylene-styrene copolymer with the chemical structure shown in Figure 5-1a) was used as the polymer matrix, silica particles as the hard sphere filler and maleated polypropylene (MaPP with chemical structure as shown in Figure 5-1b) as the wetting polymer phase under molten conditions. The maleated polypropylene was used because the maleic anhydride group of MaPP (as boxed by a red dashed square in Figure 5-1b) can react with the hydroxyl groups on the silica surface (as illustrated in Figure 5-1c), thus giving a permanent graft layer on the silica particles [154, 155]. This offers two advantages: the grafted particles can now be wetted by the polypropylene, and furthermore entanglements between the adsorbed chains and the bulk polypropylene may enhance adhesion between the particles and

wetting agent, which is critical for mechanical property enhancements. Both MaPP and silica particles may serve as filler within the SEBS matrix, since both are much stiffer than the SEBS rubber matrix. The next section discusses the results of the flexural and tensile modulus of the particle-filled immiscible polymer blends.

5.2 Results

Samples were prepared from Styrene-Ethylene-Butylene-Styrene (SEBS), maleated polypropylene (MaPP) and 0.5 – 5 micron diameter fused silica particles. The SEBS is a triblock copolymer with the chemical structure shown in Figure 5-1a with that of MAPP represented in Figure 5-1b. The melt flow index at 230^{o}C with 2kg for SEBS shows “no flow” and that of MaPP is 150g/10min. Other details of the materials are given in Appendix D.

Initial samples were prepared using a Brabender batch mixer to verify the basic hypothesis that MaPP can wet the particles and therefore induce their aggregation. These samples of SEBS/MaPP/particles ternary blends were prepared in a two-step procedure in a Brabender batch mixer. The SEBS and MaPP were first mixed together at 285^{o}C. Then, silica particles were added, in small increments, and blending continued until it was uniformly mixed. After recovering and cooling the blends, samples were washed with toluene to remove the SEBS. The residue (MaPP and particles) were examined by Scanning Electron Microscopy as shown in Figure 5-2.

Figure 5-2 illustrates the morphology of SEBS/MaPP/particles ternary mixture prepared in a Brabender batch mixer with a composition of 70/20/10. The SEBS phase was removed by selective dissolution prior to imaging. This SEM image suggests that at this sample composition,

there are two continuous phases: SEBS and a combined MaPP and particles phase with the SEBS phase removed. The tortuous voids in the sample represent the removed SEBS phase in the ternary mixture. This morphology represents a successful outcome of the goal stated in section 5.1: the particles are clearly aggregated by the particles. Even at a total dispersed phase loading of only 30vol%, the MaPP is continuous. So perhaps excellent properties may be obtained from such a ternary mixture – not only because the reinforcing phase has a high particle loading and hence likely to have a high modulus, but also because that phase is continuous. The next step therefore is a more comprehensive composition study which tests the hypothesis that mechanical properties may be improved by particle aggregation.

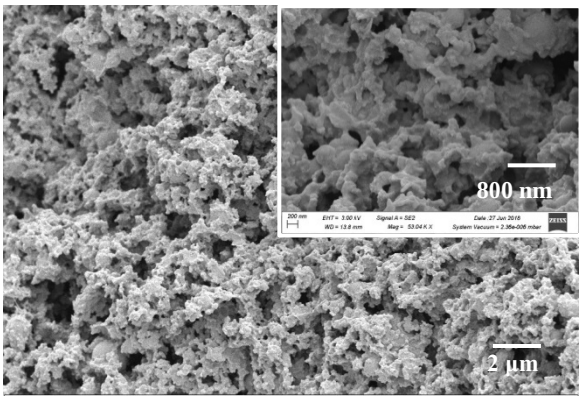

Figure 5-2 SEM image of SEBS/MaPP/particles with composition 70/20/10 prepared with a Brabender batch mixer

The sample quantities prepared by the batch mixer were insufficient for molding, so a Twin-Screw Extruder (TSE) as shown in Appendix Figure D-1 was used to mix the samples for this composition study. This provided samples in large quantities, which were then injection molded into bars. The samples prepared in the TSE-Injection Molder were also prepared in a two-

step procedure. SEBS pellets, MaPP pellets and silica particles were premixed together before being fed to the hopper of the TSE. The TSE was first preheated to 285^{o}C and fed with the premixed sample. The blended sample was extruded as a strand, cooled in a water bath and processed into pellets by a pelletizer. The sample pellets were fed into an injection molder at 285^{o}C and molded into dog-bone bars for later mechanical properties measurements. The dog-bone samples were tested for tensile and flexural modules, using tensile and three-point tests respectively. All the processing and tensile testing were conducted by undergraduate researchers at the Penn State University, Erie.

A total of 10 samples consisting of 2 pure polymers, 4 particle-filled polymers, 3 particle-filled polymer blends and 1 immiscible polymer blends were blended by TSE and injection molded into bars for flexural and tensile modulus measurement. The mechanical properties of the two pure polymers served as a reference to judge the properties of the blended samples. The compositions of 3 particle-filled immiscible polymer blends were selected to explore the mechanical properties of the SEBS phase by the aggregation of particles using capillary forces in the presence of MaPP. The ratio of MaPP to and particles of 5:10, 10:5 and 7.5:7.5 were specifically selected to achieve a combined phase dispersed within the SEBS continuous phase after injection molding. Based on our previous studies (chapter 2.0), such loadings are anticipated to force substantial aggregation with sufficient MaPP. In addition, 4 particle-filled polymers (without any MaPP) were molded to serve as controls. Lastly, the particle-free immiscible polymer blend sample was prepared as a comparison to particle-filled immiscible polymer blends in terms of mechanical properties.

Figure 5-3 shows the raw data of the tensile testing of SEBS/MaPP/particle blends at various compositions selected to have a total of 15% of the dispersed phase, i.e. the sum of the particle and the MaPP loading is 15 vol%. The addition of 15vol% MaPP to SEBS (without

particles) increased both the modulus and the ultimate strain, indicating much improvement in toughness. This is not surprising: polypropylene is stiffer than the MaPP (and hence the increase in modulus), and also highly ductile. Thus, as long as interfacial adhesion is strong, a simultaneous increase in modulus and ultimate strain is not surprising.

The mechanical properties at 15% particle loading (no MaPP) are also as expected: the modulus increases but the samples become brittle.

The mechanical properties of the three-component mixtures are unexpected: the ultimate strain reduces with particle addition, but so does the modulus. This is surprising because the particles are much stiffer than the MaPP: thus, a sample such as 85/5/10 has (on an average) a stiffer filler than the 85/15/0 sample.

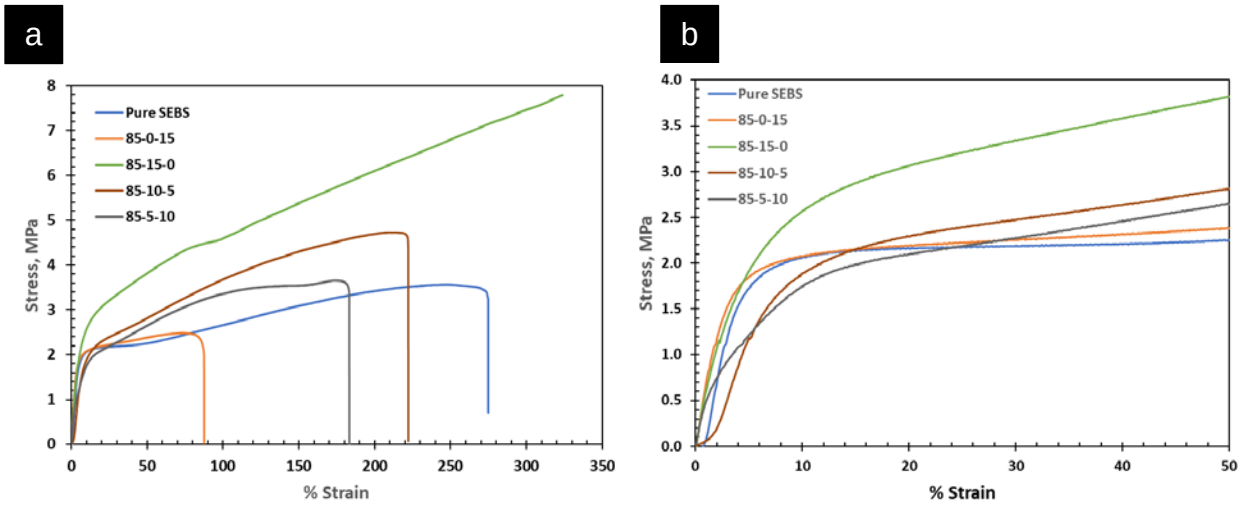

Figure 5-3 (a) Stress- strain curve of SEBS/MaPP/particles at various composition and (b) A zoomed in versoin of (a)

The mechanical properties (flexural and tensile modulus) measured from all the 10-sample composition are shown in Figure 5-4. The trends of modulus seen from flexure tests are the same as from tensile tests: the modulus of the 85-15-0 sample is higher than of the samples with particles. To understand the changes in mechanical properties, the microstructure of the prepared ternary systems was examined.

In Figure 5-5a as expected, a uniform dispersion of 15vol% particles in the SEBS matrix phase was observed. From Figure 5-5b with SEBS/MaPP/particles mixture with composition of 85/5/10, the SEBS is the only continuous phase with MaPP and particles as the dispersed phase. A non-uniform dispersion of particles on the sheet of MaPP as shown in Figure 5-5b suggests inefficient mixing. Likewise, in Figure 5-5c which has a composition of 85/10/5, a continuous phase of SEBS was created with the MaPP and particles phase forming huge particle aggregates which was also indicates ineffective mixing. A prominent situation of inefficient mixing was observed in SEBS/MaPP/particles with composition of 85/15/0 as shown in Figure 5-5d. Instead of the expected morphology of either MaPP dispersed in rubber or cocontinuous morphology, a core shell structure of the polymers was formed as shown in Figure 5-5d. The core-shell structure is made up of a core SEBS and a shell of MaPP. The core-shell structure was likely formed under high shear mixing in the TSE and injection molder due to viscosity mismatch between SEBS and MaPP. (i.e SEBS has high viscosity with melt index of “no flow” and MaPP of lower viscosity with melt index of 150kg/10min). Due to viscous segregation [156, 157] of the immiscible polymer blends, the mechanical properties measured from the molded samples were not a true representation of blended ternary mixtures at various composition.

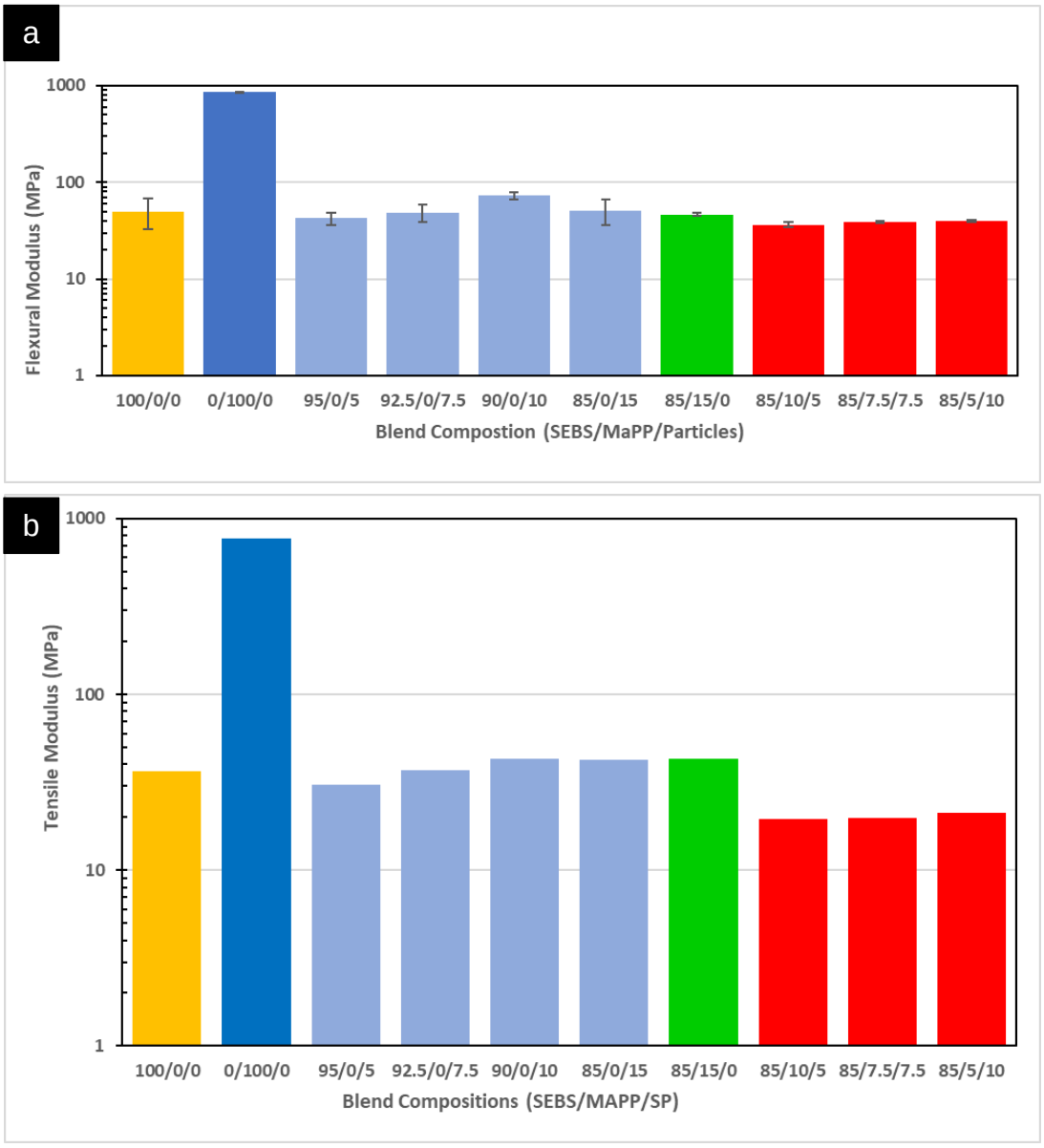

Figure 5-4 (a) Flexural and (b) tensile modulus of SEBS/MaPP/particles at various compositions

The chief problem with the processing seems to be poor mixing. Ironically, the TSE was selected for this research precisely because such extruders are usually known to give excellent mixing. But furthermore, it is possible that the injection molding step poses a significant problem

since viscous segregation simply cannot be avoided. Thus, we conclude that the TSE followed by injection molding is not suitable to test effect of particle aggregation on the properties.

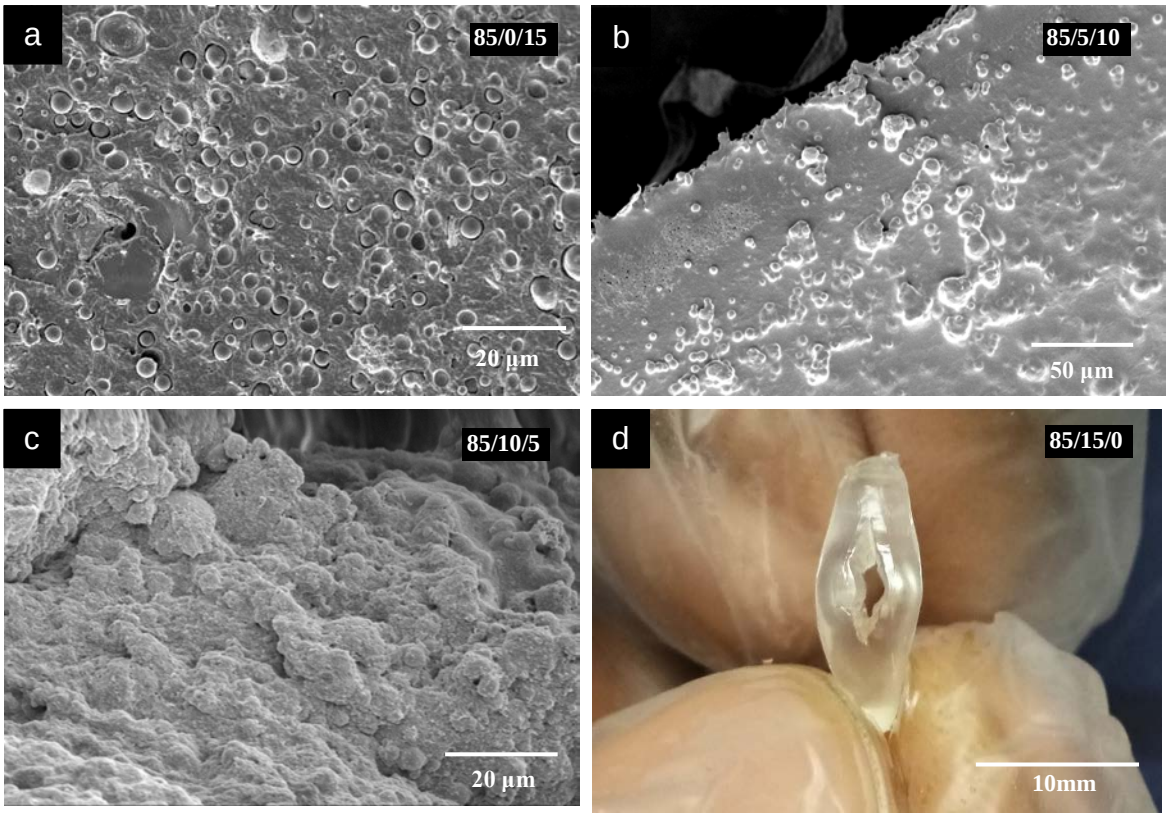

Figure 5-5 SEM images of SEBS/MaPP/particles with compositions (a) 85/0/15 (b) 85/5/10 (c) 85/10/5 and (d) Image of SEBS/MaPP/particles of 85/15/0, the whole in the sample was created after SEBS was dissolved out, showing a core-shell structure prepared with a twin screw extruder and injection molded.

One approach to avoid viscous segregation is to prepare samples with a Brabender batch mixer and then compression mold sheets from which dogbone-shapes samples can be cut. Another is to find a pair of materials with a modest viscosity mismatch.

6.0 Future Work

In this thesis, the central idea of using capillary forces to aggregate particles have been explored and applied in different ways. This included the composition-morphology relation of particle filled immiscible polymer blends which involved the creation of a composition-morphology map with fused and fumed silica as the particles used. One important finding is the fumed silica increasing the cocontinuity range of immiscible polymer blends. Capillary aggregation was also exploited with molten metals to obtain conductive plastics. There are still on-going researches in our group which will still exploit aggregation of particles as briefly explained in the next two sections.

6.1 Macroporous Materials from Sintering Capillary Aggregates Network

The fundamental concept of ternary mixture with preferentially wettable particles towards one liquid phase with the capillary aggregate network morphology formed can be explored to create sintered macroporous materials. The capillary aggregate networks appear because the wetting fluid engulfs the particles to form a combined phase with high particle loading and hence solid-like properties. The goal of this study is to sinter the particles and also remove one or both of the polymers to leave behind a macroporous sintered network. The central idea is that the macroporous network, being tightly packed, may have sufficient green strength that they may be sintered while retaining their macroporous structure.

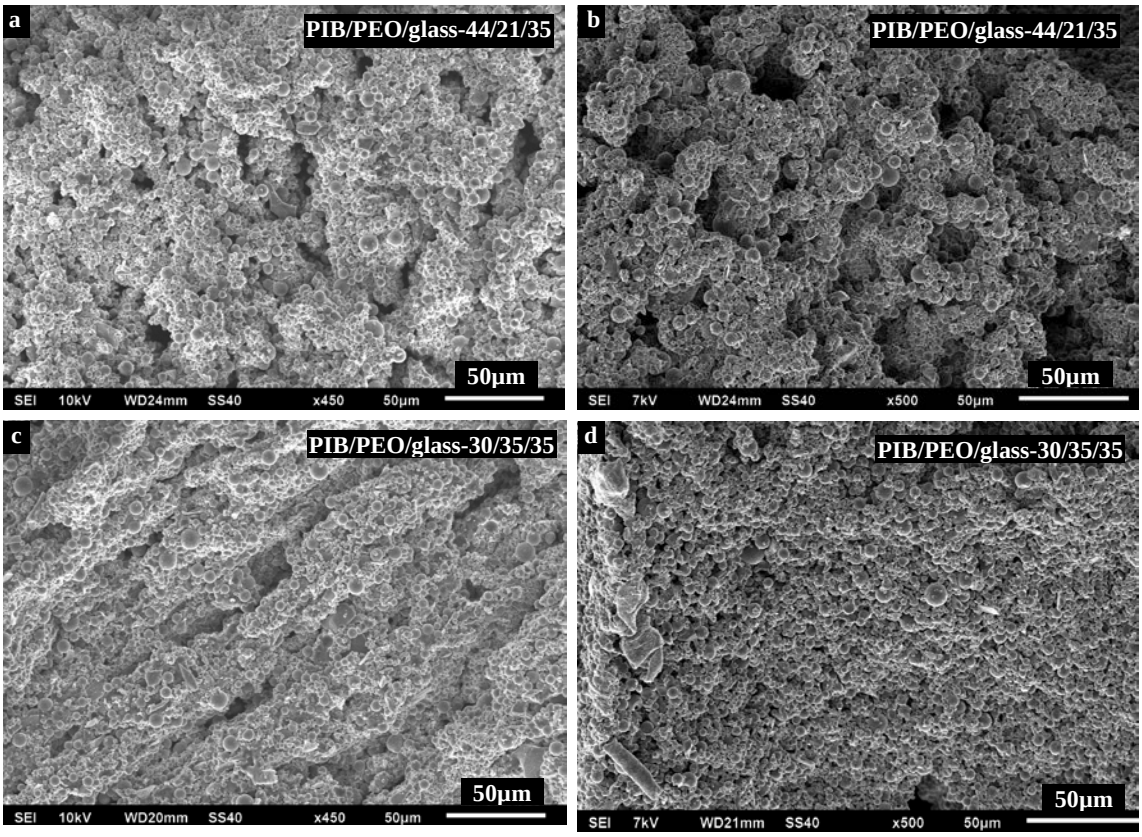

Figure 6-1 SEM images of PIB/PEO/glasss particles mixtures with compositions listed at the top right. (a&b) PIB phase extracted and (c&d) the same samples after sintering.

Initial experiments with polyisobutylene (PIB), polyethylene oxide (PEO) and spherical glass particles were conducted. They suggest that when the combined phase of PEO+glass particles (Figure 6-1c) has liquid-like rheology (PEO:glass particle ratio of 1), the capillary aggregates collapse after sintering (as shown in Figure 6-1d). Figure 6-1a with PEO:glass particle ratio of 0.6 have solid-like rheology which forms self-standing macroporous network after sintering (Figure 6-1b). In summary, sintering seems possible, but only a very narrow range of compositions allows sufficient stability during sintering to allow the macroporous network to survive. The results from chapter 3.0 show that fumed silica creates capillary aggregate network over a wide range of PEO:

particle ratio and at a much lower particle loading than with spherical particles. With such results, research is currently on-going on how to fabricate macroporous materials using fumed silica capillary aggregate network. Preliminary results of capillary aggregate network of PEO and fumed silica and sintered fumed silica (macroporous material) are shown in Figure 6-2a and Figure 6-2b respectively.

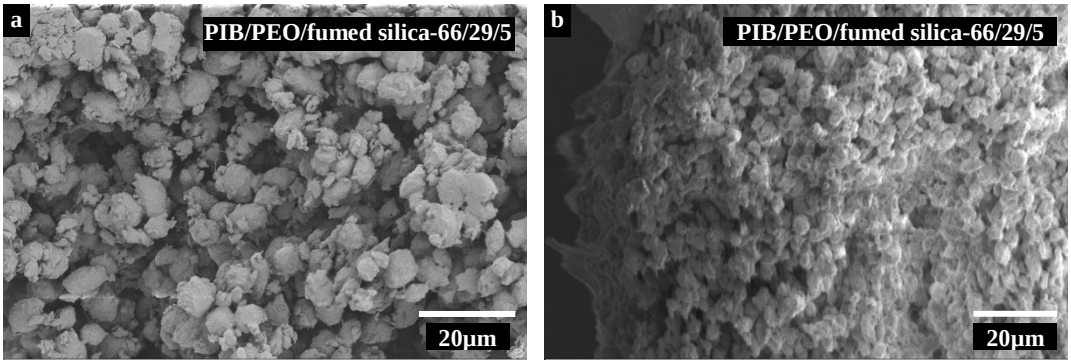

Figure 6-2 SEM images of PIB/PEO/fumed silica particles mixtures with (a) PIB phase extracted and (b) fumed silica sintered at 1130ºC. The PIB/PEO/fumed silica ratio are listed at the top right of each image.

6.2 Small Molecule Mixtures

The composition morphology relation developed for particle filled polymer blends was compared with small molecule ternary mixtures such as oil/water/particles system. In previous work and currently in this dissertation, composition-morphology relation of particle-filled polymer blends have been studied. Similar extensive studies have been performed on oil/water systems [12, 15, 158]. Both systems have significant similarities and differences in terms of one-phase continuous with dispersion and phase inversion behavior respectively. Both systems show one

phase of fluid been dispersed in another continuous phase based on composition with the continuous phase been the majority. The morphology on each side of the phase inversion composition comprises spherical drops of liquid in fluid (e.g. oil in water or vice versa). Particle aggregation in the presence of wetting fluid exist in both system due to capillarity. In oil/water mixtures, phase inversion is usually abrupt (i.e. appears in a narrow composition range with the phase inversion composition depending on mixing conditions). In contrast, blends of two immiscible polymers are often characterized by gradual phase inversion over a wider range of compositions within which co-continuous morphologies appear.

Immiscible polymer blends are processable and have high viscosity. However, oil/water mixtures have low viscosities and difficult to process. At certain compositions of oil/water mixtures with the presence of particles can realized yield stress to give solid-like properties, thereby making oil/water mixtures possible to process. At such compositions, spherical and fumed silica (non-spherical fractal-like) particles may be used to make capillary aggregates. The capillary aggregates could then be used to build porous networks that can survive flow. Such conditions can be used to explore the processability of oil/water/particle mixtures with open pore structures, making extrudates and molded pellets of ternary mixtures.

Appendix A Supplementary Material For "A Composition-Morphology of Particle-Filled Immiscible Polymer Blends"

Appendix Table A-1 Compositions for the binary and ternary blends. All compositions are listed in vol%

ϕ_{PIB}	ϕ_{PEO}	ϕ_{p}	ϱ	$\phi_p^{combined}$
96.25	3.75	0	0	0
81.25	18.75	0	0	0
77.78	22.22	0	0	0
66.67	33.33	0	0	0
61.1	38.9	0	0	0
55.56	44.44	0	0	0
50	50	0	0	0
44.44	55.56	0	0	0
37.5	62.5	0	0	0
33.33	66.67	0	0	0
22.22	77.78	0	0	0
12.5	87.5	0	0	0

Appendix Table A-1 (continued)

ϕ_{PIB}	ϕ_{PEO}	ϕ_{p}	ϱ	$\phi_p^{combined}$
88.4	1.6	10	0.16	0.86
87	3	10	0.30	0.77
84	6	10	0.60	0.63
80	10	10	1.00	0.50
70	20	10	2.00	0.33
60	30	10	3.00	0.25
55	35	10	3.50	0.22
50	40	10	4.00	0.20
40	50	10	5.00	0.17
30	60	10	6.00	0.14
20	70	10	7.00	0.13
77	3	20	0.15	0.87
65	15	20	0.75	0.57
55	25	20	1.25	0.44
50	30	20	1.50	0.40
45	35	20	1.75	0.36
40	40	20	2.00	0.33
30	50	20	2.5	0.29
10	70	20	3.50	0.22

Appendix Table A-1 (continued)

ϕ_{PIB}	ϕ_{PEO}	ϕ_{p}	ϱ	$\phi_p^{combined}$
65.3	4.7	30	0.16	0.86
55	15	30	0.5	0.67
50	20	30	0.67	0.60
35	35	30	1.17	0.46
26.25	43.75	30	1.46	0.41

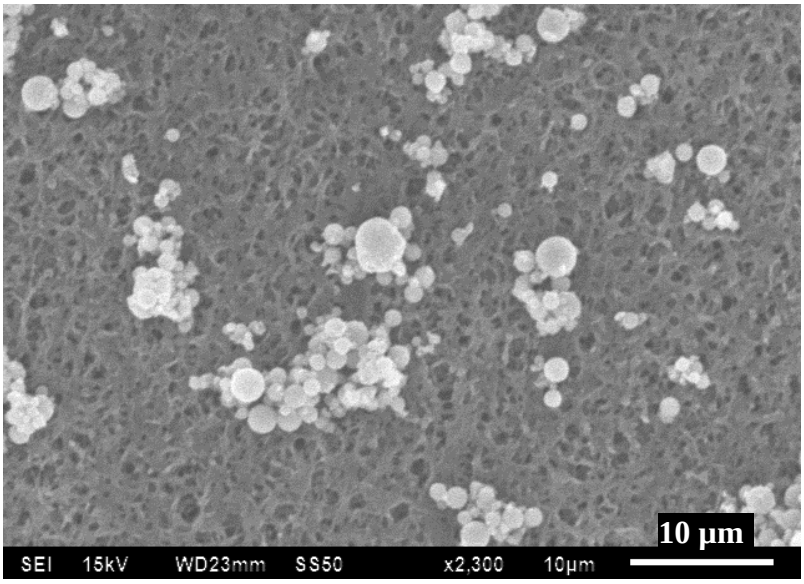

Appendix Figure A-1 SEM image of the silica particles

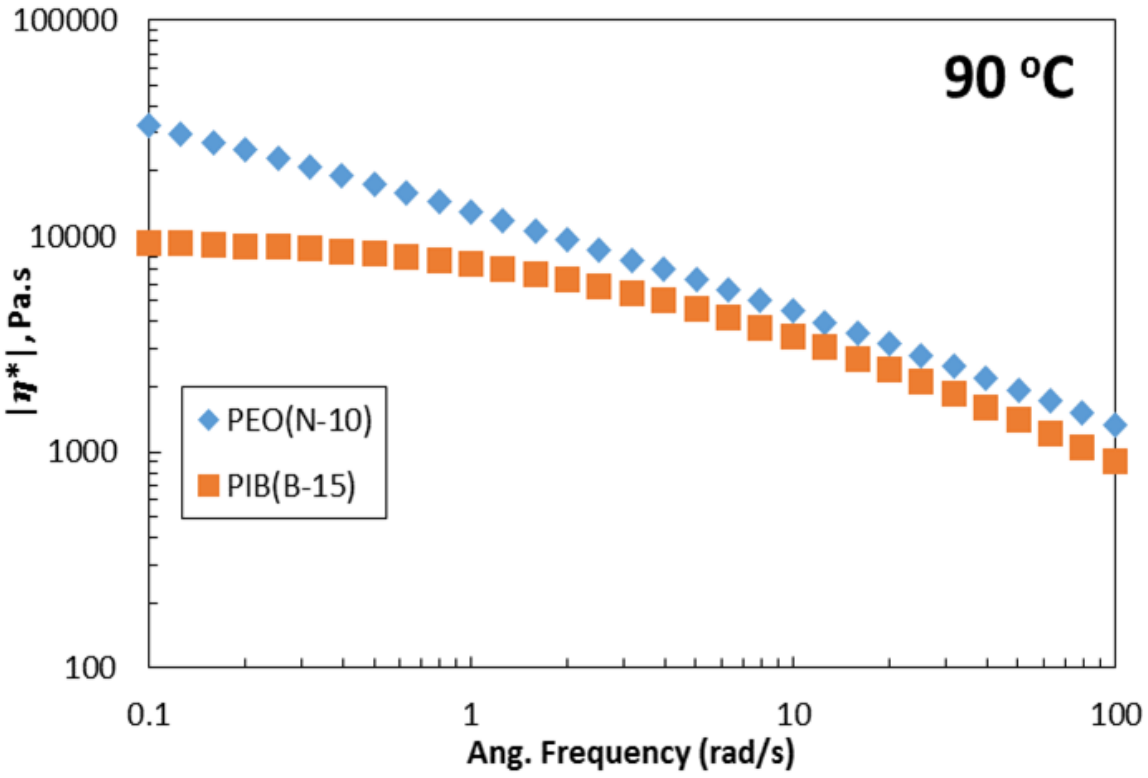

Appendix Figure A-2 Dynamic Oscillatory viscosity of PIB and PEO obtained from frequency sweep experiments

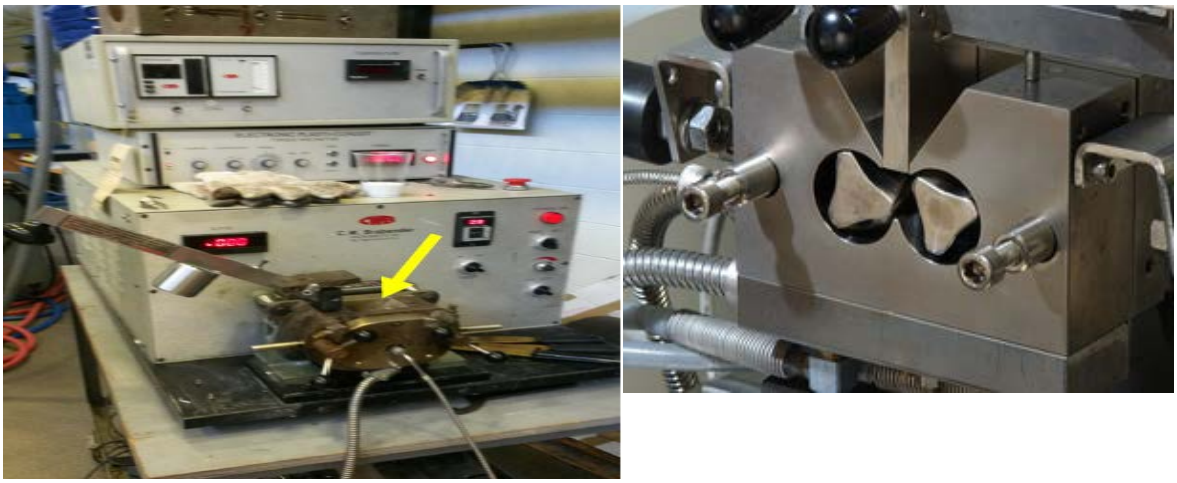

Appendix Figure A-3 Brabender Electronic Plasti-Corder batch mixer. The *left* image is an external view of the mixer with the yellow arrow point to the feed inlet. The *right* image is an internal view showing the two rotating blades

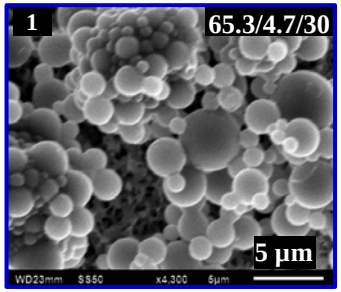
1
65.3/4.7/30
5 µm

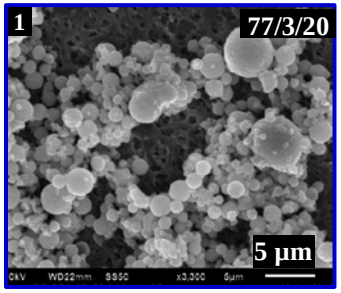
1
77/3/20
5 µm

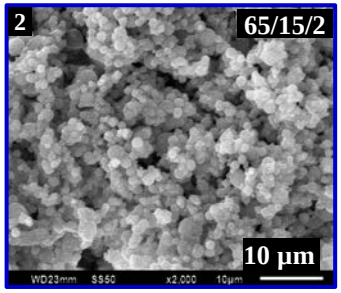
2
65/15/2
10 µm

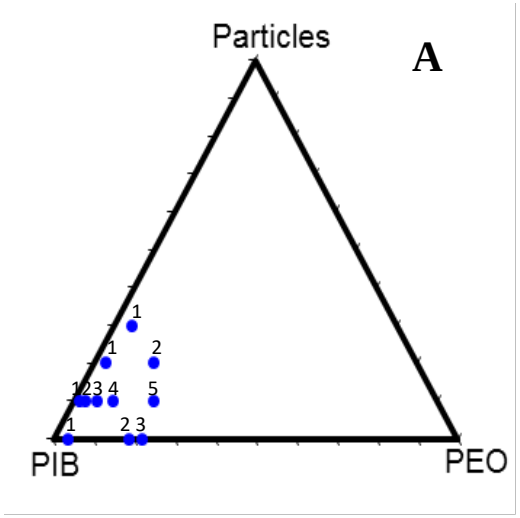
Particles
A
PIB
PEO
1
1
2
1 2 3 4
5
1
2 3

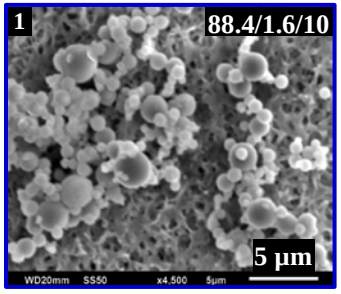
1
88.4/1.6/10
5 µm

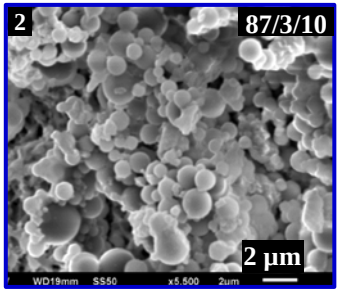
2
87/3/10
2 µm

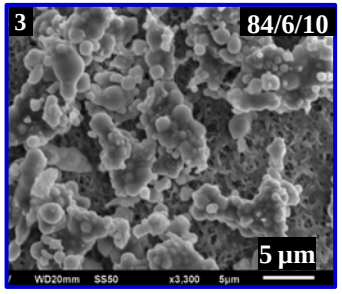
3
84/6/10
5 µm

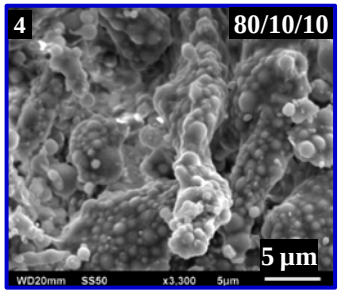
4
80/10/10
5 µm

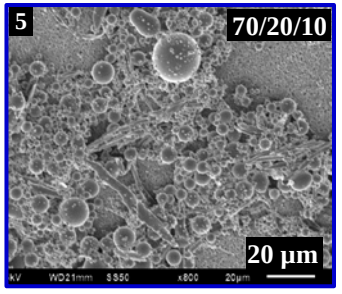
5
70/20/10
20 µm

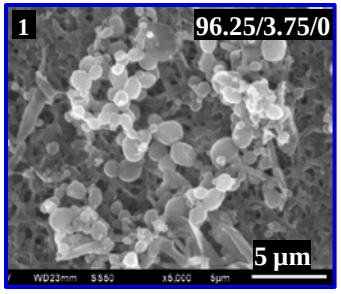
1
96.25/3.75/0
5 µm

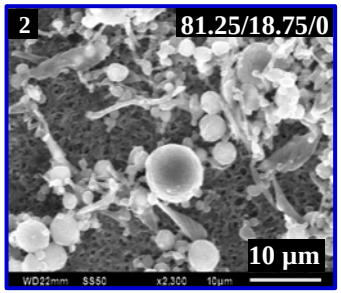
2
81.25/18.75/0
10 µm

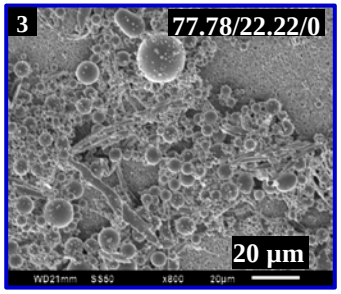
3
77.78/22.22/0
20 µm

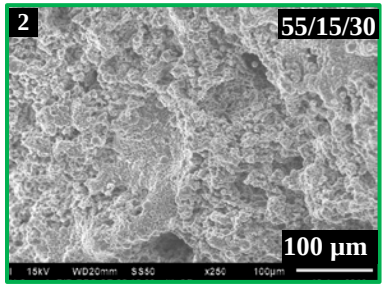
2
55/15/30
100 µm

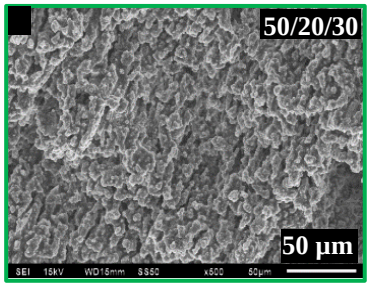
50/20/30
50 µm

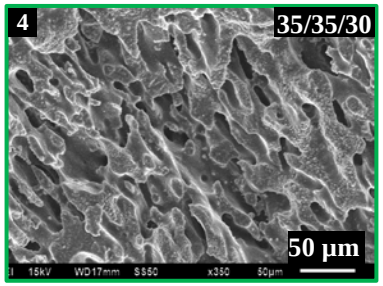
4
35/35/30
50 µm

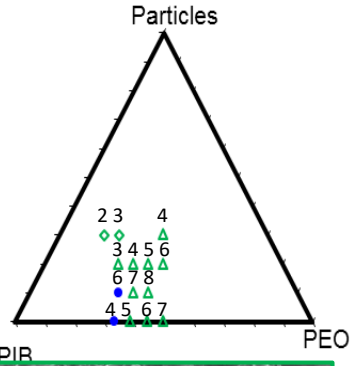
Particles
2 3 4
3 4 5 6
6 7 8
4 5 6 7
PEO
PIB

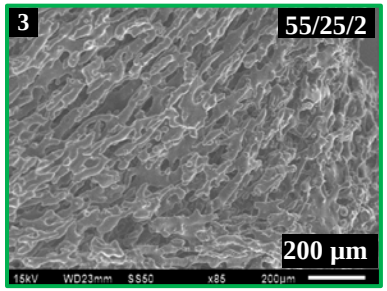
3
55/25/2
200 µm

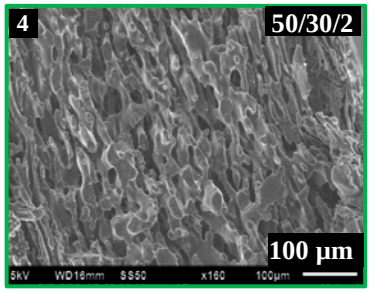
4
50/30/2
100 µm

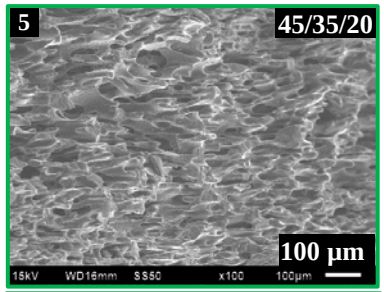
5
45/35/20
100 µm

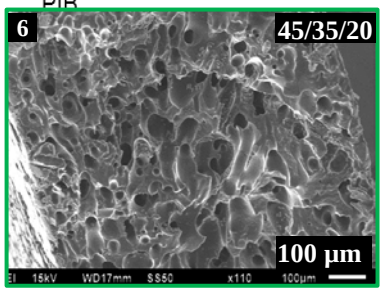
6
45/35/20
100 µm

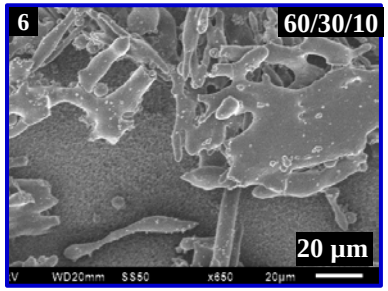
6
60/30/10
20 µm

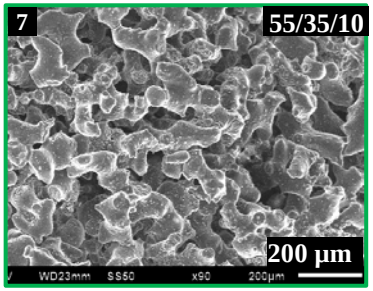
7
55/35/10
200 µm

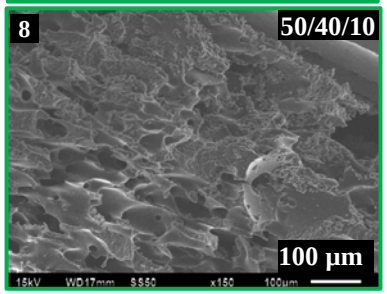
8
50/40/10
100 µm

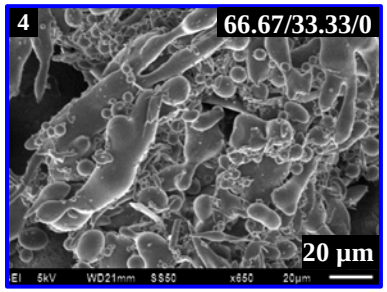
4
66.67/33.33/0
20 µm

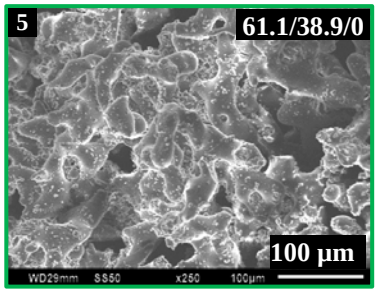
5
61.1/38.9/0
100 µm

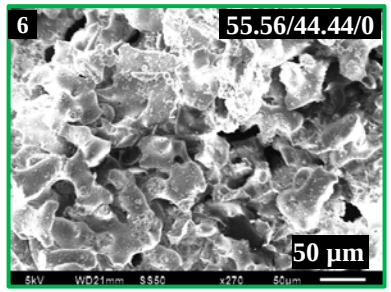
6
55.56/44.44/0
50 µm

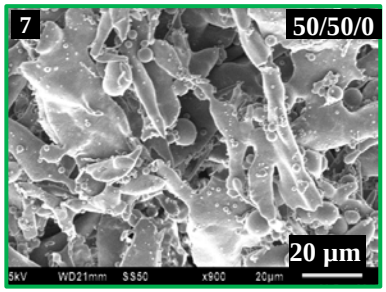
7
50/50/0
20 µm

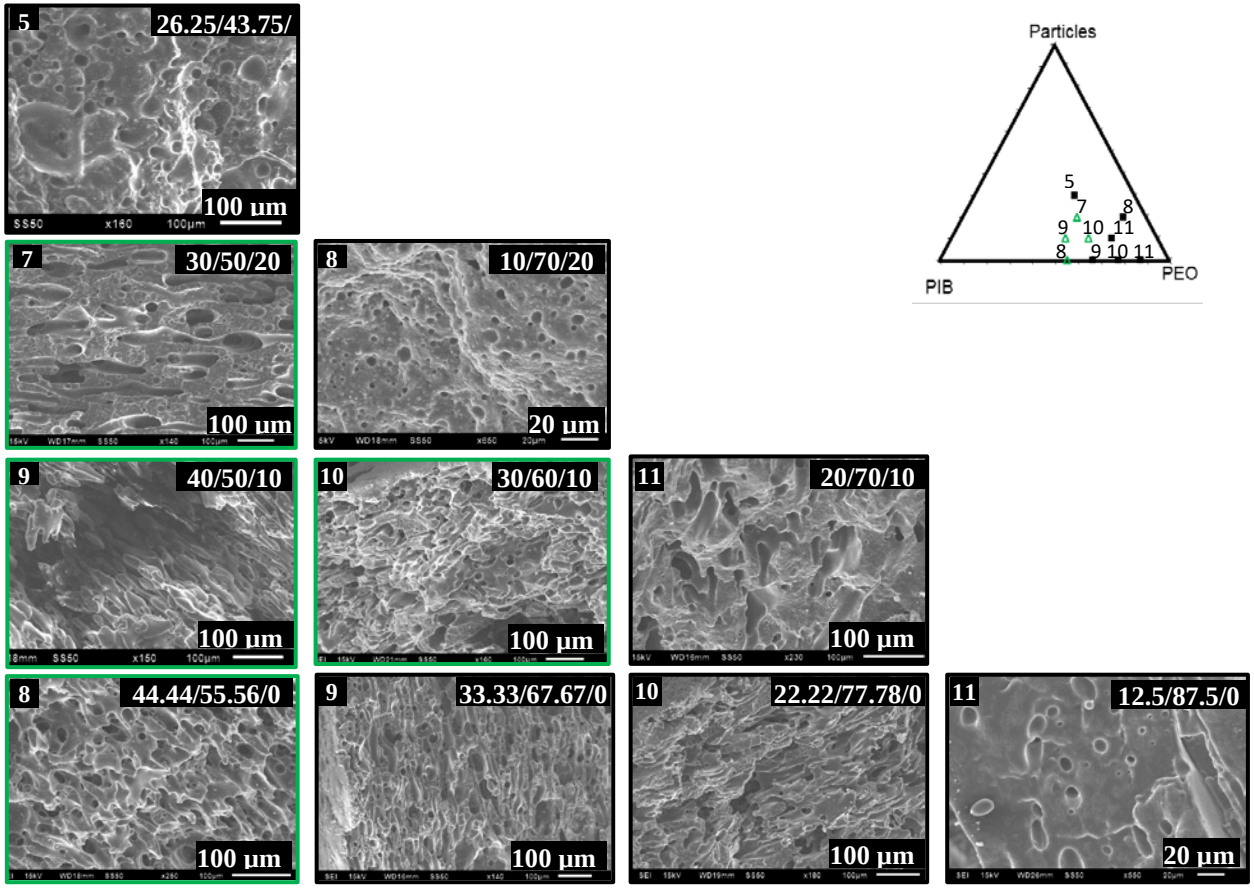

Appendix Figure A-4 Composition-rheology map for blends of PIB, PEO and silica up to 30vol% silica and representative images of all the samples. Compositions on the axes are volume fractions

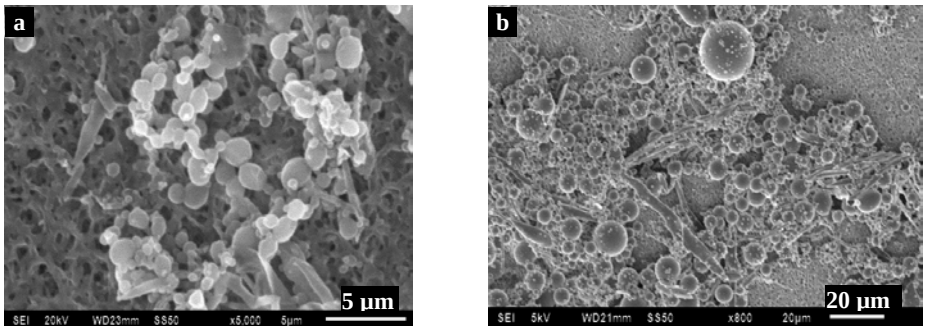

Appendix Figure A-5 SEM images showing increasing in PEO dispersed phase size with increasing PEO loading in the absence of particles: (a) PIB/PEO/silica – 96.2/3.8/0 (b) PIB/PEO/silica – 78/22/0

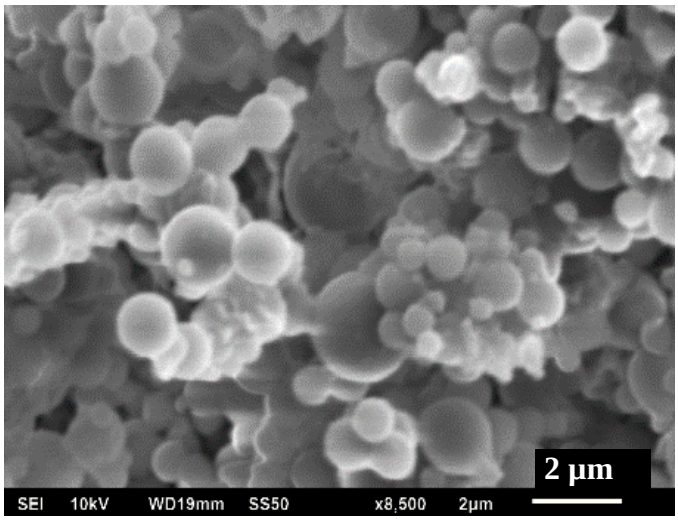

Appendix Figure A-6 SEM image of the dispersed phase (particles and PEO) of the sample PIB/PEO/silica – 87/3/10 after removal of PIB. The particles are bound together by PEO. This same figure appears as the inset to Figure 2-2a

The samples in Appendix Table A-2 were compressed into thin sheets and the PIB was washed out with heptane. The undissolved combined PEO+particle phase was washed with additional heptane, then remelted at 95ºC and compression-molded into discs for rheometry. Rheological experiments were conducted on a TA Instruments rheometer in a 25 mm parallel plate

geometry at a gap of ~1.0 mm at 95℃. Since these compression-molded combined phases have undergone exactly the same thermomechanical mixing history as the ternary blends examined, their rheological properties (Appendix Figure A-6 below) are identical to the rheology of the combined phases in the ternary blends

Appendix Figure A-6a-c shows that at a ϱ of 2.5 and 1.45, the samples have liquid-like rheology, whereas at $\varrho = 1.25$, the rheology becomes typical of a paste ($G' > G''$ at small strain, with a crossover as strain increases). The values of the low-frequency moduli as a function of ϱ are shown in Appendix Figure A-6d. These features (storage modulus exceeding loss modulus at small strain, and a crossover at modest strain) is typical of particle suspensions with high particle loading and reflect the paste-like rheology of these combined phases. The last sample in the table below, upon melting, had a crumbly consistency and could not be molded without significant voids, and hence rheometry was not attempted. Yet, this crumbly consistency itself is perhaps the strongest evidence of their strongly solid-like behavior.

Appendix Table A-2 Compositions for the ternary blends used for rheology experiment

ϕ_{PIB}	ϕ_{PEO}	ϕ_{p}	ϱ	$\phi_p^{combined}$
30	50	20	2.5	0.29
26.25	43.75	30	1.45	0.40
55	25	20	1.25	0.44
80	10	10	1.0	0.5

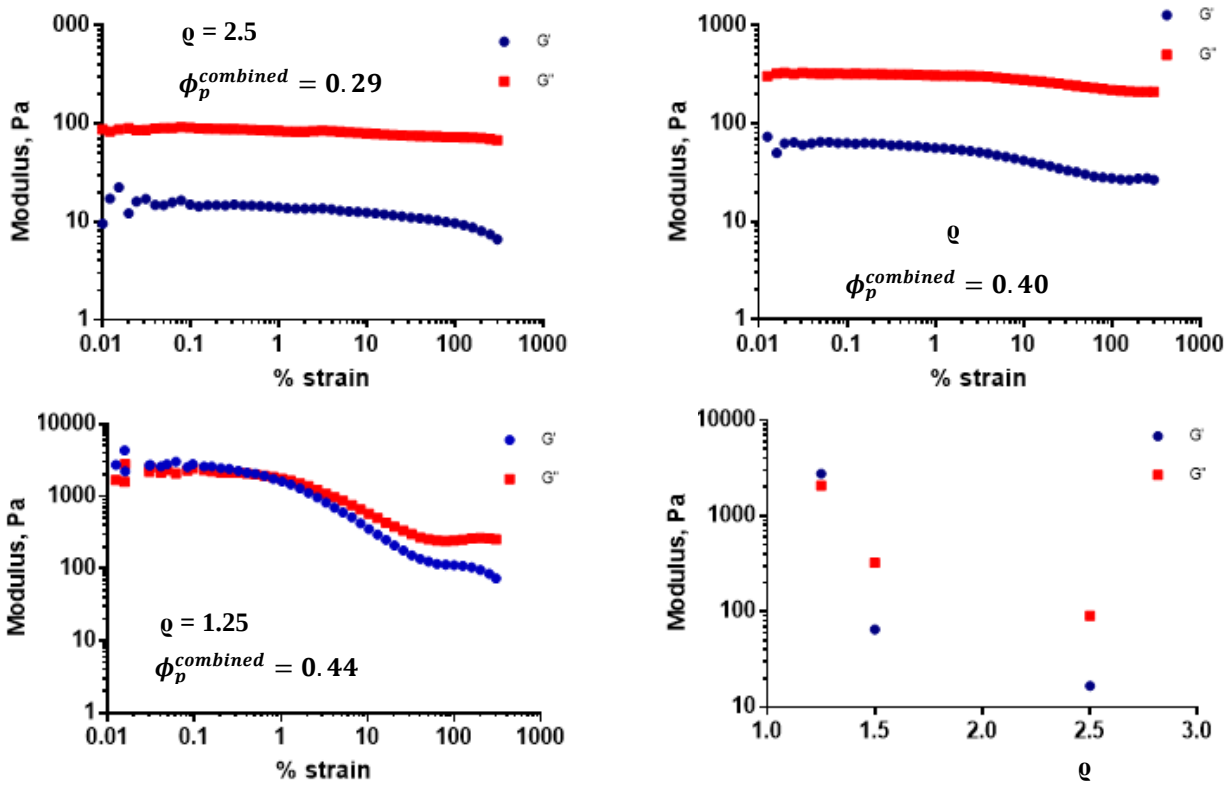

Appendix Figure A-7 Linear viscoelastic moduli G' and G" of suspensions of particles in PEO with strain at different ϱ-values

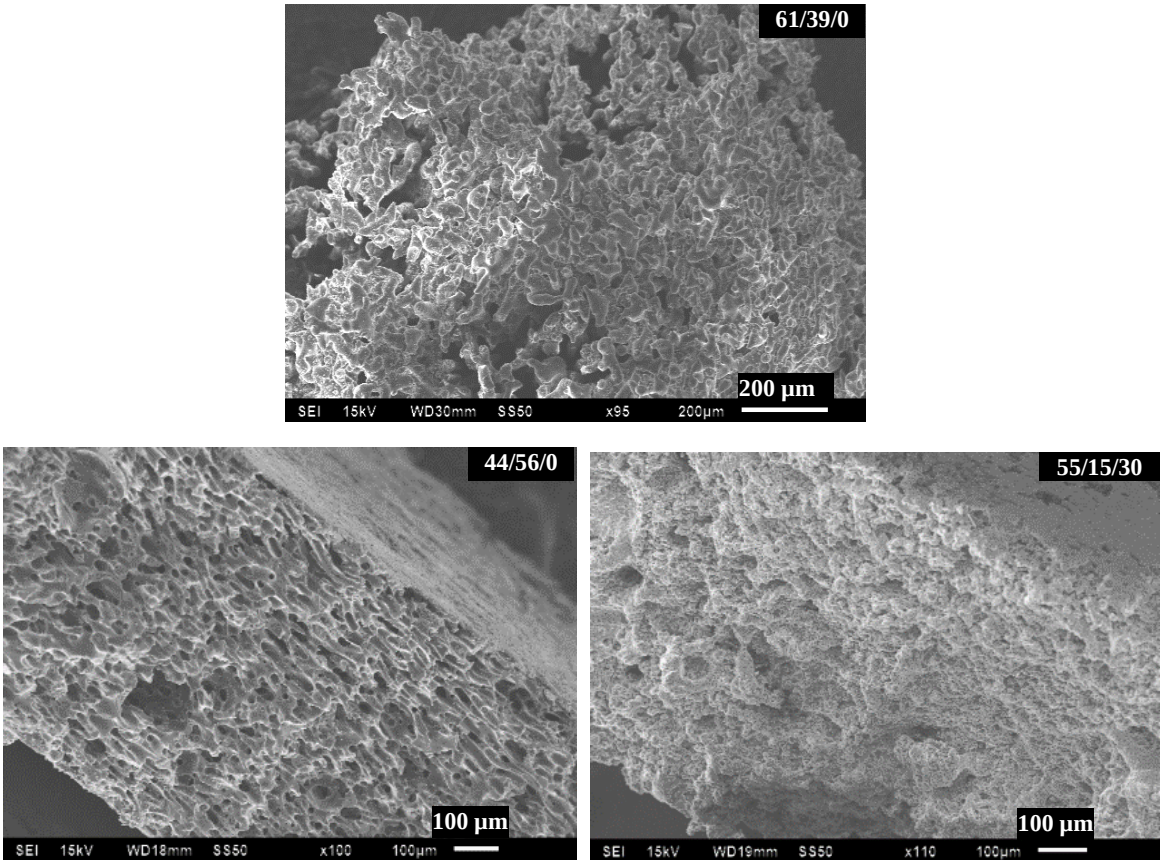

Appendix Figure A-8 Top: An example of a sample that is on the verge of losing continuity of the PEO+particle phase. Such samples are marked with circles in Figure 2-6. Bottom Samples that retain intergrity after immersion in octane, indicating that they are "firmly" in the cocontinuous regime. Bottom left is classifiedas cocontinuous, whereas bottom right as "capillary aggregate network"

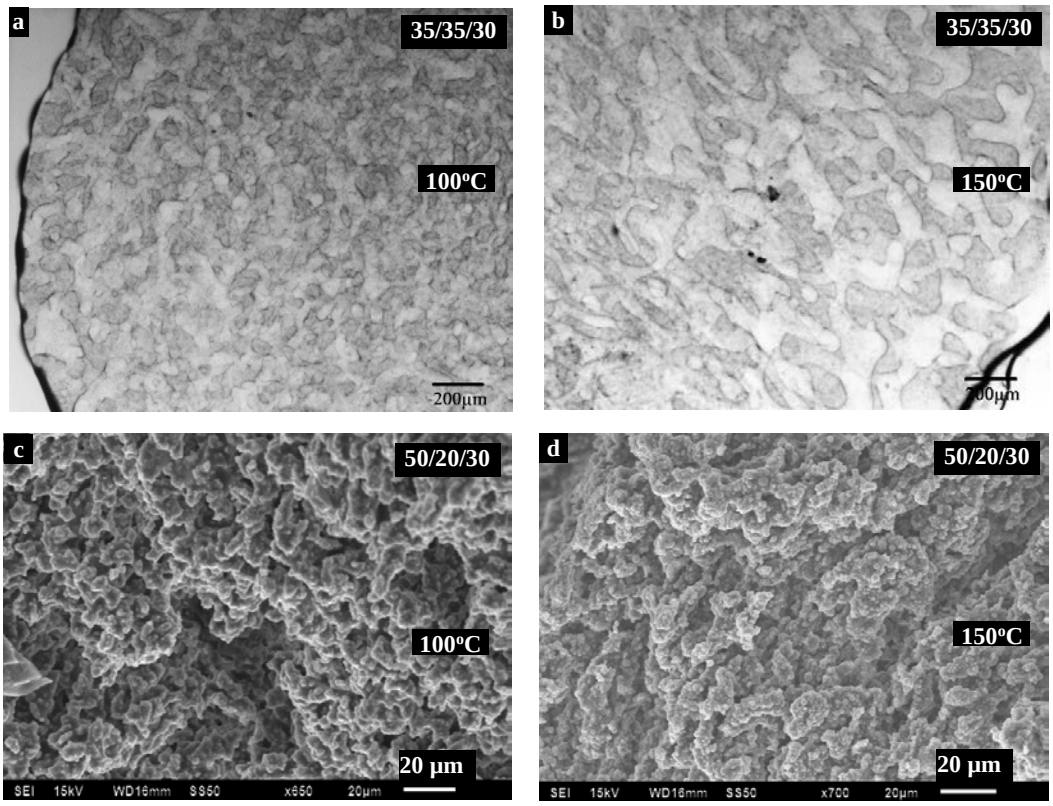

Appendix Figure A-9 Images of cocontinuous and percolating capillary aggregates upon annealing

A.1 Applying the Co-continuity Criterion for Binary Polymer Blends to a Particle-Filled Immiscible Blend

Here we present a simple model for how particles that are fully-wetted by one phase may affect phase inversion. The essential idea is that since the particles are entirely engulfed by the PEO, as a first approximation, the three-phase blend may be treated as an "effectively" two-phase blend of PIB, and the combined phase of (particles+PEO). Thus, the existing knowledge on phase inversion in two phase polymer blends may be applied. The best-known phase inversion criterion,

the Paul and Barlow model,[159] for binary blends states that the ratio of compositions at phase inversion equals the viscosity ratio. Applying this to the particle-free blend, we expect that

$$\frac{\phi_{PEO}}{\phi_{PIB}} = \frac{\eta_{PEO}}{\eta_{PIB}} \tag{A-1}$$

Treating the ternary blend as an "effective" two phase blend, we get:

$$\frac{\phi_p + \phi_{PEO}}{\phi_{PIB}} = \frac{\eta_{combined}}{\eta_{PIB}} \tag{A-2}$$

Since the combined phase is simply a suspension of spherical particles in PEO, one may use the well-known Krieger Dougherty equation for the rheology of hard sphere suspensions:

$$\eta_{combined} = \eta_{PEO}\left(1 + \frac{\phi_p^{combined}}{\phi_m}\right)^{-2.5\phi_m} \tag{A-3}$$

where ϕ_m (which corresponds to the volume fraction at which the viscosity diverges) is usually assigned a value of 0.67. Since $\phi_{eff} = \frac{\phi_p}{\phi_p + \phi_{PEO}}$, the above equations can be combined to obtain

$$\frac{\left(\phi_p + \phi_{PEO}\right)}{\left(1 - \phi_{PEO} - \phi_p\right)} = \frac{\eta_{PEO}}{\eta_{PIB}}\left(1 + \frac{\phi_p}{\phi_p + \phi_{PEO}}\frac{1}{\phi_m}\right)^{-2.5\,\phi_m} \tag{A-4}$$

Thus, at any given particle loading, one may obtain the PEO volume fraction (and hence the PEO:PIB ratio) needed for phase inversion. We reiterate that the underlying physics in the above equations captures two effects as particle loading is increased: the fact that particles increase the volume of combined phase, and that particles increase $\phi_p^{combined}$ (and hence the viscosity) of the combined phase.

The complex viscosity for the pure components shown in Appendix Figure A-2, and fortuitously, except at the lowest rates, the complex viscosity of both components decreases in

tandem. Thus, while we do not know the precise range of rates experienced by the melts in the Brabender mixer, over a wide range of shear rates, the relative viscosity $\frac{\eta_{PEO}}{\eta_{PIB}}$ is roughly 1.35, nearly independent of shear rate. Substituting this value in Eq. A4, the line of Appendix Figure A-6 is obtained. The central conclusion of this analysis is that if the ternary system is treated as an effective binary system, the particles increase the PEO:PIB ratio needed for phase inversion.

A glance at Appendix Figure A-6 shows poor agreement of Eq. A4 with the phase inversion data, even at the lowest particle loading. Any modest error in $\frac{\eta_{PEO}}{\eta_{PIB}}$ will not change this conclusion significantly. Thus, we conclude that the effects of particles on the phase inversion are more complex than can be accounted by their effect on volume fraction and viscosity of the combined phase.

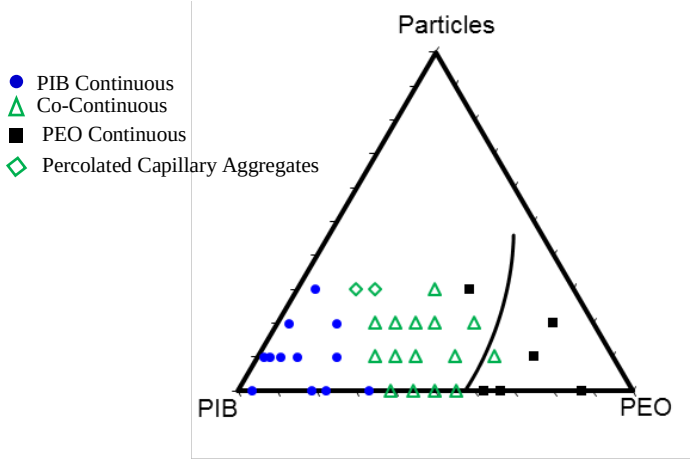

Appendix Figure A-10 A classification of phase continuity on the ternary composition diagram, and comparison of the phase inversion prediction E. A4 (*continuous black line*). The points are identical to those in Figure 2-6 in the main text.

Appendix B Supplementary Material For "Fumed Silica Induces Co-continuity Across A Wide Composition Range in Immiscible Polymer Blends"

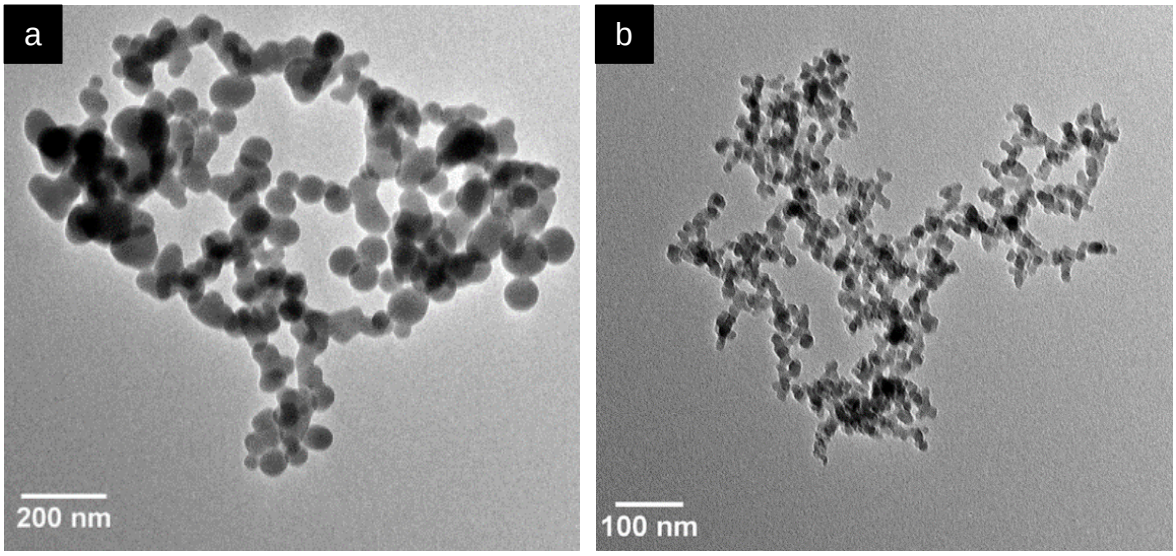

Appendix Figure B-1 TEM images of the fumed silica particles of (a) high and (b) low magnification, showing fractal-like and porous aggregate structures. The images are reprinted from Mulderig A., Beaucage, G., Vogtt, K., Jiang, H., & Kuppa, V. (2017). Quantification of branching in fumed silica. *Journal of Aerosol Science*, 109, 28-37 with copyright permission from Elsevier

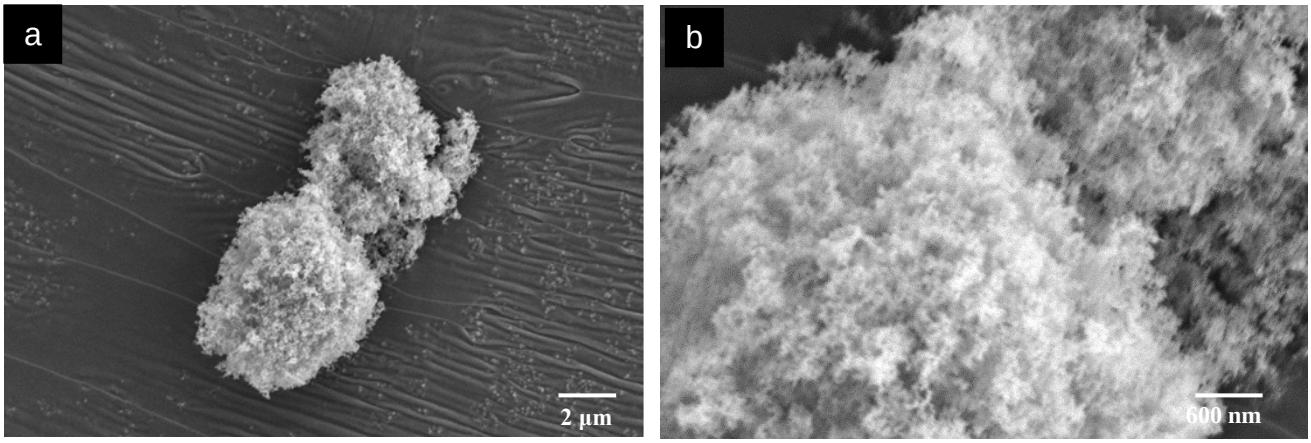

Appendix Figure B-2 SEM image of the fumed silica particles which are agglomerated at (a) low and (b) high magnification

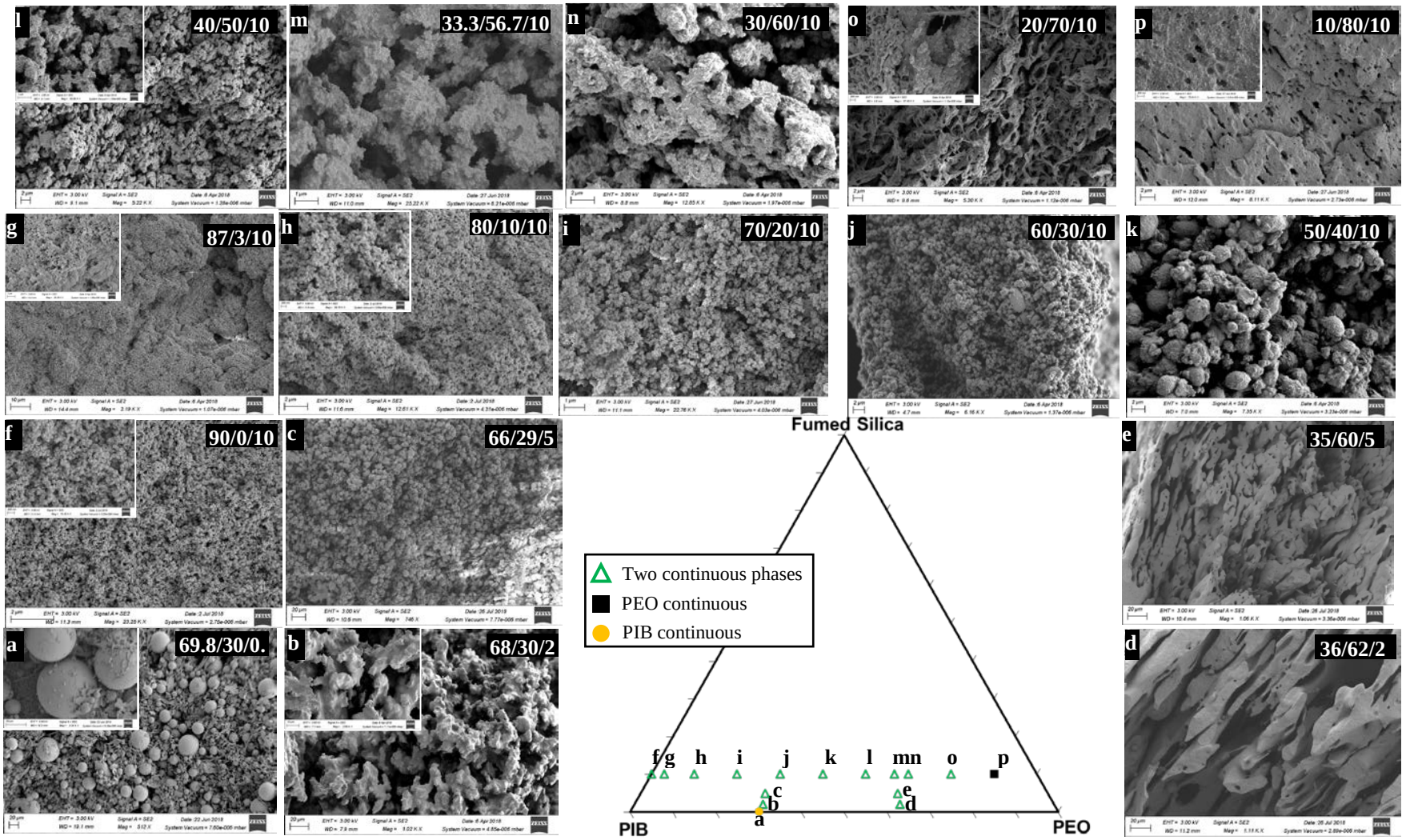

Appendix Figure B-3 Compositions examined in this research represented on a triangular composition diagram along with representative images of all the samples. The composition is noted at the top right of each image in the form PIB/PEO/silica

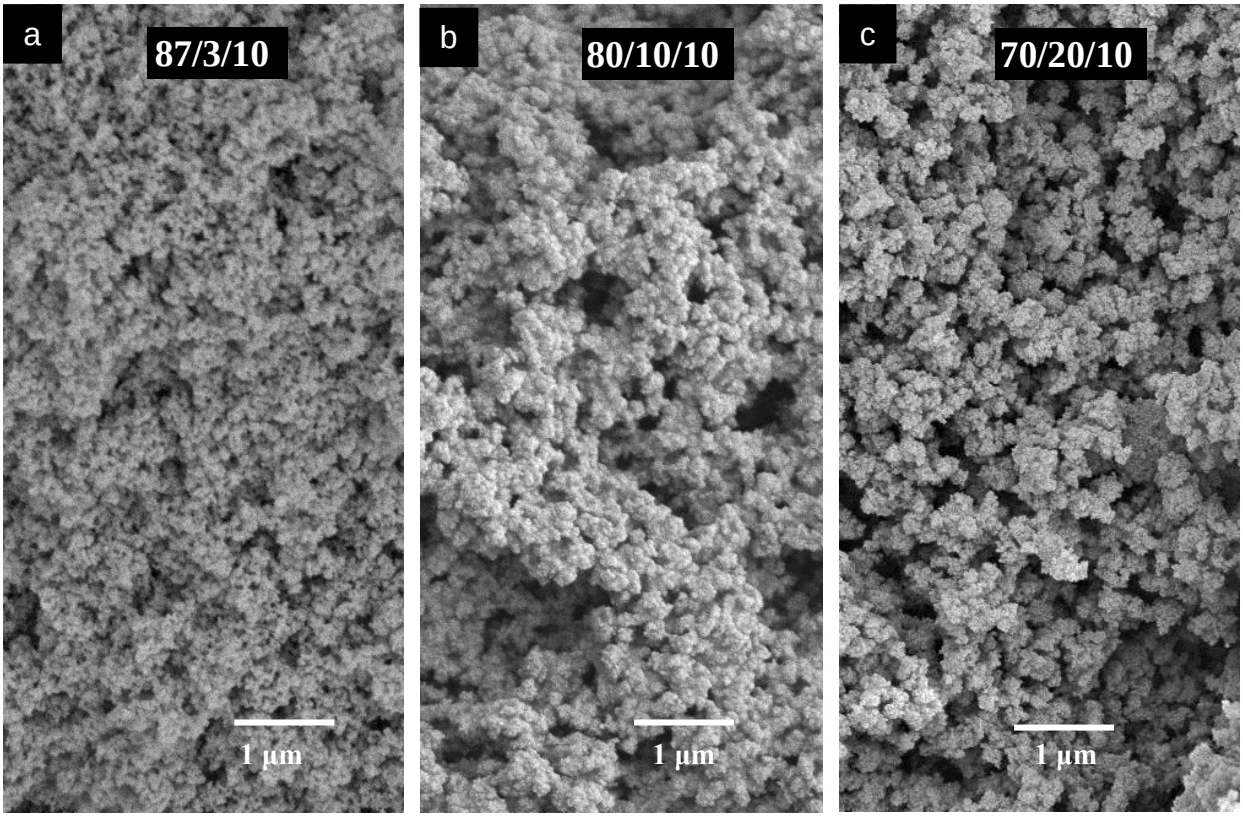

Appendix Figure B-4 Magnified version of some of the SEM images in Figure 3-3

B.1 Summary of rheology of the PEO+fumed silica combined phase

Most rheological experiments were performed on the PEO+particles combined phase that was extracted from the blends by washing out the PIB. This guarantees that we are measuring the rheology of the actual combined phases that exist in the blend. By extraction from blends with compositions PIB/PEO/particles – 36/62/2, 68/30/2, 20/70/10 and 33.3/56.7/10, PEO+particles phases with $\phi_p^{combined}$ values of 3.13%, 6.25%, 12.5% and 15% were realized. In all cases, the

combined phase remained intact after PIB extraction, i.e. each sample had two percolating phases. This was then compression-molded at 95°C under vacuum, and discs were cut out for rheometry. Incidentally, we also attempted to mold the combined phase extracted from the sample with composition PIB/PEO/silica=33.3/56.7/10 but were unsuccessful because the sample had a very crumbly consistency. One disadvantage of extracting the PEO+particles phase from ternary samples is that usually only a small quantity (several grams) remains after the PIB is removed. Therefore, an additional 50-gram batch of 10 vol% fumed silica mixed with PEO was also prepared directly in the Brabender batch mixer. This larger quantity permitted more detailed experiments, although with the caveat that this sample may differ slightly from the actual combined phase extracted from a ternary blend with a similar $\phi_p^{combined}$.

Initial tests were attempted with oscillatory rheometry. The use of parallel plates was not viable for most samples due to slip at the surface of the samples. Therefore, serrated parallel plates were used, but also proved unsuccessful. Specifically, samples with 10% or more of fumed silica were simply too solid-like to make good contact with the plates of the rheometer. Appendix Figure B-5 shows an example of a disc extracted from the sample after rheometry, and it is clear that the serrated parallel plates made good contact with only a portion of the discs despite applying a several newton normal force load.

We therefore turned to indentation tests, where although the deformation is not strictly rheometric, even highly solid-like materials can be tested, without being significantly affected by slip. The indentation test was conducted on the same rheometer using a cylindrical indenter of diameter 4 mm. Samples of 1.65 mm thickness were indented to a depth of 400 micron at a speed of 10 micron/s at 95 °C. The corresponding measurements of force are shown in Appendix Figure B-6. In all samples, the indentation force increased with time, and the magnitude of the force

increased sharply with fumed silica volume fraction. The value of the force at an indentation depth of 0.3mm micron (chosen arbitrarily) is plotted in Appendix Figure B-7 and it is clear that the load increases highly non-linearly with fumed silica loading.

Finally, even highly viscous liquids would show a significant increase in force with indentation, and a significant increase in force with particle loading. To test that the sample has solid-like characteristics, the sample with 10 vol% fumed silica was indented at three speeds. For a Newtonian liquid, the force must increase proportional to speed, whereas the force was found to be only weakly sensitive to speed (Appendix Figure B-6).

As one last test of solid-like behavior, a bar was molded from a PEO+fumed silica mixture at 10 vol% particles. This bar was supported on two solid supports placed about 32 mm apart and kept at 95^{o}C for two hours. Despite being considerably above the melting point of the PEO, the bar did not completely flow under its own weight; it only sagged partially (Appendix Figure B-5b). This indicates a significant yield stress that can resist gravity.

In summary then, the notion that the PEO+particles combined phase has solid-like rheology is supported by the following observations (1) the load in an indentation test increases steeply with particle loading, (2) the load is weakly sensitive to indentation rate (i.e. it is characteristic of a plastically-yielding material rather than a Newtonian liquid, (3) samples with 10% or more fumed silica could not be adequately "gripped" in a parallel plate rheometer, and (4) a sample with $\phi_p^{combined} = 0.2$ could not be molded due to its crumbly texture.

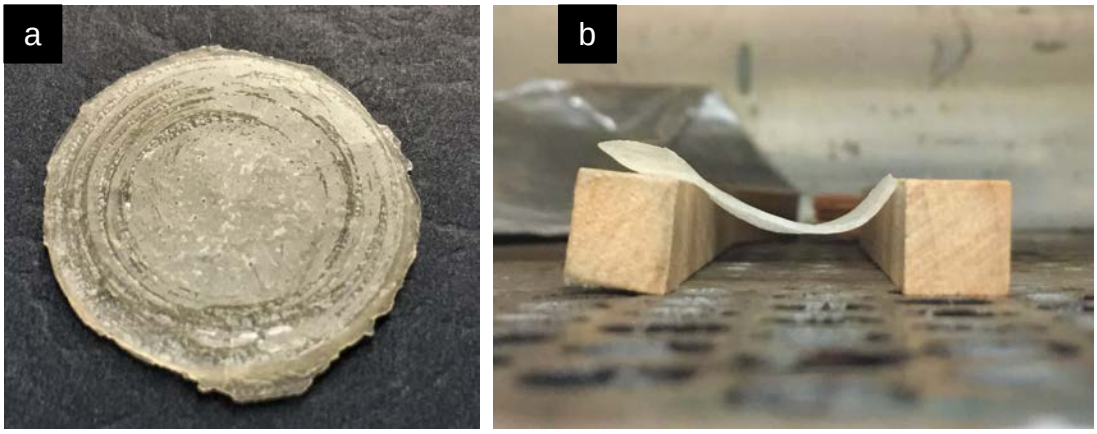

Appendix Figure B-5 Disc of PEO filled with fumed silica recovered from the parallel plate geometry of a rheometer. The concentric circles indicate regionswhere the upper plate contacted the sample. The entire mid-section did not contact the sample at all. (b) A bar of the sample supported on its two ends after 2 hours of heating at 95ºC the bar sags partially but does not flow under its own weight. Both samples correspond to 10vol% fumed silica in PEO.

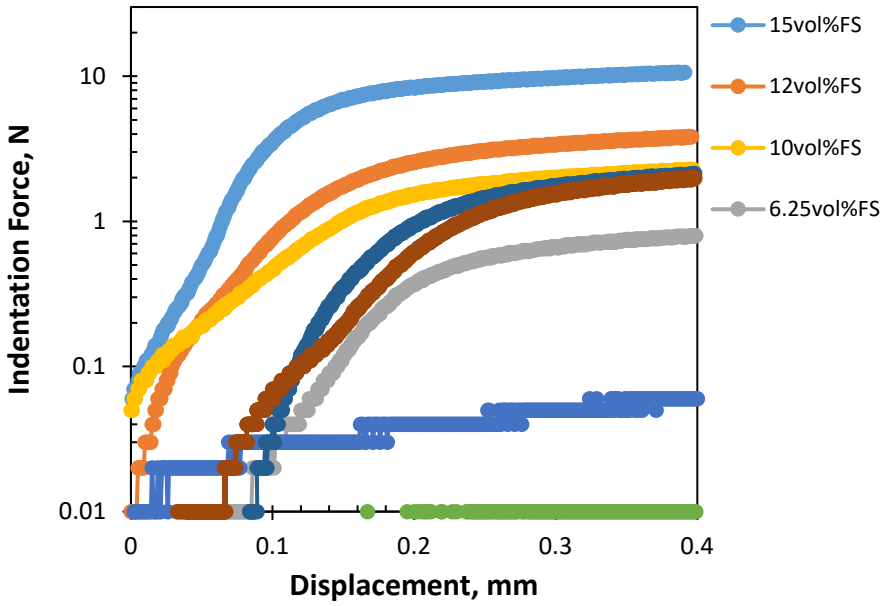

Appendix Figure B-6 Force curves obtained during indentation experiments of PEO+fumed silica mixtures at various compositions. Indentation speed was 10 micron/s unless noted otherwise in the legend

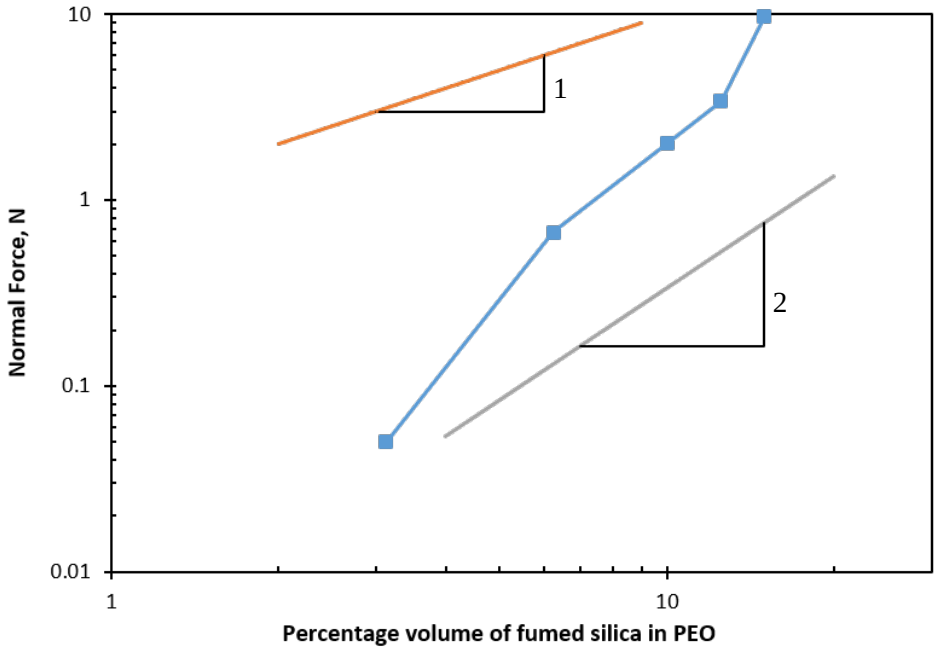

Appendix Figure B-7 Force from Appendix Figure B-6 at an indentation of 0.3 mm. Straight lines are guides to the eye to indicate the srong dependence fo force on composition and have no physical meaning

Appendix C Supplementary Materials For "Bulk Soldering: Conductive Polymer Composite Filled with Copper Particles and Solder"

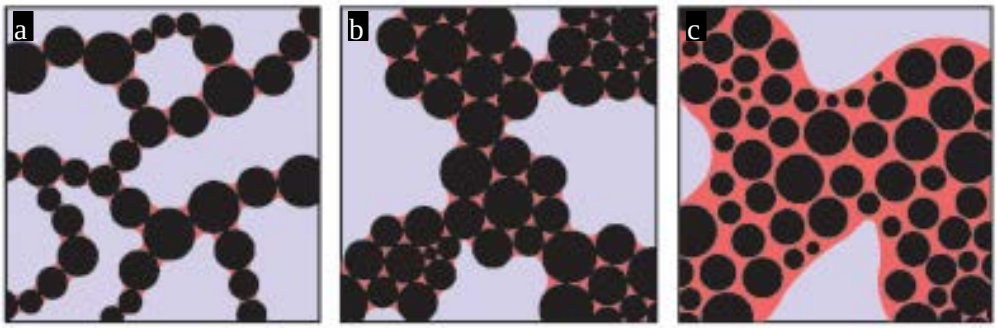

Appendix Figure C-1 Schematic diagram of the three different types of cocontinuous metallic pathways. (a) Pendular/funicular network where particle contacts invole two or few particles (b) Capillary aggregates network where the network is formed from highly filled solid-like "lumps" of wetting fluid (c) A cocontinuous morphology where the particle-filled phase is suffieciently dilute as to be liquid like. This image has been reproduced from Domenech,T., Yang, J., Heidlebaugh, S., & Velankar, S. S. (2016). Three distinct open-poremorphologies from a single particle-filled polymer blend. *Physical Chemistry Chemical Physics, 18(6),* 4310-4315 with copyright permisson from Royal Society of Chemistry

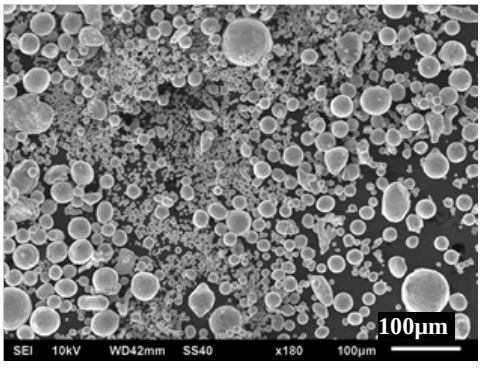

Appendix Figure C-2 SEM image of the spherical copper particles

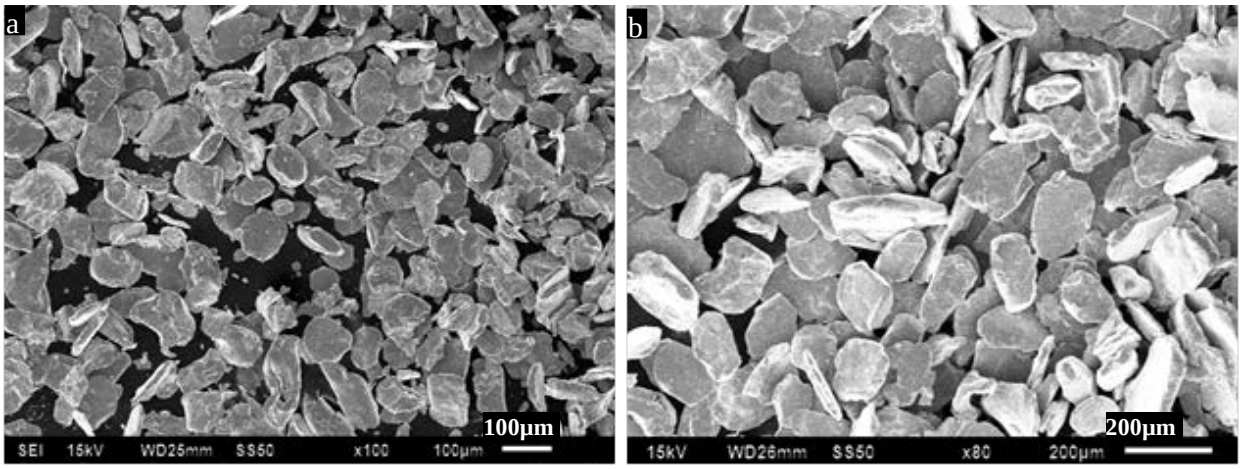

Appendix Figure C-3 SEM image of copper flakes (CuF) (a) Small and (b) Large. The CuF were obtained by ball milling the spherical copper particles in Appendix Figure C-2 in 5 g batches with milling time of 5 mins

C.1 Materials of Conductive Polymer Composites

The continuous phase of the samples was polystyrene, a mixture two grades A75 (Eastman Chemicals) and D145 (Total Petrochemicals), in a 30:70 weight ratio. This mixture composition was selected to realize a viscosity of 11 Pa.s (at 220^{o}C) that was sufficiently low to permit hand-blending at high temperature with a spatula, but sufficiently viscous that the metal particles did not sediment over experimental timescales.

Spherical copper particles (ρ = 8.9 g/cm^3, diameter = 80 – 30 µm) were purchased from Royal Metal Powders. For a limited number of experiments, copper flakes (CuF) were obtained by subjecting the spherical copper particles to ball-milling. By sieving, two different flake sizes, large (100 – 120 µm), and small (diameter = 30 – 80 µm), were obtained. SEM images of the copper particles (Appendix Figure C-2) and flakes (Appendix Figure C-3) are shown.

Solder flux (Regular flux paste, ρ = 1.1g/cm^3 T_{bp} = 150ºC) was purchased from Laco Industries Inc.

Finally, solder paste was purchased from Qualitek International Inc. This consisted of particles of $Sn_{63}Pb_{37}$ (ρ = 8.41 g/cm^3, diameter = 25 – 15 µm) dispersed in a continuous phase flux. This solder paste is typically used in the microelectronics industry and had 87 wt% metal. The melting point of the $Sn_{63}Pb_{37}$ is known to be T_m = 183ºC).

C.2 Conductive Polymer Composite Preparation

The polymer composites were prepared by hand mixing in a 5 mL, thick-walled stainless-steel container. The composition is specified by the three volume fractions denoted ϕ_{PS}, ϕ_{solder}, and ϕ_{copper}. This study examines filler metal volume fractions of ($\phi_{solder} + \phi_{copper}$) from 0 to 30%. The samples were prepared as follows. The Cu particles were first dispersed into flux with a Cu to flux volume ratio of 1:0.6 to allow the surface of the copper to be clean of oxide. A higher ratio, 1:0.9, was used for the CuF due to their higher area. This mixture was then promptly blended with the solder paste at the desired copper:solder volume ratio. All the mixing thus far was conducted at room temperature. In the second step, this mixture was blended at 165ºC to obtain a homogeneous dispersion. Since this mixing temperature is well below the melting point of the solder, the net result is a physical dispersion of copper, solder particles, and flux into the polystyrene. Finally, the cup was heated to 220ºC (which is far above the melting point of solder particles) and blending continued for 1.5 mins during which the molten solder wetted the Cu

particles. During both, the 160^{o}C mixing step and the 220^{o}C mixing step, most of the flux evaporated from the sample. The samples were then cooled rapidly.

For conductivity measurements, samples were molded into discs with a mini-molder at 225^{o}C and at 18 MPa. The molder comprises a hollow steel cylinder with two short pistons for compressing the sample. The sample was sandwiched between two Teflon sheets to avoid unwanted adhesion to the mold. This molding temperature was chosen to be above the solder melting temperature causing the solder particles to re-melt, wetting, and welding the Cu particles after cooling. The circular discs prepared had diameter of 16 mm and typical thickness of 0.8 mm.

C.3 Resistance Measurement of Conductive Polymer Composite

Both surfaces of the discs were sanded lightly with sandpaper to remove any superficial layer of polystyrene and expose the metals particles embedded in the sample. This allowed good electrical contact to be made with the electrode for easy measurement. Both surfaces of the sample were then wiped with dilute HCl to displace any metal oxide layer formed on the metal particles. A low melting bismuth alloy (melting point of 47^{o}C) was then melted on both surfaces of the discs and connected to a copper tape which served as the electrode. The setup was then sandwiched between two glass slides and held together by clips. The copper tape on both ends of the sample was connected to a multi-meter by an alligator clip to measure the resistance of the sample.

C.4 Scanning Electron Microscopy

Samples were imaged by Scanning Electron Microscopy (SEM-JEOL JSM6510). Prior to preparing samples for SEM, the circular disc was placed on a filter paper (Millipore, 0.1 µm pore size) supported on a metal wire mesh and immersed in toluene for over 10 hours to dissolve its polystyrene, leaving the metal content on the filter. This was washed further by dripping excess toluene onto the filter paper to remain any residual polystyrene. The sample was then dipped into water at 60ºC for about 24 hours to dissolve and wash away any flux that might still be left in the sample. Upon drying, the wire mesh was stuck onto on an SEM stub with carbon-tape.

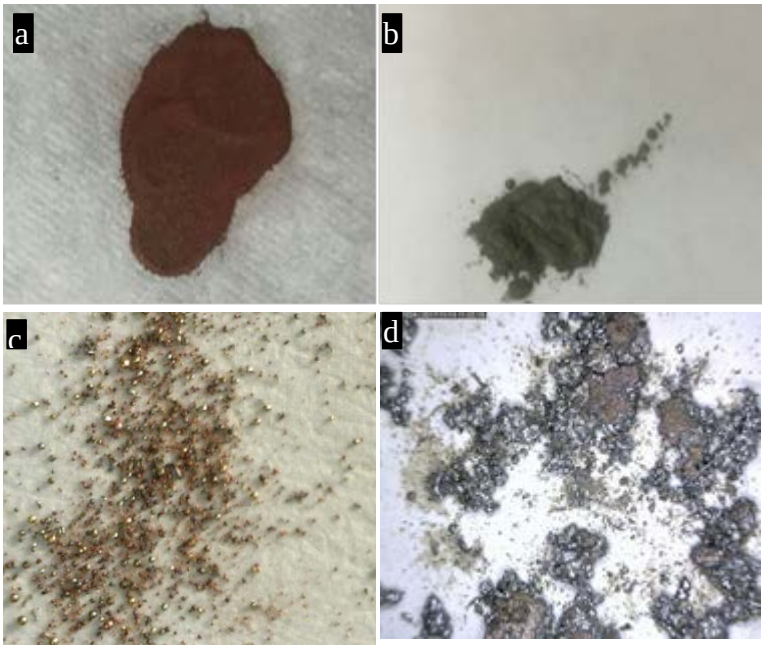

Appendix Figure C-4 Images of (a) spherical copper particles (b) solder particles (c) spherical copper particles at higher magnification (d) copper particles wetted with solder to form aggregates (a-c) correspond to particles as received, whereas (d) corresponds to the particulate phase extracted from melt-blended PS/solder/copper blends after dissolving PS.

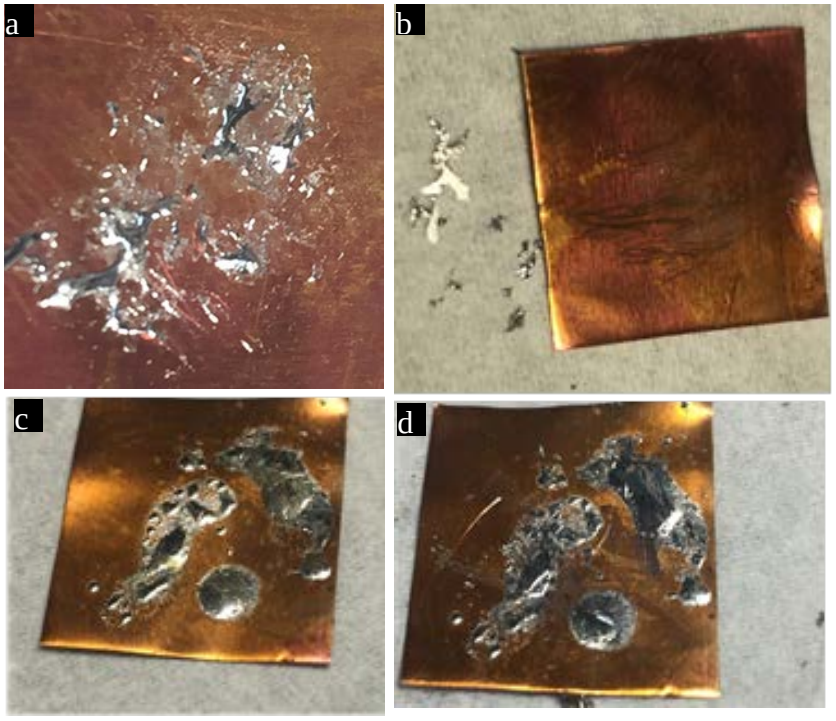

Appendix Figure C-5 images of copper foil (a)wetted with dry solder particles and (b) easily chipped off after cooling down c and d) wetted with solder paste (solder particles dispersed in flux) and impossible to be chipped away after cooling down respectively

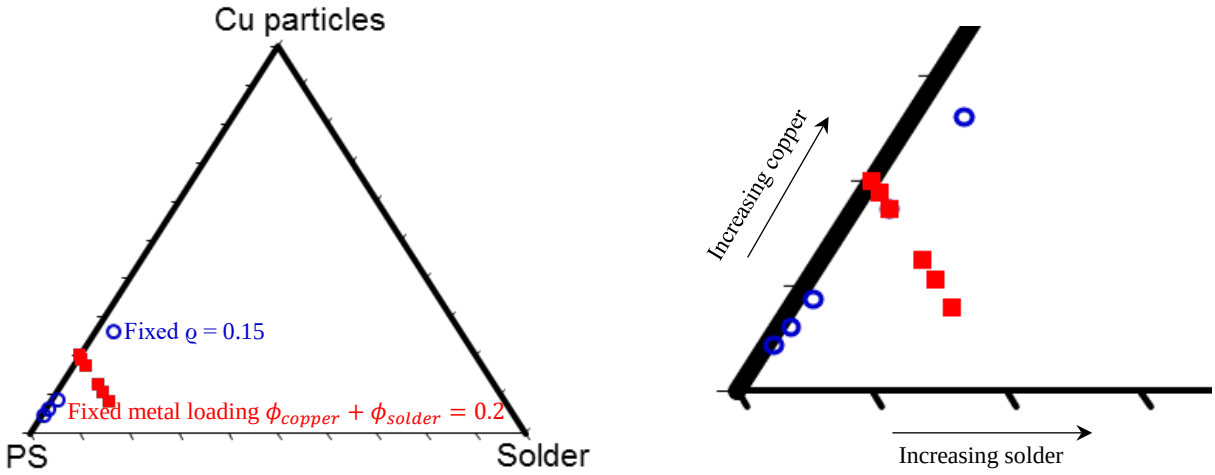

Appendix Figure C-6 Ternary diagram of PS/solder/copper samples prepared at fixed ϱ of 0.15 (open blue circles) and total metal loading (copper and solder)at 20vol% (filled red squares).

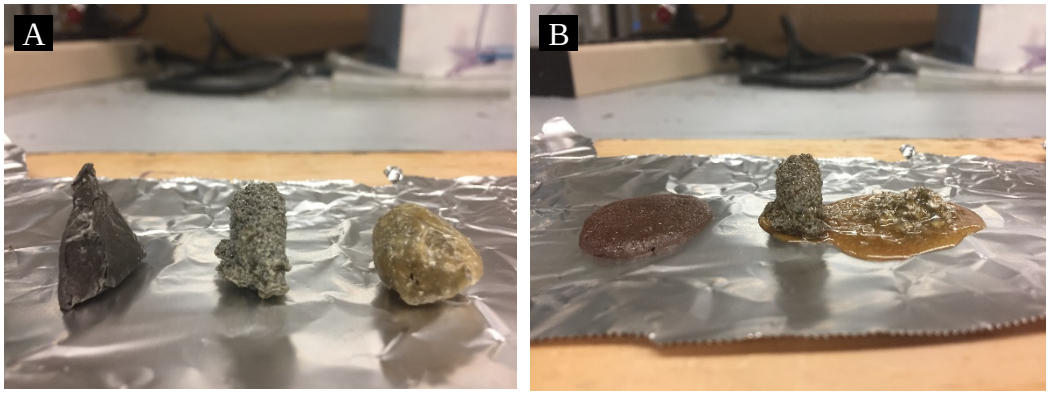

Appendix Figure C-7 Image of composites of PS/solder/copper – (1) 80/0/20, (2) 80/7.5/12.5 and (3) 80/12/8 before (A) and after (B) lumps were heated on hot plate at 220ºC for 5mins to serve as qualitative rheology test.

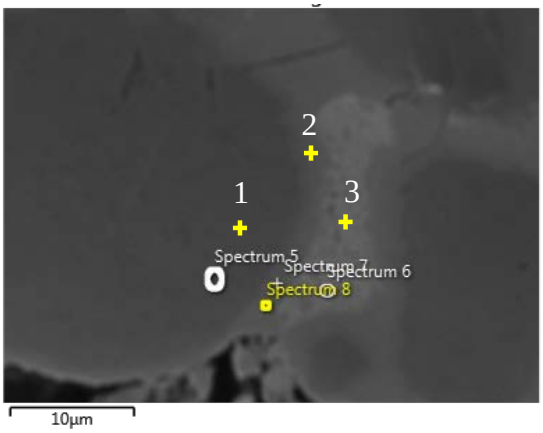

Region	Region 1	Region 2	Region 3
Copper (wt%)	99.06	55.5	0.07
Tin (wt%)	0.32	44.5	22.05
Lead (wt%)	0.61	0	77.88

Appendix Figure C-8 Image of the polished cross section with the elemental compositions coresponding to the various regions marked (+) in the image

Appendix D Supplementary Materials For "Mechanical Properties of Particle-Filled Polymer Blends"

D.1 Materials and Methods

Blends were prepared from Styrene-Ethylene-Butylene-Styrene elastomer (SEBS, Kraton, G1651, ρ = 0.91g/mol, 33% polystyrene content, MFR = no flow @ 230^{o}C/5kg), Maleated Polypropylene (MaPP, ExxonMobil, PO 1015, ρ = 0.9g/mol, MFR = 150g/10min @ 230^{o}C/2kg) and fused silica particles (Industrial Powders SS1205, ρ = 2 g/mL). These particles are polydisperse with unimodal size distribution from 0.5 to 5 mm and the mean diameter is 2 mm.

Some of the blends were prepared using a Brabender batch mixer. Due to inefficient mixing, a Twin-Screw Extruder (TSE) was later used to mix the samples, providing high shear mixing and then injection molded into bars. SEBS/MaPP/silica ternary blends prepared in the batch mixer were prepared in a two-step procedure. The mixer was first preheated to 285^{o}C, the PIB was added, and allowed to attain the 285^{o}C mixing temperature for 5 min. The was then added in small increments while blending at 92 rpm for 5 min. Silica particles were added, also in small increments, and blending continued for 5 min at same speed. For each sample blend, the amount of material at the end of the mixing process was approximately 40 g. The samples prepared in the TSE-Injection Molder were also prepared in a two-step procedure. SEBS, MaPP pellets and silica particles were premix together before being fed to the hopper of the TSE. The TSE was first preheated to 285^{o}C and fed with the premixed sample mixture. The blended sample was extruded as a strand, cooled in a water bath and processed into pellets by a pelletizer. The sample pellets are

injected into an injection molder at 285^{o}C and molded into dog-bone bars for later mechanical properties measurements.

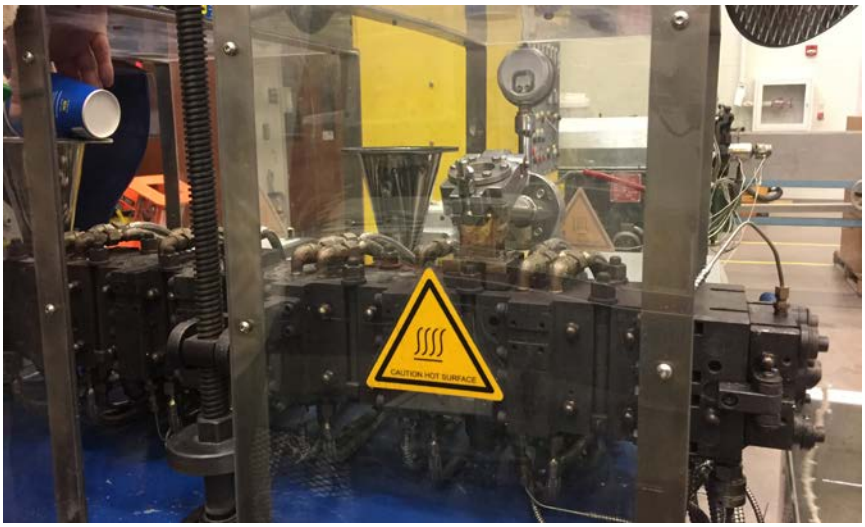

Appendix Figure D-1 Image of Twin Screw Extruder

Bibliography

1. Koos, E., *Capillary suspensions: Particle networks formed through the capillary force.* Current Opinion in Colloid & Interface Science, 2014. **19**(6): p. 575-584.

2. Utracki, L.A., P. Mukhopadhyay, and R. Gupta, *Polymer blends: introduction*, in *Polymer blends handbook*. 2014, Springer. p. 3-170.

3. Harrats, C., G. Groeninckx, and S. Thomas, *Micro-and nanostructured multiphase polymer blend systems: phase morphology and interfaces*. 2005: CRC Press.

4. Folkes, M. and P. Hope, *Polymer blends and alloys*. 1993, London: Blackie Academic & Professional: Springer.

5. Hornbaker, D., R. Albert, I. Albert, A.-L. Barabási, and P. Schiffer, *What keeps sandcastles standing?* Nature, 1997. **387**(6635): p. 765.

6. Horozov, T.S., *Foams and foam films stabilised by solid particles.* Current Opinion in Colloid & Interface Science, 2008. **13**(3): p. 134-140.

7. Lobos, J., S. Iasella, M.A. Rodriguez-Perez, and S.S. Velankar, *Improving the stability of polylactic acid foams by interfacially adsorbed particles.* Polymer Engineering & Science, 2016. **56**(1): p. 9-17.

8. Murakami, R. and A. Bismarck, *Particle-Stabilized Materials: Dry Oils and (Polymerized) Non-Aqueous Foams.* Advanced Functional Materials, 2010. **20**(5): p. 732-737.

9. Herzig, E., K. White, A. Schofield, W. Poon, and P. Clegg, *Bicontinuous emulsions stabilized solely by colloidal particles.* Nature materials, 2007. **6**(12): p. 966-971.

10. Domenech, T. and S. Velankar, *Capillary-driven percolating networks in ternary blends of immiscible polymers and silica particles.* Rheologica Acta, 2014. **53**(8): p. 593-605.

11. Domenech, T. and S.S. Velankar, *On the rheology of pendular gels and morphological developments in paste-like ternary systems based on capillary attraction.* Soft matter, 2015. **11**(8): p. 1500-1516.

12. Heidlebaugh, S.J., T. Domenech, S.V. Iasella, and S.S. Velankar, *Aggregation and Separation in Ternary Particle/Oil/Water Systems with Fully Wettable Particles.* Langmuir, 2014. **30**(1): p. 63-74.

13. Destribats, M., S. Gineste, E. Laurichesse, H. Tanner, F. Leal-Calderon, V.r. Héroguez, and V. Schmitt, *Pickering emulsions: what are the main parameters determining the emulsion type and interfacial properties?* Langmuir, 2014. **30**: p. 9313-9326.

14. Binks, B. and J. Rodrigues, *Types of phase inversion of silica particle stabilized emulsions containing triglyceride oil.* Langmuir, 2003. **19**: p. 4905-4912.

15. Binks, B. and S. Lumsdon, *Catastrophic phase inversion of water-in-oil emulsions stabilized by hydrophobic silica.* Langmuir, 2000. **16**(6): p. 2539-2547.

16. Fenouillot, F., P. Cassagnau, and J.C. Majesté, *Uneven distribution of nanoparticles in immiscible fluids: Morphology development in polymer blends.* Polymer, 2009. **50**: p. 1333-1350.

17. Al-Saleh, M.H. and U. Sundararaj, *An innovative method to reduce percolation threshold of carbon black filled immiscible polymer blends.* Composites Part A: Applied Science and Manufacturing, 2008. **39**: p. 284-293.

18. Foudazi, R. and H. Nazockdast, *Rheology and morphology of nanosilica-containing polypropylene and polypropylene/liquid crystalline polymer blend.* Journal of Applied Polymer Science, 2013. **128**: p. 3501-3511.

19. Liu, X.-Q., R.-Y. Bao, Z.-Y. Liu, W. Yang, B.-H. Xie, and M.-B. Yang, *Effect of nano-silica on the phase inversion behavior of immiscible PA6/ABS blends.* Polymer Testing, 2013. **32**(1): p. 141-149.

20. Domenech, T. and S.S. Velankar, *Microstructure, phase inversion and yielding in immiscible polymer blends with selectively wetting silica particles.* Journal of Rheology, 2017. **61**(2): p. 363-377.

21. Koos, E. and N. Willenbacher, *Particle configurations and gelation in capillary suspensions.* Soft Matter, 2012. **8**(14): p. 3988-3994.

22. Yang, J., D. Roell, M. Echavarria, and S.S. Velankar, *A microstructure-composition map of a ternary liquid/liquid/particle system with partially-wetting particles.* Soft matter, 2017. **13**(45): p. 8579-8589.

23. Amoabeng, D., D. Roell, K.M. Clouse, B.A. Young, and S.S. Velankar, *A composition-morphology map for particle-filled blends of immiscible thermoplastic polymers.* Polymer, 2017. **119**: p. 212-223.

24. Gun'ko, V., I. Mironyuk, V. Zarko, V. Turov, E. Voronin, E. Pakhlov, E. Goncharuk, R. Leboda, J. Skubiszewska-Zięba, and W. Janusz, *Fumed silicas possessing different morphology and hydrophilicity.* Journal of Colloid and Interface Science, 2001. **242**(1): p. 90-103.

25. Amoabeng, D. and S.S. Velankar, *Bulk soldering: Conductive polymer composites filled with copper particles and solder.* Colloids and Surfaces A: Physicochemical and Engineering Aspects, 2018. **553**: p. 624-632.

26. Amoabeng, D. and S.S. Velankar, *A review of conductive polymer composites filled with low melting point metal alloys.* Polymer Engineering & Science, 2017. **58**(6): p. 1010-1019.

27. Utracki, L.A., C.A. Wilkie, and SpringerLink, *Polymer Blends Handbook*. Vol. 2nd 2014.;2nd 2014;. 2014, Dordrecht: Springer Netherlands: Kluwer Academic Publishers.

28. Harrats, C., S. Thomas, and G. Groeninckx, *Micro-and nanostructured multiphase polymer blend systems: phase morphology and interfaces*. 2005: CRC Press.

29. Favis, B. and D. Therrien, *Factors influencing structure formation and phase size in an immiscible polymer blend of polycarbonate and polypropylene prepared by twin-screw extrusion.* Polymer, 1991. **32**(8): p. 1474-1481.

30. Wildes, G., H. Keskkula, and D. Paul, *Morphology of PC/SAN blends: Effect of reactive compatibilization, SAN concentration, processing, and viscosity ratio.* Journal of Polymer Science Part B: Polymer Physics, 1999. **37**(1): p. 71-82.

31. Banerjee, S.S. and A.K. Bhowmick, *Dynamic vulcanization of novel nanostructured polyamide 6/fluoroelastomer thermoplastic elastomeric blends with special reference to morphology, physical properties and degree of vulcanization.* Polymer, 2015. **57**: p. 105-116.

32. Sau, M. and S.C. Jana, *A study on the effects of chaotic mixer design and operating conditions on morphology development in immiscible polymer systems.* Polymer Engineering & Science, 2004. **44**(3): p. 407-422.

33. Xu, X., X. Yan, T. Zhu, C. Zhang, and J. Sheng, *Phase morphology development of polypropylene/ethylene-octene copolymer blends: effects of blend composition and processing conditions.* Polymer Bulletin, 2007. **58**(2): p. 465-478.

34. Akcora, P., H. Liu, S.K. Kumar, J. Moll, Y. Li, B.C. Benicewicz, L.S. Schadler, D. Acehan, A.Z. Panagiotopoulos, and V. Pryamitsyn, *Anisotropic self-assembly of spherical polymer-grafted nanoparticles.* Nature materials, 2009. **8**(4): p. 354.

35. Datta, S. and D.J. Lohse, *Polymeric comptabilizers: uses and benefits in polymer blends*. 1996, Munich; Cincinnati; New York;: Hanser.

36. Paul, D.R. and J.W. Barlow, *Polymer Blends.* Journal of Macromolecular Science, Part C, 1980. **18**: p. 109-168.

37. Sundararaj, U., C. Macosko, R. Rolando, and H. Chan, *Morphology development in polymer blends.* Polymer Engineering & Science, 1992. **32**: p. 1814-1823.

38. Macosko, C.W. *Morphology development and control in immiscible polymer blends*. in *Macromolecular Symposia*. 2000. Wiley Online Library.

39. Favis, B. and J. Chalifoux, *Influence of composition on the morphology of polypropylene/polycarbonate blends.* Polymer, 1988. **29**: p. 1761-1767.

40. Luzinov, I., C. Pagnoulle, and R. Jérôme, *Dependence of phase morphology and mechanical properties of PS/SBR/PE ternary blends on composition: transition from core–shell to triple-phase continuity structures.* Polymer, 2000. **41**: p. 3381-3389.

41. Lee, J.K. and C.D. Han, *Evolution of polymer blend morphology during compounding in a twin-screw extruder.* Polymer, 2000. **41**: p. 1799-1815.

42. Van Puyvelde, P., S. Velankar, and P. Moldenaers, *Rheology and morphology of compatibilized polymer blends.* Current Opinion in Colloid & Interface Science, 2001. **6**: p. 457-463.

43. Li, J. and B. Favis, *Characterizing co-continuous high density polyethylene/polystyrene blends.* Polymer, 2001. **42**: p. 5047-5053.

44. Li, H. and U. Sundararaj, *Morphology Development of Polymer Blends in Extruder: The effects of compatibilization and rotation rate.* Macromolecular Chemistry and Physics, 2009. **210**: p. 852-863.

45. Taguet, A., P. Cassagnau, and J.-M. Lopez-Cuesta, *Structuration, selective dispersion and compatibilizing effect of (nano) fillers in polymer blends.* Progress in Polymer Science, 2014. **39**(8): p. 1526-1563.

46. Filippone, G., N.T. Dintcheva, D. Acierno, and F. La Mantia, *The role of organoclay in promoting co-continuous morphology in high-density poly (ethylene)/poly (amide) 6 blends.* Polymer, 2008. **49**(5): p. 1312-1322.

47. Wu, G., B. Li, and J. Jiang, *Carbon black self-networking induced co-continuity of immiscible polymer blends.* Polymer, 2010. **51**: p. 2077-2083.

48. Cai, X., B. Li, Y. Pan, and G. Wu, *Morphology evolution of immiscible polymer blends as directed by nanoparticle self-agglomeration.* Polymer, 2012. **53**: p. 259-266.

49. Thareja, P., K. Moritz, and S.S. Velankar, *Interfacially active particles in droplet/matrix blends of model immiscible homopolymers: Particles can increase or decrease drop size.* Rheologica Acta, 2010. **49**: p. 285-298.

50. Ray, S.S., M. Bousmina, and A. Maazouz, *Morphology and properties of organoclay modified polycarbonate/poly(methyl methacrylate) blend.* Polymer Engineering and Science, 2006. **46**: p. 1121-1129.

51. Liu, X.-Q., R.-Y. Bao, Z.-Y. Liu, W. Yang, B.-H. Xie, and M.-B. Yang, *Effect of nano-silica on the phase inversion behavior of immiscible PA6/ABS blends.* Polymer Testing, 2013. **32**: p. 141-149.

52. Si, M., T. Araki, H. Ade, A. Kilcoyne, R. Fisher, J.C. Sokolov, and M.H. Rafailovich, *Compatibilizing bulk polymer blends by using organoclays.* Macromolecules, 2006. **39**: p. 4793-4801.

53. Trifkovic, M., A.T. Hedegaard, M. Sheikhzadeh, S. Huang, and C.W. Macosko, *Stabilization of PE/PEO cocontinuous blends by interfacial nanoclays.* Macromolecules, 2015. **48**: p. 4631-4644.

54. Li, W. and J.G. Goossens, *The Control of Silica Nanoparticles on the Phase Separation of Poly (methyl methacrylate)/Poly (styrene-co-acrylonitrile) Blends.* Macromolecular Chemistry and Physics, 2013. **214**: p. 2705-2715.

55. Lee, S.H., M. Bailly, and M. Kontopoulou, *Morphology and Properties of Poly (propylene)/Ethylene-Octene Copolymer Blends Containing Nanosilica.* Macromolecular Materials and Engineering, 2012. **297**: p. 95-103.

56. Lee, H.-s., P.D. Fasulo, W.R. Rodgers, and D. Paul, *TPO based nanocomposites. Part 1. Morphology and mechanical properties.* Polymer, 2005. **46**: p. 11673-11689.

57. Martin, G., C. Barrès, P. Sonntag, N. Garois, and P. Cassagnau, *Co-continuous morphology and stress relaxation behaviour of unfilled and silica filled PP/EPDM blends.* Materials Chemistry and Physics, 2009. **113**: p. 889-898.

58. Steinmann, S., W. Gronski, and C. Friedrich, *Influence of selective filling on rheological properties and phase inversion of two-phase polymer blends.* Polymer, 2002. **43**: p. 4467-4477.

59. Premphet, K. and P. Horanont, *Phase structure and property relationships in ternary polypropylene/elastomer/filler composites: Effect of elastomer polarity.* Journal of Applied Polymer Science, 2000. **76**: p. 1929-1939.

60. Premphet, K. and P. Horanont, *Phase structure of ternary polypropylene/elastomer/filler composites: effect of elastomer polarity.* Polymer, 2000. **41**: p. 9283-9290.

61. Plattier, J., L. Benyahia, M. Dorget, F. Niepceron, and J.-F. Tassin, *Viscosity-induced filler localisation in immiscible polymer blends.* Polymer, 2015. **59**: p. 260-269.

62. Al-Saleh, M.H. and U. Sundararaj, *Electromagnetic interference (EMI) shielding effectiveness of PP/PS polymer blends containing high structure carbon black.* Macromolecular Materials and Engineering, 2008. **293**: p. 621-630.

63. Nagarkar, S. and S.S. Velankar, *Rheology and morphology of model immiscible polymer blends with monodisperse spherical particles at the interface.* Journal of Rheology 2013. **57**: p. 901-926.

64. Thareja, P. and S. Velankar, *Particle-induced bridging in immiscible polymer blends.* Rheologica Acta, 2007. **46**: p. 405-412.

65. Vermant, J., S. Vandebril, C. Dewitte, and P. Moldenaers, *Particle-stabilized polymer blends.* Rheologica Acta, 2008. **47**: p. 835-839.

66. Vandebril, S., J. Vermant, and P. Moldenaers, *Efficiently suppressing coalescence in polymer blends using nanoparticles: role of interfacial rheology.* Soft Matter, 2010. **6**: p. 3353-3362.

67. Vermant, J., G. Cioccolo, K.G. Nair, and P. Moldenaers, *Coalescence suppression in model immiscible polymer blends by nano-sized colloidal particles.* Rheologica Acta, 2004. **43**: p. 529-538.

68. Bai, L., J.W. Fruehwirth, X. Cheng, and C.W. Macosko, *Dynamics and rheology of nonpolar bijels.* Soft Matter, 2015. **11**: p. 5282-5293.

69. Tong, W., Y. Huang, C. Liu, X. Chen, Q. Yang, and G. Li, *The morphology of immiscible PDMS/PIB blends filled with silica nanoparticles under shear flow.* Colloid and Polymer Science, 2010. **288**: p. 753-760.

70. He, Y., Y. Huang, Q. Li, Y. Mei, M. Kong, and Q. Yang, *Morphological hysteresis in immiscible PIB/PDMS blends filled with fumed silica nanoparticles.* Colloid and Polymer Science, 2012. **290**: p. 997-1004.

71. Zou, Z.-M., Z.-Y. Sun, and L.-J. An, *Effect of fumed silica nanoparticles on the morphology and rheology of immiscible polymer blends.* Rheologica Acta, 2014. **53**: p. 43-53.

72. Kohonen, M.M., D. Geromichalos, M. Scheel, C. Schier, and S. Herminghaus, *On capillary bridges in wet granular materials.* Physica A: Statistical Mechanics and its Applications, 2004. **339**: p. 7-15.

73. Wang, J.-P., E. Gallo, B. François, F. Gabrieli, and P. Lambert, *Capillary force and rupture of funicular liquid bridges between three spherical bodies.* Powder Technology, 2017. **305**: p. 89-98.

74. Velankar, S.S., *A non-equilibrium state diagram for liquid/fluid/particle mixtures.* Soft Matter, 2015. **11**(43): p. 8393-8403.

75. Dil, E.J. and B.D. Favis, *Localization of micro and nano-silica particles in a high interfacial tension poly (lactic acid)/low density polyethylene system.* Polymer, 2015. **77**: p. 156-166.

76. Elias, L., F. Fenouillot, J.C. Majeste, and P. Cassagnau, *Morphology and rheology of immiscible polymer blends filled with silica nanoparticles.* Polymer, 2007. **48**: p. 6029-6040.

77. Kong, M., Y. Huang, G. Chen, Q. Yang, and G. Li, *Retarded relaxation and breakup of deformed PA6 droplets filled with nanosilica in PS matrix during annealing.* Polymer, 2011. **52**: p. 5231-5236.

78. Herzig, E., K. White, A. Schofield, W. Poon, and P. Clegg, *Bicontinuous emulsions stabilized solely by colloidal particles.* Nature Materials, 2007. **6**: p. 966-971.

79. Domenech, T., J. Yang, S. Heidlebaugh, and S.S. Velankar, *Three distinct open-pore morphologies from a single particle-filled polymer blend.* Physical Chemistry Chemical Physics, 2016. **18**: p. 4310-4315.

80. Tucker III, C.L. and P. Moldenaers, *Microstructural evolution in polymer blends.* Annual Review of Fluid Mechanics, 2002. **34**: p. 177-210.

81. Jalali Dil, E. and B.D. Favis, *Localization of micro- and nano-silica particles in heterophase poly(lactic acid)/poly(butylene adipate-co-terephthalate) blends.* Polymer, 2015. **76**: p. 295-306.

82. Binks, B.P., *Particles as surfactants—similarities and differences.* Current Opinion in Colloid & Interface Science, 2002. **7**: p. 21-41.

83. Binks, B. and S. Lumsdon, *Catastrophic phase inversion of water-in-oil emulsions stabilized by hydrophobic silica.* Langmuir, 2000. **16**: p. 2539-2547.

84. Heidlebaugh, S.J., T. Domenech, S.V. Iasella, and S.S. Velankar, *Aggregation and separation in ternary particle/oil/water systems with fully wettable particles.* Langmuir, 2014. **30**: p. 63-74.

85. Nagarkar, S.P. and S.S. Velankar, *Morphology and rheology of ternary fluid–fluid–solid systems.* Soft Matter, 2012. **8**: p. 8464-8477.

86. Iveson, S.M., J.A. Beathe, and N.W. Page, *The dynamic strength of partially saturated powder compacts: the effect of liquid properties.* Powder Technology, 2002. **127**: p. 149-161.

87. Trifkovic, M., A.T. Hedegaard, M. Sheikhzadeh, S. Huang, and C.W. Macosko, *Stabilization of PE/PEO cocontinuous blends by interfacial nanoclays.* Macromolecules, 2015. **48**(13): p. 4631-4644.

88. Iveson, S.M., J.A. Beathe, and N.W. Page, *The dynamic strength of partially saturated powder compacts: the effect of liquid properties.* Powder Technology, 2002. **127**(2): p. 149-161.

89. Thareja, P., K. Moritz, and S.S. Velankar, *Interfacially active particles in droplet/matrix blends of model immiscible homopolymers: Particles can increase or decrease drop size.* Rheologica acta, 2010. **49**(3): p. 285-298.

90. Nagarkar, S.P. and S.S. Velankar, *Morphology and rheology of ternary fluid–fluid–solid systems.* Soft matter, 2012. **8**(32): p. 8464-8477.

91. Dil, E.J. and B.D. Favis, *Localization of micro-and nano-silica particles in heterophase poly (lactic acid)/poly (butylene adipate-co-terephthalate) blends.* Polymer, 2015. **76**: p. 295-306.

92. Gubbels, F., R. Jérôme, E. Vanlathem, R. Deltour, S. Blacher, and F. Brouers, *Kinetic and thermodynamic control of the selective localization of carbon black at the interface of immiscible polymer blends.* Chemistry of materials, 1998. **10**(5): p. 1227-1235.

93. Domenech, T., J. Yang, S. Heidlebaugh, and S.S. Velankar, *Three distinct open-pore morphologies from a single particle-filled polymer blend.* Physical Chemistry Chemical Physics, 2016. **18**(6): p. 4310-4315.

94. Caggioni, M., A.V. Bayles, J. Lenis, E.M. Furst, and P.T. Spicer, *Interfacial stability and shape change of anisotropic endoskeleton droplets.* Soft Matter, 2014. **10**(38): p. 7647-7652.

95. Boode, K. and P. Walstra, *Partial coalescence in oil-in-water emulsions 1. Nature of the aggregation.* Colloids and Surfaces A: Physicochemical and Engineering Aspects, 1993. **81**: p. 121-137.

96. Koos, E. and N. Willenbacher, *Capillary forces in suspension rheology.* Science, 2011. **331**(6019): p. 897-900.

97. Galloway, J.A. and C.W. Macosko, *Comparison of methods for the detection of cocontinuity in poly (ethylene oxide)/polystyrene blends.* Polymer Engineering & Science, 2004. **44**(4): p. 714-727.

98. Pötschke, P. and D. Paul, *Formation of co-continuous structures in melt-mixed immiscible polymer blends.* Journal of Macromolecular Science, Part C: Polymer Reviews, 2003. **43**(1): p. 87-141.

99. Dittmann, J., E. Koos, and N. Willenbacher, *Ceramic capillary suspensions: novel processing route for macroporous ceramic materials.* Journal of the American Ceramic Society, 2013. **96**(2): p. 391-397.

100. Amoabeng, D., A.J. Tempalski, B. Young, B.P. Binks, and S.S. Velankar, *Fumed Silica Induces Co-continuity Across A Wide Composition Range in Immiscible Polymer Blends.* Polymer, 2019: p. Submitted.

101. Fenouillot, F., P. Cassagnau, and J.-C. Majesté, *Uneven distribution of nanoparticles in immiscible fluids: Morphology development in polymer blends.* Polymer, 2009. **50**(6): p. 1333-1350.

102. de Luna, M.S. and G. Filippone, *Effects of nanoparticles on the morphology of immiscible polymer blends–challenges and opportunities.* European Polymer Journal, 2016. **79**: p. 198-218.

103. Yang, J., N. Heinichen, and S.S. Velankar, *The effect of particle wettability on the of rheology particulate suspensions with capillary force.* Colloids and Surfaces A: Physicochemical and Engineering Aspects, 2018. **558**: p. 164-170.

104. Yang, J. and S.S. Velankar, *Preparation and yielding behavior of pendular network suspensions.* Journal of Rheology, 2017. **61**(2): p. 217-228.

105. Aerosil. *https://www.aerosil.com/product/aerosil/en/industries/plastics-thermoplastics/*. February 2019].

106. Cabot-Corporation. *http://www.cabotcorp.com/~/media/files/brochures/fumed-metal-oxides/brochure-cab-o-sil-fumed-silica-for-silicone-elastomers.pdf*. February 2019].

107. Flörke, O.W., H.A. Graetsch, F. Brunk, L. Benda, S. Paschen, H.E. Bergna, W.O. Roberts, W.A. Welsh, C. Libanati, and M. Ettlinger, *Silica.* Ullmann's Encyclopedia of Industrial Chemistry, 2000.

108. Evonik-Industries *https://www.aerosil.com/product/aerosil/downloads/technical-overview-aerosil-fumed-silica-en.pdf*.

109. Boldridge, D., *Morphological characterization of fumed silica aggregates.* Aerosol Science and Technology, 2010. **44**(3): p. 182-186.

110. Ehrburger, F. and J. Lahaye, *Thermoporometric study of the intra-aggregate porosity of pyrogenic silica dispersed in aqueous and non-aqueous liquids.* Colloids and surfaces, 1987. **23**(1-2): p. 105-117.

111. Lee, S., M. Kontopoulou, and C. Park, *Effect of nanosilica on the co-continuous morphology of polypropylene/polyolefin elastomer blends.* Polymer, 2010. **51**(5): p. 1147-1155.

112. Li, J., P.L. Ma, and B.D. Favis, *The role of the blend interface type on morphology in cocontinuous polymer blends.* Macromolecules, 2002. **35**(6): p. 2005-2016.

113. Galloway, J.A., H.K. Jeon, J.R. Bell, and C.W. Macosko, *Block copolymer compatibilization of cocontinuous polymer blends.* Polymer, 2005. **46**(1): p. 183-191.

114. Odent, J., Y. Habibi, J.-M. Raquez, and P. Dubois, *Ultra-tough polylactide-based materials synergistically designed in the presence of rubbery ε-caprolactone-based*

copolyester and silica nanoparticles. Composites Science and Technology, 2013. **84**: p. 86-91.

115. Steinmann, S., W. Gronski, and C. Friedrich, *Influence of selective filling on rheological properties and phase inversion of two-phase polymer blends.* Polymer, 2002. **43**(16): p. 4467-4477.

116. Cassagnau, P., *Melt rheology of organoclay and fumed silica nanocomposites.* Polymer, 2008. **49**(9): p. 2183-2196.

117. Raghavan, S.R. and S.A. Khan, *Shear-thickening response of fumed silica suspensions under steady and oscillatory shear.* Journal of colloid and interface science, 1997. **185**(1): p. 57-67.

118. Raghavan, S.R., H. Walls, and S.A. Khan, *Rheology of silica dispersions in organic liquids: new evidence for solvation forces dictated by hydrogen bonding.* Langmuir, 2000. **16**(21): p. 7920-7930.

119. Kohonen, M.M., D. Geromichalos, M. Scheel, C. Schier, and S. Herminghaus, *On capillary bridges in wet granular materials.* Physica A: Statistical Mechanics and its Applications, 2004. **339**(1): p. 7-15.

120. Lawrence, S.S., P. Walia, and J. Willett, *Starch-filled ternary polymer composites. I: Dynamic mechanical properties.* Polymer Engineering & Science, 2003. **43**(6): p. 1250-1260.

121. Sirianni, A., C. Capes, and J. Puddington, *Recent experience with the spherical agglomeration process.* The Canadian Journal of Chemical Engineering, 1969. **47**(2): p. 166-170.

122. Chevalier, Y. and M.-A. Bolzinger, *Emulsions stabilized with solid nanoparticles: Pickering emulsions.* Colloids and Surfaces A: Physicochemical and Engineering Aspects, 2013. **439**(Supplement C): p. 23-34.

123. Binks, B.P. and T.S. Horozov, *Colloidal particles at liquid interfaces*. 2006: Cambridge University Press.

124. Dittmann, J., J. Maurath, B. Bitsch, and N. Willenbacher, *Highly porous materials with unique mechanical properties from smart capillary suspensions.* Advanced Materials, 2016. **28**(8): p. 1689-1696.

125. Lee, M.N. and A. Mohraz, *Bicontinuous macroporous materials from bijel templates.* Advanced Materials, 2010. **22**(43): p. 4836-4841.

126. Gonzenbach, U.T., A.R. Studart, E. Tervoort, and L.J. Gauckler, *Macroporous Ceramics from Particle-Stabilized Wet Foams.* Journal of the American Ceramic Society, 2007. **90**(1): p. 16-22.

127. Dinsmore, A., M.F. Hsu, M. Nikolaides, M. Marquez, A. Bausch, and D. Weitz, *Colloidosomes: selectively permeable capsules composed of colloidal particles.* Science, 2002. **298**(5595): p. 1006-1009.

128. Mohraz, A., *Interfacial routes to colloidal gelation.* Current Opinion in Colloid & Interface Science, 2016. **25**: p. 89-97.

129. Bauhofer, W. and J.Z. Kovacs, *A review and analysis of electrical percolation in carbon nanotube polymer composites.* Composites Science and Technology, 2009. **69**(10): p. 1486-1498.

130. Bhattacharya, S.K. and A.C.D. Chaklader, *Review on metal-filled plastics .1. Electrical-conductivity.* Polymer-Plastics Technology and Engineering, 1982. **19**(1): p. 21-51.

131. Radzuan, N.A.M., A.B. Sulong, and J. Sahari, *A review of electrical conductivity models for conductive polymer composite.* International Journal of Hydrogen Energy, 2017. **42**(14): p. 9262-9273.

132. Mamunya, Y., A. Boudenne, N. Lebovka, L. Ibos, Y. Candau, and M. Lisunova, *Electrical and thermophysical behaviour of PVC-MWCNT nanocomposites.* Composites Science and Technology, 2008. **68**(9): p. 1981-1988.

133. Arjmand, M., M. Mahmoodi, G.A. Gelves, S. Park, and U. Sundararaj, *Electrical and electromagnetic interference shielding properties of flow-induced oriented carbon nanotubes in polycarbonate.* Carbon, 2011. **49**(11): p. 3430-3440.

134. Liao, K.-H., Y. Qian, and C.W. Macosko, *Ultralow percolation graphene/polyurethane acrylate nanocomposites.* Polymer, 2012. **53**(17): p. 3756-3761.

135. Bigg, D.M., *Mechanical, thermal, and electrical properties of metal fiber-filled polymer composites.* Polymer Engineering & Science, 1979. **19**(16): p. 1188-1192.

136. Wu, G., B. Li, and J. Song, *Enhancing the electrical and thermal stability of metallic fiber-filled polymer composites by adding tin–lead alloy.* Polymer bulletin, 2011. **67**(6): p. 1105-1110.

137. Sichel, E.K., P. Sheng, J.I. Gittleman, and S. Bozowski, *Observation of fluctuation modulation of tunnel junctions by applied ac stress in carbon polyvinylchloride composites.* Physical Review B, 1981. **24**(10): p. 6131.

138. Balberg, I., *Tunneling and nonuniversal conductivity in composite-materials.* Physical Review Letters, 1987. **59**(12): p. 1305-1308.

139. Amoabeng, D. and S.S. Velankar, *A Review of Conductive Polymer Composites Filled With Low Melting Point Metal Alloys.* Polymer Engineering & Science, 2017: p. Accepted.

140. Mrozek, R.A., P.J. Cole, L.A. Mondy, R.R. Rao, L.F. Bieg, and J.L. Lenhart, *Highly conductive, melt processable polymer composites based on nickel and low melting eutectic metal.* Polymer, 2010. **51**(14): p. 2954-2958.

141. Zou, M., J. He, Y. Lei, F. Zhang, Q. Zhao, T. Liu, H. Ma, and Y. Yi, *Effect of the eutectic Sn-Cu alloy-to-Cu content ratio on the structure and properties of conductive polyamide-66 composites.* Composites Science and Technology, 2016. **133**: p. 200-207.

142. Michaeli, W. and T.G. Pfefferkorn, *Electrically conductive thermoplastic/metal hybrid materials for direct manufacturing of electronic components.* Polymer Engineering & Science, 2009. **49**(8): p. 1511-1524.

143. Yang, Q., M.H. Beers, V. Mehta, T. Gao, and D. Parkinson, *Effect of Thermal Annealing on the Electrical Conductivity of Copper–Tin Polymer Composites.* ACS applied materials & interfaces, 2016. **9**(1): p. 958-964.

144. Sun, H., X. Zhang, and M.M. Yuen, *Enhanced conductivity induced by attractive capillary force in ternary conductive adhesive.* Composites Science and Technology, 2016. **137**: p. 109-117.

145. Bossler, F. and E. Koos, *Structure of particle networks in capillary suspensions with wetting and nonwetting fluids.* Langmuir, 2016. **32**(6): p. 1489-1501.

146. Lau, J.H., *Solder joint reliability: theory and applications*. 1991: Springer Science & Business Media.

147. Humpston, G. and D.M. Jacobson, *Principles of soldering*. 2004: ASM international.

148. Bekaert-Company. *http://www.bekaert.com/en/products/basic-materials/materials-plastic/beki-shield-stainless-steel-fibers-for-conductive-plastics*. May 2017].

149. RTP-Company. *https://www.rtpcompany.com/products/conductive/typical-conductive-additives/*. November 2017].

150. Kim, H. and K. Tu, *Kinetic analysis of the soldering reaction between eutectic SnPb alloy and Cu accompanied by ripening.* Physical review B, 1996. **53**(23): p. 16027.

151. Maurath, J., B. Bitsch, Y. Schwegler, and N. Willenbacher, *Influence of particle shape on the rheological behavior of three-phase non-brownian suspensions.* Colloids and Surfaces A: Physicochemical and Engineering Aspects, 2016. **497**: p. 316-326.

152. Zuiderduin, W., C. Westzaan, J. Huetink, and R. Gaymans, *Toughening of polypropylene with calcium carbonate particles.* Polymer, 2003. **44**(1): p. 261-275.

153. Polat, K., I. Orujalipoor, S. İde, and M. Şen, *Nano and microstructures of SEBS/PP/wax blend membranes: SAXS and WAXS analyses.* Journal of Polymer Engineering, 2015. **35**(2): p. 151-157.

154. Bikiaris, D.N., A. Vassiliou, E. Pavlidou, and G.P. Karayannidis, *Compatibilisation effect of PP-g-MA copolymer on iPP/SiO2 nanocomposites prepared by melt mixing.* European Polymer Journal, 2005. **41**(9): p. 1965-1978.

155. Nandi, S., S. Bose, S. Mitra, and A.K. Ghosh, *Effect of maleic anhydride grafted polyethylene on engineering properties and morphology of fumed silica filled polyethylene blown films.* Journal of Plastic Film & Sheeting, 2012. **28**(3): p. 207-227.

156. Reignier, J. and B.D. Favis, *Core–shell structure and segregation effects in composite droplet polymer blends.* AIChE journal, 2003. **49**(4): p. 1014-1023.

157. Han, C.D., *Measurement of the rheological properties of polymer melts with slit rheometer. II. Blend systems.* Journal of Applied Polymer Science, 1971. **15**(10): p. 2579-2589.

158. Binks, B. and S. Lumsdon, *Stability of oil-in-water emulsions stabilised by silica particles.* Physical Chemistry Chemical Physics, 1999. **1**(12): p. 3007-3016.

159. Paul, D.R. and J.W. Barlow, *Polymer Blends.* Journal of Macromolecular Science, Part C, 1980. **18**(1): p. 109-168.